Master thesis in Energy Science

Spectral analysis of supply-demand matching in power systems with high levels of VRE

Jeroen van Winden

February 2018

Key concepts:
Variable renewable energy, Fourier transformation, spectral analysis, grid flexibility, electricity storage

Utrecht University

Contact information

Name:	Jeroen J. van Winden
Institution:	Utrecht University (UU)
Student number:	3956423
Tel. number:	+316 5131 4499
E-mail:	j.j.vanwinden@students.uu.nl
	jjvw@live.nl
Weblink:	www.linkedin.com/in/jjvanwinden
UU supervisor:	Gert Jan Kramer
UU course code:	GEO4-2510 (ENSM)
UU second reader:	Wilfried van Sark

Abstract

High levels of variable renewable energy (VRE) induce supply-demand mismatches due to variability in electricity generation. To accommodate these fluctuations in residual load, power grid flexibility is required, which entails the ability of the power system to absorb or supply electricity when required. Flexibility can be enhanced through electricity storage, interconnection, demand-side management and flexible power plant dispatch. Since the residual load fluctuations depend on different cycling components of supply and demand, flexibility is required on specific cycling timeframes. This study investigates a spectral analysis which maps these supply- and demand fluctuations and the subsequent effect of deploying flexibility measures. Through direct Fourier transformation, generation and demand profiles are decomposed into individual time-varying components, showing on which timeframes dominant cycling components fluctuate. This visualises the residual load for different solar PV/wind-ratios in frequency and phase spectra. Subsequently, the effect of deploying flexibility measures is reflected as changes in these frequency spectra. To generate residual load curves, a power system model is created where three storage technologies and several other flexibility measures can be deployed.

The frequency spectra show how solar PV generation is well-described by two diurnal and one seasonal fluctuations, where the latter is in antiphase with the seasonal demand fluctuation. Wind generation is shown to fluctuate more noisily, but is especially dominated by monthly fluctuations. Increased wind penetration thus induces residual loads on monthly timeframes whereas solar PV generation induces large daily and seasonal residual loads. The amplitudes of onshore wind fluctuations were furthermore higher than offshore wind. The generation mix inducing the lowest fluctuation volume was found to be a solar PV penetration of 25-40%. Additionally, inverse Fourier transformation exposed the extent to which supply and demand correspond on individual cycling timeframes.

In terms of storage, battery storage reduces fluctuations on <12-hour timeframes in the frequency spectrum. The reducing effect increases with PV penetration due to increased discharge cycles. Compressed air energy storage is shown to be a cheaper option with stronger reduction potential on diurnal and weekly timeframes. Power-to-hydrogen conversion reduces fluctuations on diurnal, monthly and seasonal timeframes, but at high cycling costs. Even after combining storage with other flexibility measures, especially monthly fluctuations pose problematic supply-demand mismatches, inducing instances when VRE generation is close to zero and storage caverns are depleted. Additional findings include overgeneration has the potential to reduce fluctuations on all timeframes, especially when combined with gas-to-power combustion. Interconnection, interruptible loads and curtailment are furthermore shown to be important flexibility measures due to instances of high surplus/deficit. Concludingly, the research successfully investigated the application of spectral analyses in VRE integration research and provides a foundation for a new approach to flexibility strategies.

Content

List of figures

List of tables

List of abbreviations

AA-CAES	Adiabatic compressed air energy storage
AMI	Advanced metering infrastructure
BES	Battery energy storage
CAES	Compressed air energy storage
DFT	Discrete Fourier transformation
DLC	Direct load control
DR	Demand response
DSI	Demand-side integration
DSM	Demand-side management
DSO	Distribution system operator
E2P	Energy-to-power [ratio]
EES	Electrical energy storage
EV	Electric vehicle
EHP	Electric heat pump
FFT	Fast Fourier transformation
G2P	Gas-to-power
iFFT	Inverse fast Fourier transformation
LCOS	Levelised cost of storage
LF	Load factor
P2G	Power-to-gas
P2P	Power-to-power
PHS	Pumped hydro storage
PSO	Power system operation
PR	Price response
PV	Photovoltaic(s)
TCC	Total capital cost
TSO	Transmission system operator
RES	Renewable energy source(s)
V2G	Vehicle-to-grid
VoLL	Value of lost load
VRE	Variable renewable energy

1. Introduction

In response to increasing concerns about the effects of fossil-based electricity generation, there has been a rapid increase in the use of renewable energy sources (RES) over the last decades (REN21, 2017). An especially notable increase can be recognised in the capacity of solar photovoltaic (PV) and wind power, which are expected to account for the majority of additionally installed (non-hydro) renewables in the future (IEA, 2014). Hence, future reliance on solar and wind power is projected to be unavoidable in reaching (inter)national climate goals and slowing down the depletion of the global carbon budget.

Yet, on an hourly and daily basis cloud cover, wind speeds and solar irradiation levels influence the energy output of solar PV panels and wind turbines (World Energy Council, 2016a). Furthermore, seasonal climate conditions cause a discrepancy between the energy output during different months and seasons. The electricity generated by these technologies is therefore referred to as variable renewable energy (VRE Since the power system relies on the presumption of a constant balance between generation and consumption (World Energy Council, 2016a), increased reliance on VRE raises challenges regarding power grid security and reliability (Luo et al., 2015; ESMAP, 2015). Nonetheless, experience shows that European solar and wind power cycling is occasionally complementary, posing an opportunity for VRE integration (Music et al., 2013; IEA, 2014).

Literature acknowledges VRE implementation of 5 to 10% of total annual electricity generation can be achieved without significant challenges in the energy system (IEA, 2014; ESMAP, 2015). At higher VRE shares, increased grid flexibility is needed to deal with residual loads[1] at times of over- and undersupply of VRE. Grid flexibility broadly describes the ability of the power system to supply and absorb electricity whenever required. Literature suggests four concepts that may be deployed to increase grid flexibility: dispatchable generation, adaptation of the physical grid infrastructure, demand-side management (DSM) and electrical energy storage (EES[2]) (IEA, 2014). An optimal mix of such flexibility measures is required for high VRE integration or even full reliance on VRE sources (ESMAP, 2015).

Dispatchable generation capacity allows electricity generation to follow the demand by flexibly operating conventional power plants. Improved grid infrastructure involves physically adapting the grid to better cope with VRE, e.g. by increasing grid interconnectedness (IRENA, 2015b; IEA, 2014). DSM concerns measures to promote demand response (DR), where consumers shift their demand to avoid or shift peak loads (ESMAP, 2015). Finally, EES[3] allows the time-shifting of large energy volumes and is thus recognised to have the largest potential to form a synergy with high levels of VRE (IRENA, 2015a; IEC, 2011). Common short-term storage options include electrochemical batteries, supercapacitors and -conductors, compressed air energy storage (CAES), pumped hydro-storage (PHS) and flywheels. Common long-term EES technologies are sensible/latent heat storage and power-to-gas (P2G) conversion in the form of hydrogen or synthetic methane (World Energy Council, 2016b; IRENA, 2015a).

Literature acknowledges the need for sufficient grid flexibility and proposes an array of measures such as EES to enhance grid flexibility. Yet despite this widespread recognition, it is reported that more investigation is required for determining exactly how flexibility measures allow these ambitious VRE targets (IEA, 2014). Furthermore, stakeholders lack common vision on the need of energy storage and the challenges of its implementation, posing a barrier for EES implementation (DG ENER, 2013). Hence, there seems to be a research gap where flexibility measures are directly linked to

[1] Electricity demand minus VRE generation (World Energy Council, 2016b)

[2] EES includes both electricity stored in the form of electricity as well as by conversion into another storable medium (Luo et al., 2015).

[3] I.e. grid-connected EES

the fluctuational behaviour of the residual load. VRE induces supply-demand discrepancies due to different time-varying cycling components, but the interplay between the time-varying components, demand and the need for flexibility remains implicit. Since individual components fluctuate on specific timeframes (hourly, daily, weekly, seasonally), the deployment of flexibility measures should be dependent on these cycling components. By explicitly formulating the link between these variables, limitations and opportunities for high VRE shares can be insightfully explicated. This notion has implications for the level to which VRE can be integrated into the grid as well as the for the effective deployment of flexibility measures.

1.1 Research proposal

Identifying the individual cycling components of a complex signal can be achieved through Fourier transformation. A Fourier analysis implies that any signal function can be described by a set of sinusoidal functions with different amplitudes, phases and frequencies (Morin, 2009). It can thus be used to recreate any discrete or continuous signal using individual sinusoidal fluctuations. This research proposes to apply this methodology to separate supply and demand curves into their individual sinusoidal fluctuations. This visualises their cycling behaviour in a frequency spectrum and a phase spectrum, where the former shows the amplitude and frequency sinusoids and the latter indicates their phase-shift. Using these spectra, the individual time-varying fluctuations that dominate the residual load can be depicted comprehensively. Since flexibility measures affect the fluctuation profiles of supply and demand in the power system, their effect is directly reflected as changes in the frequency and phase spectrum. Hence, the effect of flexibility measures can be quantified by comparing the spectra in power system configurations with and without flexibility measures. Similarly, the spectra can be used to analyse whether certain installed ratios of solar PV and wind power are less prone to time-varying fluctuations than others.

In order to find residual load curves for different power system configurations, the research includes the creation of a customisable power system model. The model allows different levels of VRE generation to be combined with the deployment of flexibility measures such as EES or interconnection. It thus provides the input signals for the spectral analyses.

Although applying a Fourier analysis in VRE research is not a novel application, this research investigates a new approach in the sense that it uses spectral analysis to explicate power system dynamics and explore VRE integration potential. Whereas literature generally derives the frequency spectrum for single case studies, this research uses spectral analysis to show how the residual load's frequency spectrum is dependent on the system configuration. Moreover, it investigates the use of frequency spectra to quantify the effect of flexibility measures on individual cycling timeframes. In conclusion, the research investigates an alternative methodology for analysing and visualising the challenge of VRE integration. In doing so, it aims to expose explicit relations between VRE integration and flexibility, answering the following main and sub questions:

- **To what extent do flexibility measures accommodate different cycling components of residual load at high VRE levels?**

i) On what timeframes do supply and demand fluctuate?

ii) How does the residual load fluctuate at different VRE generation mixes?

iii) How is the effect of flexibility measures reflected in frequency spectra?

iv) What cost dynamics influence the deployment of EES?

1.2 Report layout

The first section of the research consists of a literature review to summarise the concept of grid flexibility as well as the measures that can be deployed to enhance flexibility [chapter 2]. Additionally, this section discusses the theoretical background on Fourier analyses and Fourier transformations. Subsequently, the second step concerns the methodology for modelling a power system [chapter 3]. This section explains how the different power system components are modelled, including the way in which EES and other flexibility measures are incorporated. For the model's input data, the Netherlands is used as a reference case. Then the methodology for executing the Fourier analyses is described, including the processing steps required for executing a spectral analysis [chapter 4]. After the power model and the Fourier analyses have been discussed, the research results are set forth in chapter 5 and 6. Chapter 5 concerns the results of running supply and demand curves through the spectral analysis in order to map the power system fluctuations. This includes comments on optimal configurations and supply-demand complementarity. Subsequently, in section 6 the effect of deploying flexibility measures is visualised in the frequency spectra. Afterwards, the implications and limitations of the research results are discussed [chapter 7]. Finally, the main conclusions and recommendations for further research are included in chapter 8 and 9.

2. Theory

The following section contains a theoretical background regarding the different storage technologies as well as other possible flexibility measures. After concisely defining the concept of flexibility in the light of supply-demand matching, an overview is provided on the EES technologies that can be applied to enhance grid flexibility. Then a summary is given of the other flexibility measures that can be deployed, where Appendix XVI includes a more elaborate literature review of all the concepts. This provides a substantiation on the concept of grid flexibility as well as practical applications of the flexibility measures. Finally, an introduction to the concept of Fourier analyses and transformations is included.

2.1 Definition of grid flexibility

Grid flexibility is a concept which has implications in a variety of components of an energy system. In general terms, flexibility is the ability to supply and absorb energy whenever required and ensure a supply and demand equilibrium (IEA, 2014). Hence, a flexible system is able to apprehend the equilibrium despite risks and unforeseen events (Blanco & Faaij, 2018). Nevertheless, flexibility is rather viewed in relation to a system's responsive capabilities on different timeframes (Gracceva & Zeniewski, 2014). As shown in Figure 1, a dynamic and responsive an energy system is required on multiple timeframes to form a secure energy supply. A system's intra-hourly response capabilities, such as frequency or voltage control, are rather described as grid stability. Resilience is in turn the ability to react to system shocks such as major power dropouts or fuel depletion. Adequacy and robustness both concern energy security in terms of a stable economic and geopolitical power system. Flexibility is thus defined more specifically as a (power) system's ability to change supply and demand in response to short term uncertainty or mismatches is forecasted and delivered energy.

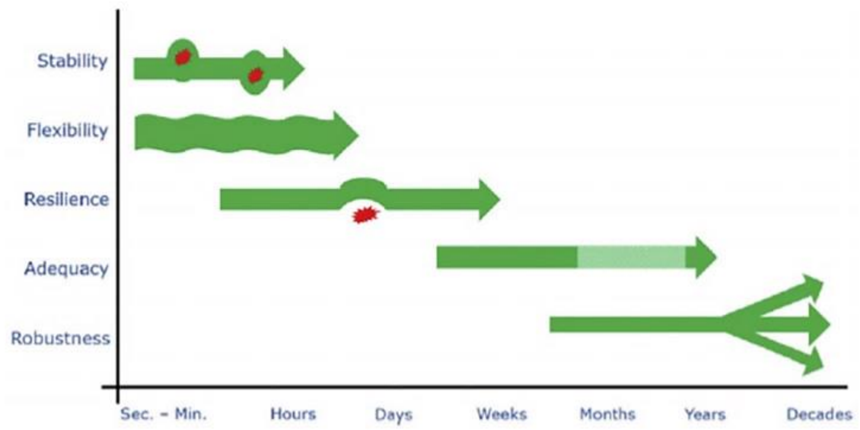

Figure 1: Five properties of a secure energy system (Gracceva & Zeniewski, 2014; p. 338)

For the power grid specifically, IEA (2014) divides the measures for enhancing grid flexibility into four main components, elaborated on in the following sections: electrical energy storage (EES), dispatchable generation, demand-side management (DSM) and adaptation of the physical grid. Blanco & Faaij (2018) supplements the possibility of installing excess capacity, where an VRE overcapacity is installed to reduce deficits and further increase storable surpluses. Furthermore, curtailment[4], geographical and technological system diversity and an optimal ratio between solar PV and wind generation are stated to enhance grid flexibility.

[4] Which involves purposely spilling electricity by shutting off wind turbines or solar PV installations

2.2 Electrical energy storage (EES)

Electrical energy storage concerns the notion that electricity surpluses are shifted over time, by either directly storing electricity or converting it into another storable medium. The following section contains concise descriptions on the classification and application of the different storage technologies. The technological data on each type of EES are adapted from ESMAP (2015), IEC (2011), World Energy Council (2016b), Pierie et al. (2015), Verzijlbergh et al. (2015) and Luo et al. (2015).

2.2.1 Classification of EES technologies

Although there are multiple ways of classifying electricity storage technologies, two common methods are classification according to physical form of energy storage and classification according to energy-to-power ratios. Figure 2 shows the EES technologies categorised according their physical form of energy storage. Only the EES technologies that can return energy in the form of electricity (P2P) are incorporated. Hence, latent and sensible heat storage as well as solar fuels are disregarded.

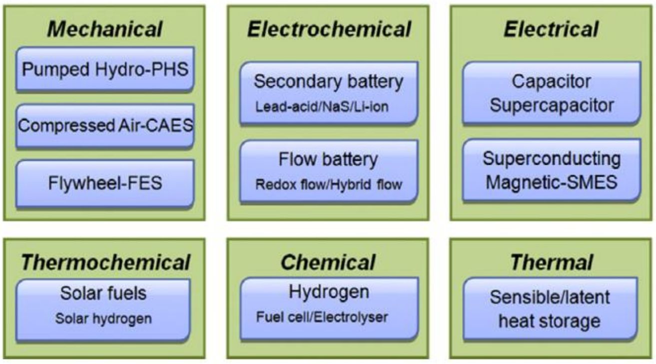

Figure 2: Classification of EES technologies to energetic state (Luo et al., 2015, p. 514)

Storage technologies are furthermore well defined by the ratio of energy-to-power ratio (E2P ratio), as shown in Figure 3. The E2P ratio - or discharge time - denotes how long a storage facility can discharge energy at its rated power and is thus an indicator of the application potential for EES technologies. A technology with a low E2P ratio can generally deliver or absorb high power for a short period of time and therefore excels in short-term fluctuation reduction. On the other hand, technologies with high E2P ratios can provide power for longer periods of time, making them suitable for shifting larger amounts of energy over longer timeframes (World Energy Council, 2016b). Since supercapacitors, superconductors and flywheels[5] have E2P ratios of <0.25h (World Energy Council, 2016b), these technologies generally have their application in increasing grid stability rather than grid flexibility. Hence, these technologies are disregarded as well. The following section includes a technology description on the remaining P2P storage technologies.

[5] A technology description is annexed in Appendix IX

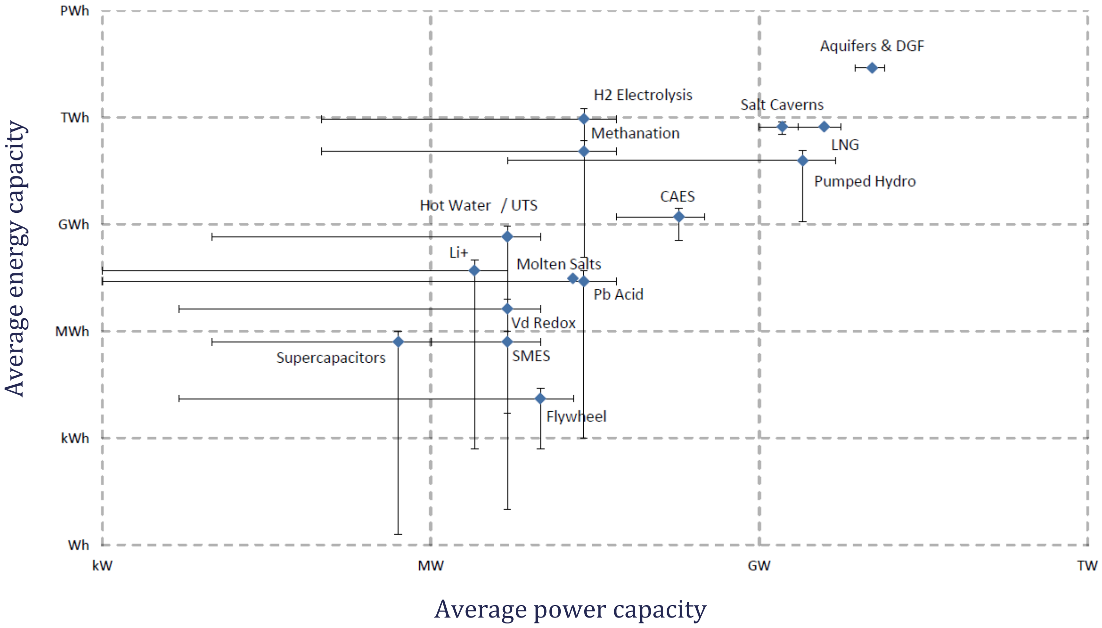

Figure 3: Classification of EES technologies to E2P ratio (Pierie et al., 2015, p. 20)

2.2.2 Pumped hydro storage (PHS)

The most commercialised EES technology is PHS, covering 99% of the global industrial-sized EES capacity. In PHS, water is pumped up to an elevated reservoir at times of low electricity demand. If peak demands occur, the water can be released through a turbine to generate electricity at capacities of up to multiple GWs. PHS is one of the few technologies that can deliver both high power and energy, making it suitable for frequency control, load levelling, hourly control but also long-term energy storage. Its exact E2P ratio generally lies between those of medium and long term EES technologies and is reported varying from single hours up to weeks. PHS facilities are further characterised by a cycle efficiency ranging between 70 and 85%, long lifetimes (~40 years) and fast response times (3 minutes). Barriers to implementation include the requirement of suitable geographical sites and high initial investment costs.

2.2.3 Compressed air energy storage (CAES)

CAES uses electricity to compress air, which is then stored in subterranean (salt) caverns or storage tanks. In conventional CAES, the compressed air is heated by combustion of a fuel (diabatic) or residual heat sources, which in turn drives turbines to generate electricity. Hence, conventional CAES can be considered a means of reducing natural gas usage in conventional gas turbines. An emerging renewable alternative is advanced adiabatic CAES (AA-CAES), which avoids additional fuel requirements by storing the heat released in compression phase and using it for the decompression (Das & McCalley, 2012). This does however require an additional means of thermal energy storage (TES) (stoRE, 2012). Rated power of CAES installations can be hundreds of MW per unit at cycle efficiencies of 40-75%, depending on whether an additional energy source is required. It is suggested that CAES is especially capable of smoothing power output from wind turbines as ((de)compression rates reach full power within the hour and storage capacity can be sized accordingly. Common E2P ratios of CAES are similar to the E2P of PHS, with reported full cycling times of multiple hours. Downsides are the requirement of suitable storage caverns, low diabatic cycle efficiencies and the notion that diabetic CAES requires additional fuel input, which is generally natural gas.

2.2.4 Battery energy storage (BES)

BES involves a range of electrochemical batteries which use electricity to invoke a chemical reaction or vice versa. The traditional solid-state battery consists of two solid electrolytes immersed in a liquid. Battery cells can be connected in series or parallel to increase the storage and power capacity, generally at a constant ratio. The E2P ratio of batteries is reported between 1-10 hours for each type and to a large extent fixed per battery. Alternatively, redox flow batteries utilise two chemical solutions which are separated by a membrane to invoke a chemical reaction. Such flow batteries allow the decoupling of energy and power capacity. Different types of solid-state and flow batteries exist, which are elaborated individually on in appendix IX. The response time of all batteries is seconds or less.

2.2.5 Power-to-gas (P2G)

The storage of electricity in the form of gas is an option with higher E2P ratios (50-500+ h) and thus suitable for long-term storage. P2G can either be deployed in the form of hydrogen (H_2) or in the form synthetical natural gas (SNG) after further processing. The first step of both options is electrolysis, where the electricity is used to form H_2 and oxygen (O_2) from water. The H_2 can be stored for months in empty (salt) caverns, combusted or be injected into the natural gas grid up to H_2 concentrations of ~5%. After extracting the hydrogen from the storage cavern, it is used together with oxygen to generate electricity in in fuel cells or used in conventional turbines This storage option has total cycle efficiencies of around 30-50% and can be sized from multiple kWs to GWs.

Alternatively, the H_2 can be further processed together with CO_2 to form methane (CH_4), which is in turn refined into synthetic natural gas (SNG) for injection into gas grids or usage in transport (Vlap et al., 2015). The gas can be stored in subterranean caverns or empty gas- and oil fields, where the latter requires additional ‘cushion’ gas injection. Completing the storage cycle, the SNG is combusted in a regular gas turbine to produce electricity. The additional processing steps lower the cycle efficiency to 30-35% and increase investment costs. Again, the power-to-gas and gas-to-power capacities can be varied freely, as well as the storage capacity utilised. Furthermore, a P2G installation has a start-up rate of ~40 minutes (Vlap et al., 2015) and response times of ~10 minutes.

2.2.6 Flywheels

This EES technology uses electricity to spin a mass around a magnetic bearing with very low friction. An electric motor speeds up the rotor to store electricity and in turn a generator slows it down to generate electricity. Flywheels are characterised by low E2P ratios (<0.25h) and instantaneous response times, thus being suitable for very short-term storage. Rated capacities reach up to multiple MWs at low energy capacities and their efficiencies lie between 70-80%. Applications thus mainly involve the ensuring of uninterrupted power supply and frequency regulation. Disadvantages of flywheels are the high level of self-discharge (3-40%/h) and the wear-down of mechanical components.

2.2.7 Supercapacitors

Supercapacitors store electricity in electrostatic fields between two electrical conductors. Where conventional capacitors have a low energy density, super- or ultracapacitors can have a hundredfold of conventional energy densities. These capacitors utilise nanomaterials to greatly increase capacitance, but the energy density remains below BES technologies. Supercapacitors have a high efficiency (90-94%), a very low E2P ratio (<0.25h), immediate response times and can be cycled millions of times without degradation. Its applications lie in frequency and voltage control as well as peak shaving. Downsides are high costs and high self-discharge levels, making them unsuitable for large scale or longer-term energy storage.

2.2.8 Superconducting magnetic energy storage (SMES)

SMES systems store electricity in the magnetic field of a superconducting coil. Due to the superconducting coil, almost no electricity is lost in resistance and efficiencies are very high (>90%). Like for supercapacitors, the cycle lifetime is very high and full discharge can occur within 1 minute almost without degradation. SMES is currently applied to short-term power quality operations but research is being done for applying SMES to renewable integration. Disadvantages are the high current costs, the need for cryogenic cooling equipment and the possible harmful effects of the magnetic fields.

2.3 Other flexibility measures

Besides EES, other drivers of grid flexibility are demand-side management (DSM), dispatchable generation and grid adaptation. Since DSM becomes increasingly important with changing demand patterns, a section is furthermore included on the effects of demand-side electrification. Note again that this section provides summarising information, whereas Appendix XVI includes the full literature reviews.

2.3.1 Demand-side management

DSM is a broad concept encompassing a variety of tools which aim to manage the energy demand of consumers (Kakran & Chanana, 2018), which include both residential and industrial users. IEA (2016) defines DSM as the planning, implementation and monitoring of actions that aim to alter consumers' demand pattern. Additionally, the umbrella term of demand-side integration (DSI) is proposed, which encompasses both DSM and demand response (DR). DR is in turn the reactive behaviour that consumers display, possibly influenced by DSM measures. Figure 4**Error! Reference source not found.** includes the summary of different concepts related to DSM, which is explained in detail in Appendix XVI. This appendix additionally contains a quantification of the effect of different DSM measures as reported in literature.

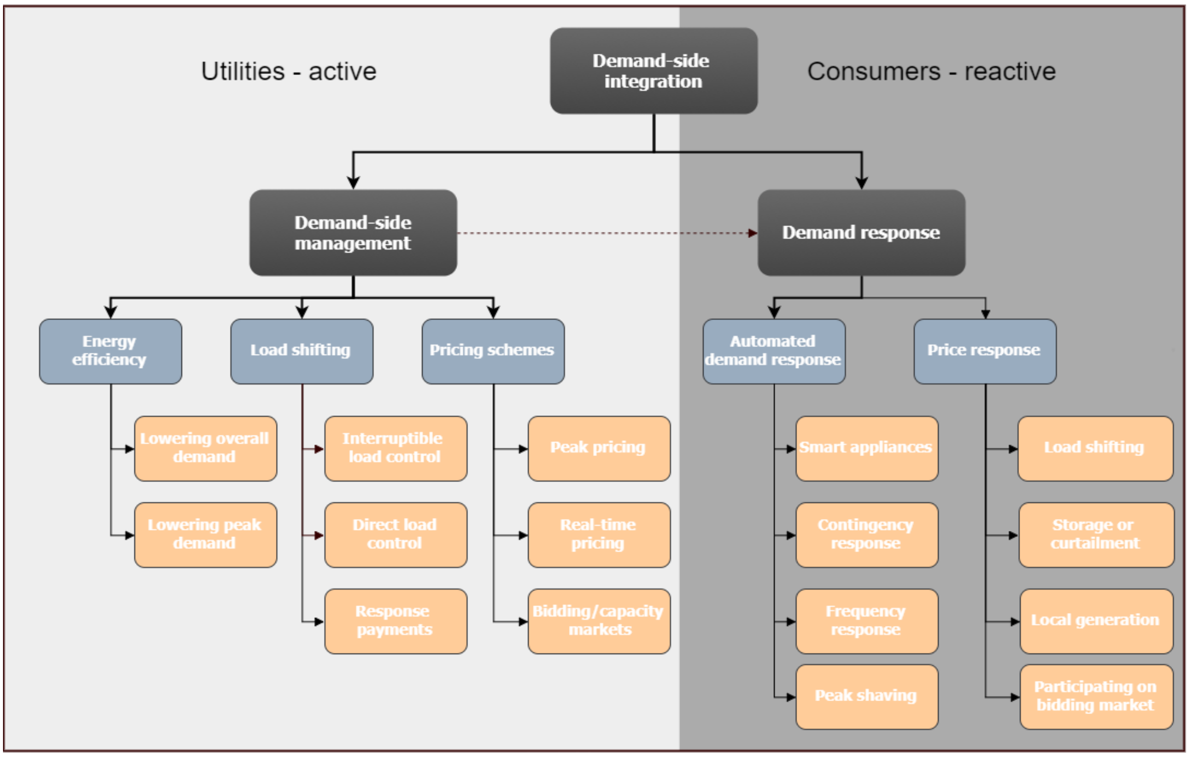

Figure 4: Overview of DSM concepts

2.3.2 Demand-side electrification

Electrification implies to which extent different sectors use electrified processes rather than other resources. The shift towards increasingly electrified processes causes a change in the consumers' demand profiles and induces increased potential for DSM in the power sector. Although the concept can be argued to have implications in all demand sectors, its influence can broadly be divided into the residential, transport and industrial sector. A more elaborate discussion of the related concepts is again included in Appendix XVI.

Residential electrification concerns switching from fossil resources to electricity for space heating/cooling, water heating and cooking. Since the energy used for cooking is generally a minor contribution, it mostly implies a shift to electric or hybrid heat pumps (EHPs) for space and water heating. Literature such as Love et al. (2017) and UK Power Network (2014) propose daily EHP load profiles specified per month, which indicated the influence of electrification on current demand patterns [Figure 5]. Most notably, a peak occurs in the morning, followed by a dip in the afternoon and finally a lower peak in the evening.

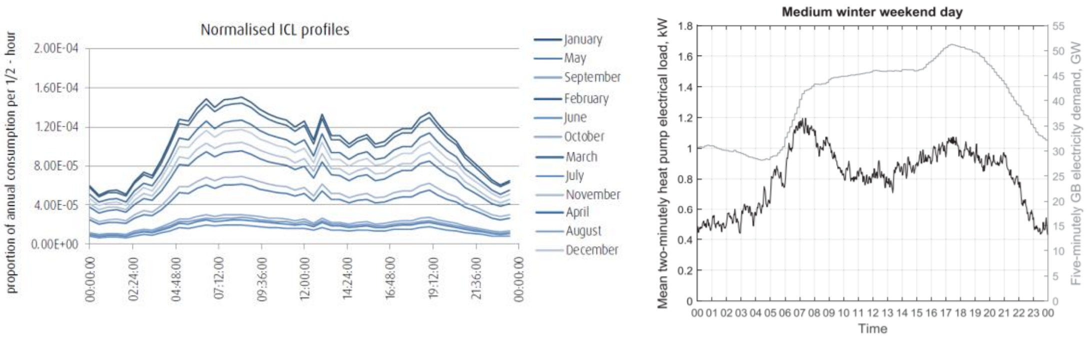

Figure 5: Single EHP load profile per month [UK Power Network, 2014, p. 17 (L); Love et al., 2017, p. 337 (R)]

The electrification of transport naturally concerns the use of (hybrid-)electric vehicles (EVs) as opposed to fossil-fuelled vehicles as a mode of transport. Whereas electric passenger cars account for the majority of global EV deployment, EVs can also include electric trains, buses, trams or marine vehicles. The way in which the daily demand profile of a household changes in response to electric passenger vehicle adoption is dependent on the charging behaviour of the consumers. Factors that influence the demand profile include the time of day when charging occurs, the charging duration, the *smartness* of the charging and the amount of charging done at home rather than at public charging stations (Movares, 2013). For home charging specifically, UK Power Networks (2014) proposes hourly charging loads for electric vehicles per household [Figure 6].

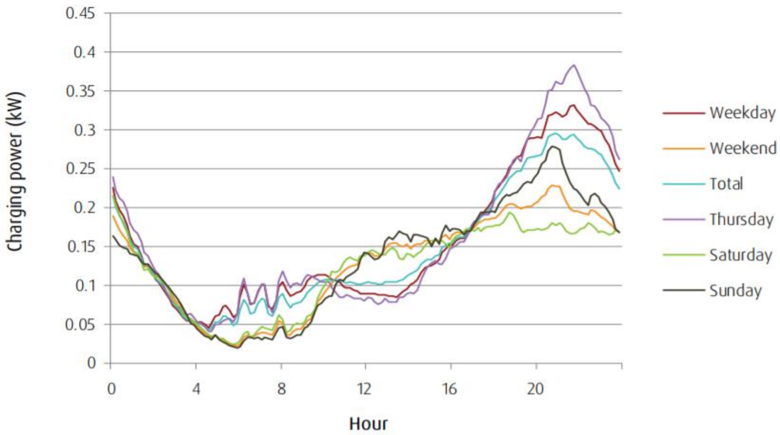

Figure 6: Average EV charging profiles per weekday [UK Power Network, 2014, p. 27]

In terms of industrial electrification, the fact that different industrial processes shift towards electricity as their resource implies the daily electricity demand profile of large consumers is prone to change. Simultaneously, increased electrification induces a larger DSM potential since an increasing share of processes can be controlled, shifted or interrupted. The daily electricity profile and its potential for load shifting is however strongly dependent on the type of industrial processes. Appendix XVI includes a review on the different types of industrial electrification reported in literature.

2.3.3 Dispatchable generation

Deploying dispatchable generation is the most traditional form of providing grid flexibility. Dispatchable or flexible generation implies the selective operation of power plants whenever VRE generation is insufficient to meet demand. Different aspects of power plants that influence their flexibility include short-term start-up, operation capabilities at a range of generation levels, ramping rates and response times (IEA, 2014; Verzijlbergh et al., 2015). Table 1 shows the flexibility characteristics for several conventional generation power plants: an open-cycle gas turbine (OCGT), a natural gas combined cycle plant (NGCC), a supercritical pulverized coal plant (SCPC), a nuclear power plant (NPP) and a bio energy plant (Bio). It can be concluded that OCGTs and SCPCs are generally the most flexible power plants[6] and NPPs the least flexible due to their long start-up times. Appendix XVI includes an additional comment on the utilisation effect, which describes how dispatchable generation negatively influences the economic viability of power plant operation.

[6] Excluding pumped hydro plants

Table 1: Power plant flexibility characteristics

Parameter	Unit	OCGT[2,5,6]	NGCC[2,4,5,6]	SCPC[1]	NPP[3, 4, 5]	Bio[4,7]
Minimum load	[%]	15-25	40-60	50	30-50	50
Cold start time	[min]	-	120-250	90	>1440	-
Warm start time	[min]	<20	90-200	45	>1440	180
Hot start time	[min]	<20	45-90	30	780-1440	-
Ramp up rate	[%/min]	20-30	4-5	2	1-5	3
Efficiency	[%]	30-42	38-60	40-45	30-33	30-35
CO_2 intensity	[g/kWh]	400	400	~800	~0	~0

[1] NETL (2012), [2] IEA (2014), [3] NEA (2011), [4] Eurelectric (2011b), [5] IEA (2012), [6] ESMAP (2015), [7] IRENA (2012)

2.3.4 Grid adaptation

Adaptation of the physical grid describes all alterations to the existing power grid which aim to increase the system's responsive capabilities. Besides enhancing flexibility and adaptability, grid adaptation is often required to accommodate other flexibility measures. IEA (2012) proposes a distinction between three categories of grid adaptation. Firstly, grid extension involves interconnection between regions and countries as well as connecting new generation capacity. Subsequently, grid renewal concerns the upgrading and smartening of existing transmission and Distribution networks. Thirdly, renewable integration involves specific grid adaptations to enhance VRE integration, such as spreading out generation sources to reduce fluctuations (i.e. the pooling effect). The possible grid adaptations within each category are summarised in Table 2 and explained in greater detail in Appendix XVI.

Table 2: Investment options for grid adaptation

Investment	Adaptation	Effects on grid
Grid extension	Connecting new capacity	+ Reduces demand-bottlenecks
	Interconnection	+ Smoothens power fluctuations + Increases supply-demand balance + Reduces regulation reserves, congestion and required back-up capacity - High investment costs - Requires complementary generation/demand profiles - Requires integral transformation
Grid renewal	Upgrade power lines and connection nodes (transmission & distribution)	+ Bi-directional energy flows + Enables distributed energy sources - Increased control and monitoring complexity
	Smarter grids	+ Accommodates other flexibility measures + Improves stability, resilience and power quality + Reduces system costs + Enables distributed energy sources - Hardware- and IT intensive
VRE integration	Geographical spread	+ Reduces system-level variability + Reduces curtailment

		- Requires ample interconnection and forecasting
	Connecting VRE sources to grids	+ Additional generation (over)capacity + Connects remote VRE sources - Negative effect on grid components - Requires FRT capabilities, protection systems and smart adaptations

2.4 Fourier analysis

The following section explains the theoretical background of the Fourier analysis. The methodology section [4] includes any additional steps required for executing the analysis and processing the results. Fourier's theory is built upon the suggestion that any mathematical formula can be described by cumulating an indefinite number of periodical sinusoidal functions (Lunter & Wayenburg, 2003). This implies that any given waveform can be recreated using a specific set of (co)sinuses. Each sinusoid is characterised by a different frequency *f,* amplitude *A* and phase ϕ [Figure 7]. The frequency indicates how often one full fluctuation occurs per time segment and is directly linked to a fluctuation's period 1/f. The amplitude describes the magnitude of that fluctuation and the phase in turn describes the sinusoid's relative starting position, where one full fluctuation spans a phase of 360° or 2π radians. If the phase shift between two waves is 180°, they are in complete anti-phase. The relative phase of two waves thus indicates to what extent their peaks align or alternate.

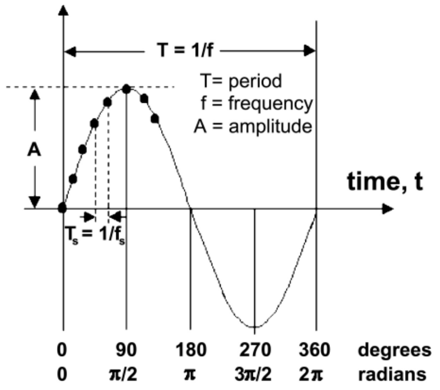

Figure 7: Characteristics of a sinusoid wave (NIST, 2016)

Although the Fourier theory describes signals using sinusoids, even cumulation into square or triangular signals is possible if enough sinusoids are cumulated, as illustrated in Figure 8. The reason why Fourier's notion is valuable, is because it implies that any complex signal can simply be described by a set of separate sinusoidal signals. Hence, if a complex waveform is acquired through data sample collection or signal processing, the analysis is used to identify what exact combination of sines and cosines determines the original waveform. If the frequency, amplitude and phase of the underlying sines and cosines are identified, this provides comprehensible insight into the different fluctuating components of the original waveform.

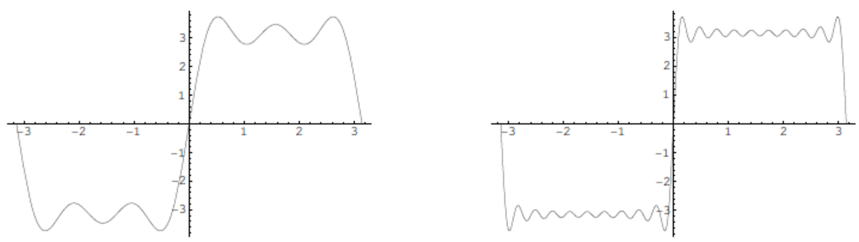

Figure 8: Recreation of a square waveform by cumulating 3 (L) and 10 sinusoids (R) (Lunter & Wayenburg, 2003, p. 75)

Decomposition of a waveform into its separate sinusoidal functions is achieved through a discrete Fourier transformation (DFT) (Morin, 2009). *Discrete* implies that the function is performed over non-continuous signals or samples (Kerr, 2009). Waveforms are generally plotted as signal amplitude versus time and are thus referred to as being shown in the time domain. However, a DFT transforms the signal into a *frequency spectrum*, where the frequency or period is plotted on the x-axis rather than time [Figure 9]. In the frequency domain, a peak in the plot of the DFT indicates the presence of a sinusoid. The height of the peak indicates the corresponding amplitude. As shown in the figure, the original signal can be found by cumulating all the individual sinusoids. For additional explanation on DFTs, an example of interpreting a DFT is annexed in appendix V.

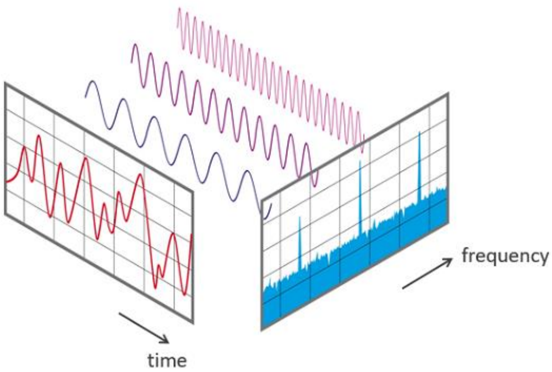

Figure 9: Relation between the time domain and frequency domain (NTi Audio, 2017)

Alternatively, executing an *inverse* discrete Fourier transform (iDFT) changes a signal from the frequency domain back into the time domain. Performing such an iDFT over the full frequency spectrum thus returns the original waveform. On the other hand, performing an iDFT over a segment of the frequency spectrum (i.e. a *frequency band*), returns only the frequencies within that range into the time domain. In Figure 9, this would entail that if the frequency spectrum was filtered to only show one of the three peaks, the iDFT would lead to the corresponding sine wave rather than the original waveform. A segment of the frequency spectrum can be isolated using a band-pass filter, which gives any frequencies outside the chosen frequency band an amplitude of 0. An example is shown in Figure 10, where f_l is the minimum frequency of and f_u is the maximum frequency of a single band. Since the signal was set to 0 for each frequency outside the band, the time domain shows the waveform of an individual temporal component. The specific values of the frequency bands are arbitrary and can be adapted to the researcher’s requirements (Makarov et al., 2012).

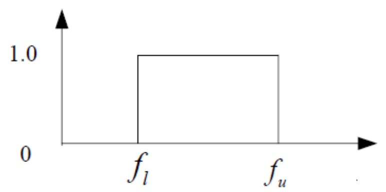

Figure 10: Band-pass cut-off in the frequency spectrum (Makarov et al., 2012; p. 4)

Introduction to the method

The method section explains the steps taken to answer the sub and main questions of the research. Figure 11 shows a representation of the five steps taken in the research process. First, the input data are collected which provide the basis for the power system model. Subsequently, the model is designed according to a power system framework, where different flexibility measures are incorporated. After completion of the model, verification and validation steps are deployed to determine the model's applicability and reliability [Appendix X]. After model completion, the Fourier analyses are applied to different input signals to expose the power system fluctuations. Subsequently, the residual load is analysed for different compositions of the power system to expose the flexibility requirements for different scenarios. This step furthermore includes the visualisation of the effect of EES in the frequency spectra.

The research process can broadly be divided into a modelling section (step 1-3) and an analysis section (step 4-5). For clarity, method Part I explains the modelling process, setting forth the different model components, the model input data and the used data sources. The method for the Fourier analyses is then discussed in method Part II, including which input signals are analysed and additional processing steps.

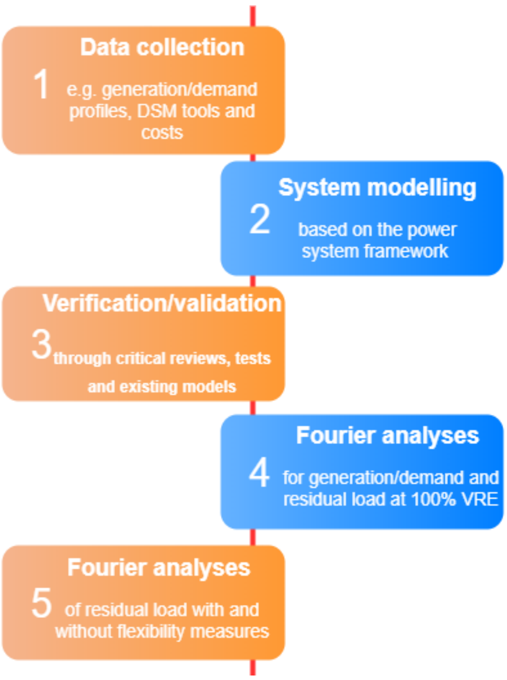

Figure 11: Research method

3. Method Part I - modelling

The power system modelling is done in the form of a spreadsheet model, combined with MATLAB for computational capabilities. A detailed model characterisation is included in Appendix I and the provisional model title is the *Renewable Energy SPECtral analysis Tool* (RESPECT). The validation and verification steps taken are annexed in Appendix X. Note that the model is not intended to give a complete representation of the Dutch power system but aims to simplify as much as possible, given that power models are generally highly complex. To still ensure an adequate representation of the essential power system components, the model is built upon a model framework, as proposed in Pietzcker et al. (2017). This report proposes an assessment framework of 18 important drivers in power system modelling, annexed in Appendix IV. The drivers are categorised into five themes: power system operation (PSO), temporal demand matching, storage (EES), grid operation and investment dynamics. The model lay-out is built upon the different components of this framework. Figure 12 shows the resulting model lay-out, including the way in which it enables the Fourier analyses. The way in which each driver is modelled specifically is discussed in the following section.

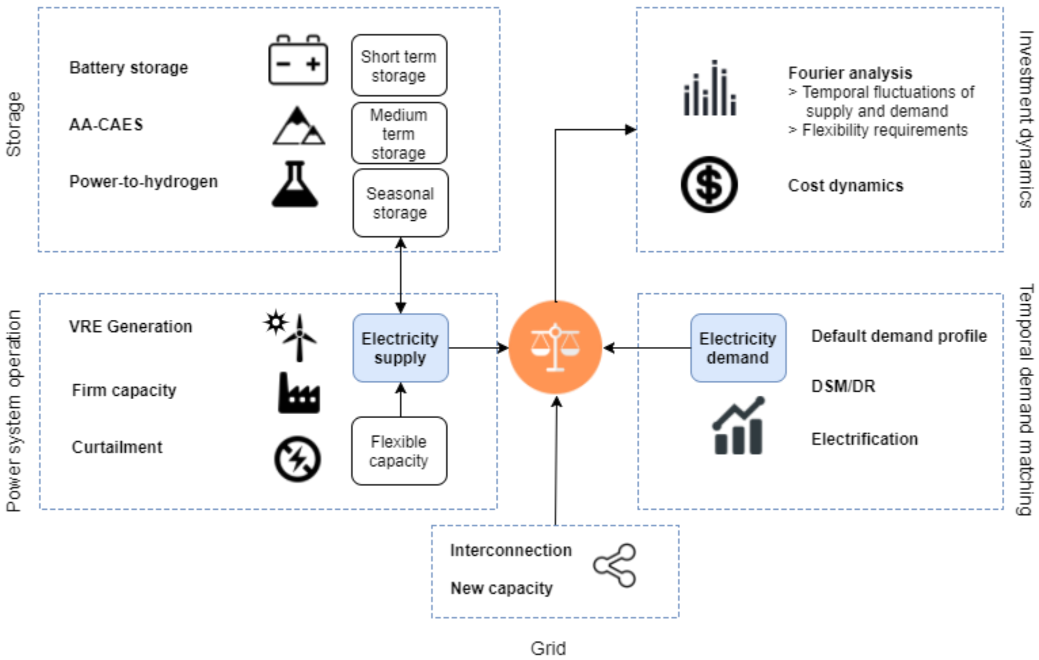

Figure 12: Power system model lay-out

3.1 Power system operation

The theme of power system operation broadly concerns the supply side of the power system. Its drivers include the VRE generation as well as the installed capacity and dispatch of back-up generators. Thirdly, the flexibility measure of curtailment is categorised within this theme.

3.1.1 VRE generation

In terms of VRE generation, the model includes separate generation curves for solar PV, onshore wind and offshore wind. Their hourly output is based on a historical Dutch load curve which is converted into an hourly share of the annual output. The historical load curves are retrieved from the 2016 quarter-hourly generation data as reported by ENTSO-E (2016a), cumulated into 8760 hours from Friday January 1st 12:00 until Saturday December 31st 12:00. The hourly shares of the annual generation are derived using equation 7, where subscript *j* denotes a generation technology. For offshore wind, a correction was applied to normalise the energy generation to installed capacity (adapted from CBS, 2017a), since significant additional VRE generation capacity was installed throughout the year 2016. The method for correcting the values is annexed in appendix VII. Figure 13 shows an exert of the resulting generation profiles, shown for the first week of January and August.

$$\%E_{j,t=i} = \frac{E_{\mathrm{his,j},t=i}}{E_{\mathrm{his,j},tot}} \qquad \forall \mathrm{j}, \forall \mathrm{i} \qquad (1)$$

$\%E_{j,\,t=i}$ = share of annual generation in hour i [MWh per MWh/yr]
$E_{his,\,j,\,t=i}$ = historical electricity generation in hour i [MWh]
$E_{his,\,j,\,t=i}$ = historical total annual generation [MWh/yr]

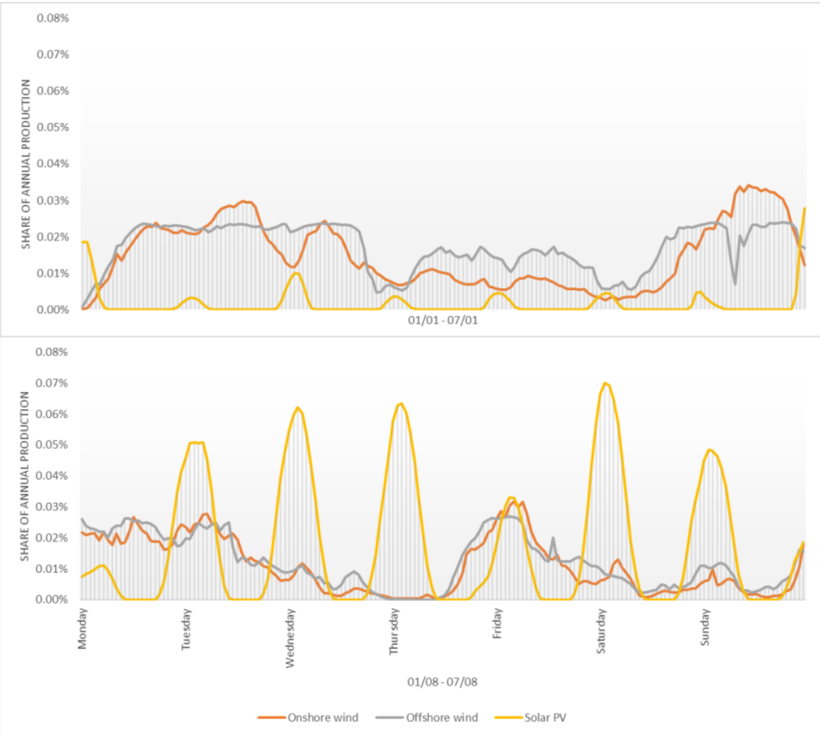

Figure 13: Historical generation profile for a week in January and August 2016 [% of annual total/h]

The fact that the generation profiles are included as *shares* per hour, allows a variable installed capacity to be transformed into hourly generation data if the load factor (LF) of each technology is known. As a result, the installed capacities of VRE generation technologies can be manually varied in the model[7]. The load factors are adapted from Quintel (2017) which assumes 10% for solar PV, 25% for onshore wind and 40% for offshore wind. The hourly electricity generation for a technology *j* then becomes:

$$E_{j,\ t=i} = C_j \times LF_j \times \%E_{j\ ,t=i} \times 8760 \qquad \forall j, \forall i \qquad (2)$$

$E_{j,\ t=i}$ = electricity generation in hour i [MWh]
C_j = installed capacity [MW]
LF_j = load factor [%]
$\%E_{j,\ t=i}$ = share of annual generation in hour i [MWh per MWh/yr]

3.1.2 Flexible capacity and dispatch

Secondly, an installed level of back-up or *firm* capacity can be opted for in the model, which is defined as a guaranteed energy level at a certain moment (IRENA, 2017). To differentiate between flexible and inflexible capacity, three types of firm power plants are included in the model. Two types of flexible capacities can be included, based on the characteristics of an OCGT and a SCPC [Table 1]. Hence, both natural gas and coal can be used for power generation, where a variable number of 400 MW power plants can be manually chosen for both power plants. De Boer et al. (2014) shows that of the total 28 GW Dutch installed power plant capacity, about 2/3 or ~20 GW use gas and 1/5 or ~6 GW use coal as a fuel. It is assumed that both flexible power plants can reach full operation within an hour so specific ramping rates are not incorporated in the model. The power plants are however limited by a minimum load factor, reported at 25% for the NGCCs and 50% for the SCPCs (IEA, 2012; NETL, 2012)[8].

The inflexible power plant is based on a nuclear power plant (NPP). The NPP is assumed to be a must-run generation facility at a constant load of 495 MW throughout the year, the installed capacity of the only Dutch NPP (ANVS, 2017). The dispatch of flexible capacity in the model is not based on an actual merit order since no representation of the power market is included in the model. Rather, a merit order is prescribed for the generation technologies as shown in Figure 15. VRE technologies are in practice always deployed first, despite the possibility that cheaply operated generators must reduce their operation as a result (REN21, 2017). The load that remains after the VRE generation is referred to as the residual load, as visualised in Figure 14. Note that a positive residual load indicates that additional energy is required to reach demand, whereas a negative residual load indicates a surplus of energy. As can be deduced, the residual load is defined as:

$$E_{res,t=i} = E_{load,t=i} - (E_{PV\ ,t=i} + E_{wind\_on\ ,t=i} + E_{wind\_off\ ,t=i}) \qquad \forall i \qquad (3)$$

$E_{res,\ t=i}$ = residual load in hour i [MWh]
$E_{load,\ t=i}$ = total load in hour i [MWh]
$E_{j,\ t=i}$ = Generation by technology j in hour i [MWh]

[7] The default 2016 installed capacities for The Netherlands are 2040 MW of solar PV, 3283 MW for onshore wind and 957 MW for offshore wind (CBS, 2017b).
[8] Example: if 450 MW is to be generated, one power plant of 400 MW is fully operated and 50 MW remains. This is beneath the minimum load of a power plant so only one power plant becomes operational.

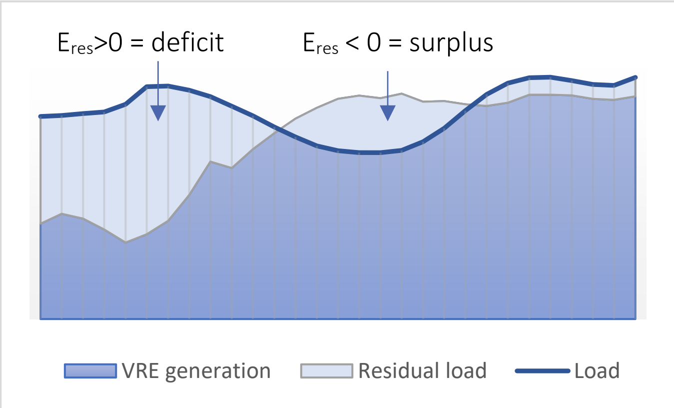

Figure 14: Visualisation of residual load

A positive residual load is first generated by the baseload capacity of the NPP, since it provides inflexible generation capacity. Subsequently, the flexible firm capacity is dispatched where coal is opted before gas. As a result, the prescribed merit order of the power plants is as shown in Figure 15.

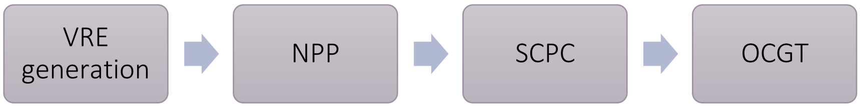

Figure 15: Electricity generation merit order

3.1.3 Curtailment

If an oversupply of electricity occurs, measures need to be taken to relieve the grid from the surplus. This can be achieved through reducing the load of flexible firm capacity, charging storage mediums or by exporting electricity. If all such options are exhausted, the final option is curtailment, which is thus described by:

$$E_{curt,t=i} = \sum_j E_{j,t=i} - E_{load,t=i} - E_{stored,t=i} - E_{exp,t=i} \qquad \forall i \text{ if } E_{curt,t=i}>0 \qquad (4)$$

$E_{curt,\ t=i}$ = curtailed energy in hour i [MWh]
$\Sigma E_{j,\ t=i}$ = total generation in hour i [MWh]
$E_{load,\ t=i}$ = total load in hour i [MWh]
$E_{stored,\ t=i}$ = stored electricity in hour i [MWh]
$E_{exp,\ t=i}$ = exported electricity in hour i [MWh]

3.2 Temporal demand matching

The theme of temporal demand matching concerns the demand profile that determines the equilibrium between supply and demand. The framework proposes the driver of demand profile evolution, resulting from the notion that a demand profile is not fixed but can change with socio-economic or technologic developments. As discussed in Appendix XVI, this for example happens when sectors increase the levels of electrification or if DSM measures are deployed. Hence, to account for such changes, the model includes simplified options for varying demand patterns as a result of DSM and electrification[9]. Although the framework further proposes the driver of solar/wind-complementarity, this factor is already covered in the theme of power system operation.

3.2.1 Default demand curve

In order to provide input for the equilibrium, the model first prescribes a default hourly demand curve. Similar to the generation profiles, a historical demand curve is adapted from ENTSO-E (2016b) and transformed into an hourly share of the annual total. Again, 2016 load data are adapted, running from Friday January 1st 12:00 until Saturday December 31st 12:00. The default annual total electricity demand is set at the 2016 CBS value of 415 PJ (Schoots et al., 2016), but can be manually altered to reflect changes in demand. Figure 13 shows the development of the hourly profile for a week in January and August as a percentage of the total annual demand.

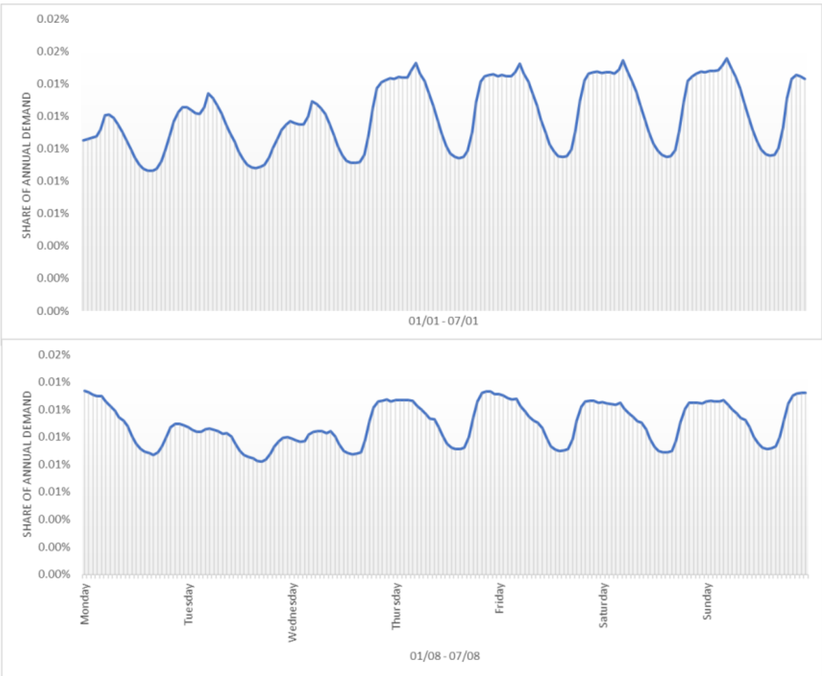

Figure 16: Historical demand profile for a week in January and August 2016 [% of annual total/h]

[9] Note that Pietzcker et al. (2017) categorises DSM under *storage*, since it often entails using EVs as storage and grid operation devices. However, in this research DSM is rather dealt with as a driver of the demand profile. Therefore, the categorisation under this theme seems more appropriate.

3.2.2 Demand profile evolution - DSM

The way in which the default demand curve changes in response to DSM mechanisms is based on the theory section on DSM. To differentiate between the different DSM tools and their resulting DR, different alterations to the default demand curve are possible in the model.

3.2.2.1 *Peak pricing*

Peak pricing is incorporated to simulate a variety of DSM tools which aim to shift demand away from peak hours as well as the resulting price response. If this demand type is selected, the demand peaks above a certain threshold are divided amongst times of low demand. The threshold is specified per month, based on the maximum demand and a certain set peak reduction. Figure 17 shows how the default demand curve is altered in response to peak pricing. Note how the demand at peak times is cut at the threshold and shifted towards times of low demand. The level of peak reduction can be manually chosen within a range, leading to a maximum allowable load level for each month.

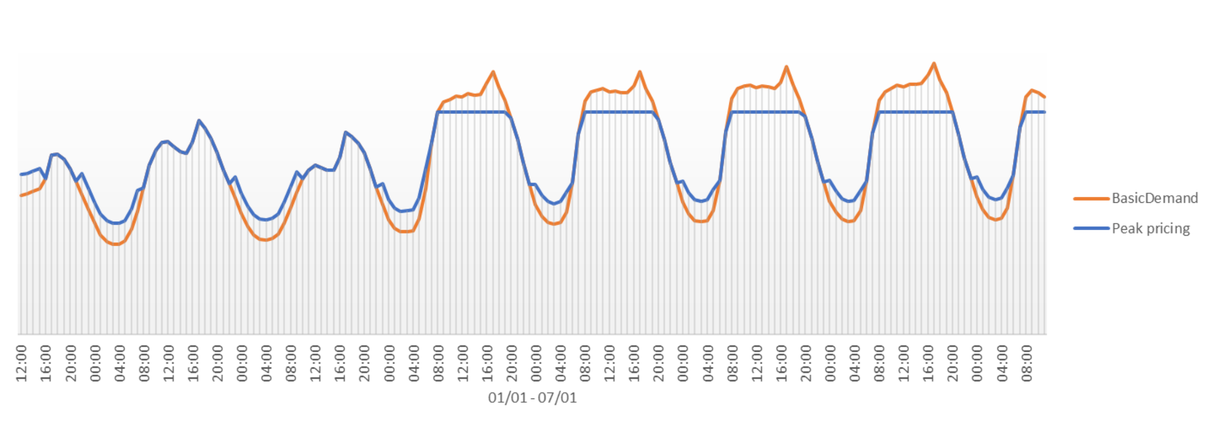

Figure 17: Default demand curve vs peak pricing demand curve

3.2.2.2 *Load following*

Secondly, a level to which demand follows generation levels (i.e. *load following*) can be switched on within the model. This simulates the DSM measures of DLC and automated load-following. The mechanism allows a certain share of the demand to be dependent on the VRE generation level. Hence, if load following is set at 10%, 90% of the demand will consist of the default demand curve and 10% of the demand will be distributed over the year proportional to VRE generation. To illustrate, Figure 18 shows how the demand curve is altered due to load following in case of 10% and 50% load following. In the former case, the figure shows how the demand is higher than the default demand at times of high VRE generation, but lower than the default demand when VRE generation drops. In the latter case, it can be recognised that the demand takes the shape of the VRE generation curve. Although 50% load following is unrealistically high, it illustrates how the demand curve evolves in response to the load following settings.

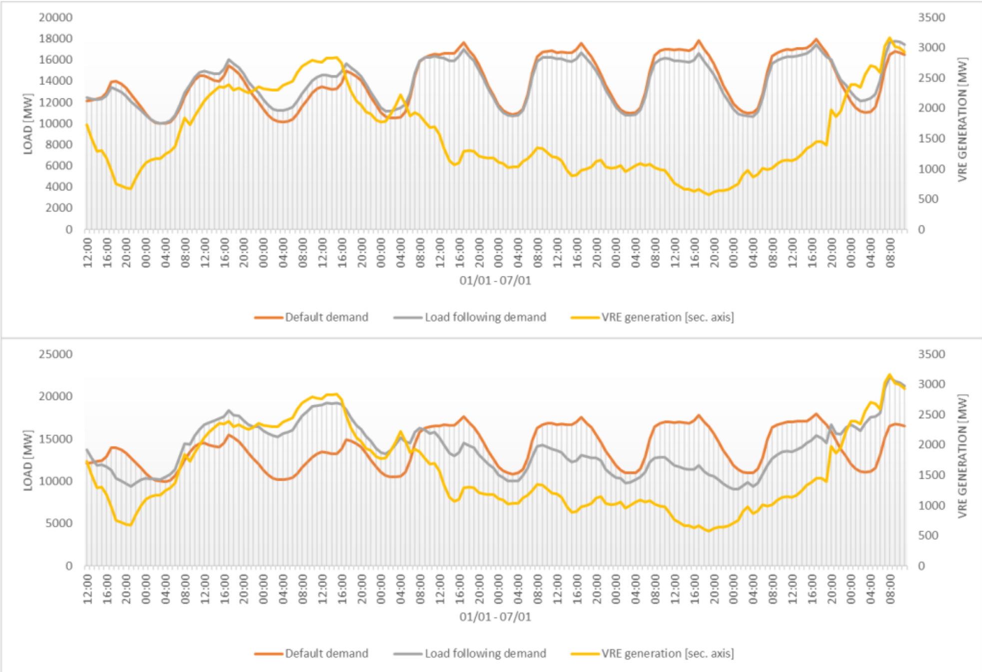

Figure 18: Default demand curve vs. load following demand curve at 10% (top) and 50% (bottom)

3.2.2.3 *Energy efficiency investment and interruptible load*

Furthermore, the possibility of investing in energy efficiency can be simulated through manually lowering the total annual electricity demand. Automatically, this diffusely lowers the hourly energy demand. Finally, the possibility of an interruptible load is included, where a variable load can be decreased by a certain amount of MWs whenever demand cannot be met.

3.2.3 Demand profile evolution - electrification

The types of electrification included in the model are the transport sector shifting to electric vehicles (EV) and the residential sector shifting to electric heat pumps (EHP). Ideally industrial electrification would be included as well but time restrictions caused the modelling of DSM to be limited to two sectors. Additionally, the industrial load curve evolution is strongly dependent on specific industrial processes which are rather reflected in bottom-up modelling.

3.2.3.1 *Electric vehicles*

In terms of electric vehicles (EVs), the model assumes that only passenger cars are increasingly electric since the electrification of other Dutch vehicles is negligible compared to passenger cars (RvO, 2017). Furthermore, it is assumed that the charging only occurs at home at a rate which is constant throughout the year. The charging profile is based on the theory section, and includes a distinction between the charging behaviour in weekends and on weekdays. Figure 19 shows the hourly charging load profile for a single EV for a full day, where t=0 corresponds to the time of 00:00 am. Within the model, the percentage of passenger vehicles that is electric can be varied between 0 and 100%, where the total amount of passenger cars is set at the 2016 value of 8.1 million (CBS, 2017c). The total load that results from the charging of electric vehicles is added to the hourly demand profile in the model.

As discussed, the EV batteries furthermore have the potential to be used for local storage. Despite that notion that it remains uncertain to what extent EV battery storage provides benefits, it is assumed that a share of the electric vehicles can be used as additional storage capacity. The model allows vehicle-to-grid storage to be switched on, which increases the battery capacity by 20 kW per electric vehicle at an E2P ratio of 5 hours. Any benefits that 'smart charging' can pose are not considered since the charging behaviour is not dynamic. Nevertheless, smart charging can be considered a DSM measure and be approximated using the load following settings.

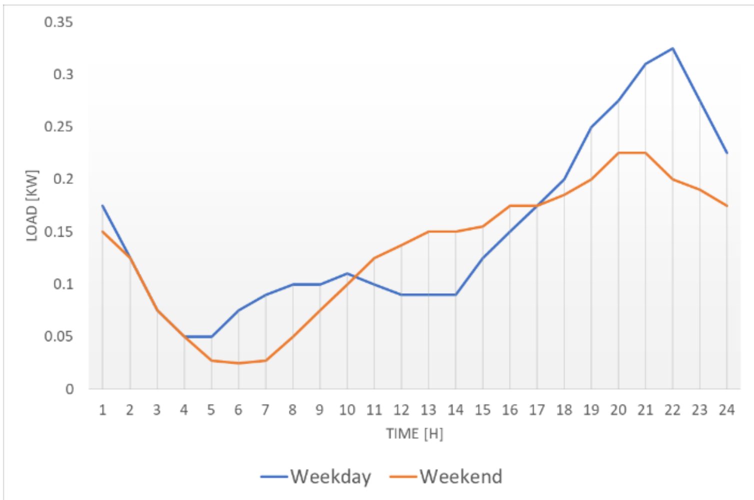

Figure 19: Modelled daily home charging load of a single EV

3.2.3.2 *Electric heat pumps*

The effect of electrification in the residential sector is modelled in terms of electric heat pump (EHP) implementation. Based on the theory section, an hourly load profile for single EHPs was specified per month [Figure 20]. The amount of EHPs is assumed to be linked to the number of households that are physically able to install an EHP. RvO (2014) reports a Dutch heat pump potential of 5.4 million residences, or 74% of all residences. As a result, the share of residences with an EHP can be varied manually between 0-74%. Again, the total hourly load resulting from the heat pumps is added to the demand curve.

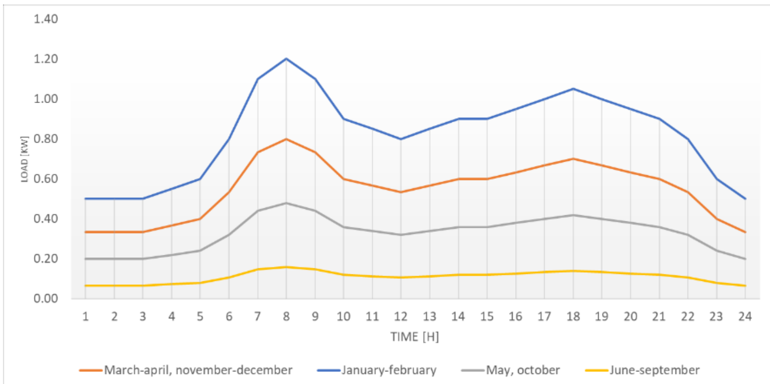

Figure 20: Modelled hourly load profile of a single electric heat pump

3.3 Storage (EES)

The third component of the model involves the electricity storage options. The drivers of this theme are storage short-term and seasonal storage. To simulate this driver, the model attains three different storage types to simulate both a low, medium and high E2P ratio: battery storage (BES), compressed air energy storage (CAES) and power-to-gas storage (P2). PHS is not considered due to geographical limitations. Furthermore, using the Norwegian PHS facilities is rather considered as interconnection. The characteristics for the three storage types are shown in Table 3 and discussed below.

Table 3: Storage technology characteristics

		Efficiency	Default E2P	Power capacity	Energy capacity
Technology		[%]	[h]	[GW_{max}]	[GWh_{max}]
P2G	Charging	60	>1 year	-	552,000
	Discharging	50		-	
BES[a]	Full-cycle	90	5	0.001	0.005
AA-CAES	Charging	80	9	-	69
	Discharging	90		-	

[a] *Values for a single battery*

3.3.1 Battery energy storage (BES)

The power/energy capacities of single batteries are assumed to be the transmission/distribution size of 1 MW, as reported in ESMAP (2015). Furthermore, a default E2P ratio is assumed of 5 hours, based on the general reported ratio of 1-10 hours and reported energy/power capacities (World Energy Council, 2016b; ESMAP, 2015). The amount of batteries installed can be manually chosen with a maximum of 10,000, leading to a maximum installed capacity of 10 GW capable of providing an energy capacity of 50 GWh. The full-cycle efficiency is assumed to be the maximum value of 90%. An hourly self-discharge level can be manually included and degradation levels are assumed to be negligibly low within the timeframe of one year.

3.3.2 Compressed air energy storage (CAES)

The CAES installation is assumed to be advanced adiabatic CAES (AA-CAES) requiring no additional fuel inputs. With the emergence of such advanced CAES designs, this type of storage can be considered a way of storing energy fully renewably[10]. For CAES in the Netherlands, a maximum storage capacity of 69 GWh is reported in the form of salt caverns (De Boer et al., 2014). The cycle efficiency is assumed to be 70-75% based on Zakeri & Syri (2015). It is further assumed that the default E2P ratio is 9 hours, based on the common cycling time, but this changes with varying the installed (de)compression capacities and storage capacity. Although the decompression and compression capacity can be altered separately, Gardner & Haynes (2007) reports that the largest operational CAES installation has a 3:1 discharging to charging ratio.

[10] Alternatively, CAES may be combined with biofuels to run renewably.

3.3.3 Power-to-H_2

Finally, the P2G is assumed to be power-to-hydrogen, converted into electricity through expansion in a gas turbine. The assumption that the H_2 is used to generate power leads to an underestimation of the value of P2G storage, since it has more promising applications outside the power system (ENEA Consulting, 2016). To partly account for the possibility that P2G is not used for power-to-power purposes, the model includes the option of turning off H_2 usage for electricity production. In this case, the H_2 is assumed to be delivered to other sectors and is not combusted.

An average full-cycle P2P efficiency of 30% is adapted, resulting from a power-to-gas efficiency of 60% and a gas-to-power efficiency of 50% (De Boer et al., 2014; Belderbos et al., 2017). The E2P ratio is practically unlimited due to the large storage capacity but naturally changes with the installed G2P capacity. Again, both the installed P2G capacity and G2P capacity can be varied manually. The total utilised storage capacity is equal to the highest occurring gas reserve[11].

3.4 Grid

In the theme of *grid*, the first driver is transmission and distribution. This driver is incorporated in the form of international connectedness of the grid. Interconnectedness with other countries allows over- and underproduction of electricity to be partly abated through electricity import/export. Figure 21 shows the available capacities for import/export to other countries for the year 2016 (based on TenneT, 2015). The 2150 MW to Belgium and Germany consists of 1300 MW of constant capacity and a maximum of 850 MW of variable monthly capacity. The import/export capacity can be manually increased to simulate the driver of grid expansion. In terms of the national grid, the model components are not geospatially specified so generation technologies are considered as one point-source. The driver of the pooling effect[12] is thus not incorporated, which may cause the model to overestimate the power fluctuation between regions. Finally, the model assumes the grid to be fully 'smart' and up-to-date. Hence, it is assumed that the grid has been equipped with an AMI to accommodate all the flexibility measures described in other themes. E.g. if a DSM measure requires the installation of demand-side hardware to allow response mechanisms, it is assumed that such installations are present.

Figure 21: Bi-directional capacity of 2016 Dutch connection to international grids [MW]

[11] This allows the costs for the storage section to be derived.
[12] Reduced power output fluctuations due to geographical spreading of VRE sources (Pietzcker et al., 2017)

3.4.1 Flexibility merit order

Additionally, with all the power system framework components modelled, a merit order for all flexibility measures is implemented to prescribe how the grid flexibility measures are deployed. First, any demand profile evolution is processed. Subsequently, the three storage options are deployed to increase grid flexibility. The first EES option considered is the charging or discharging of battery capacity and if no further battery capacity is available, CAES and power-to-gas are deployed respectively. If the storage options are exhausted, the flexible dispatch of coal and gas turbines is maximised. Afterwards, the possibilities of import, export and electricity curtailment are considered. Finally, the model allows the possibility of interrupting a part of the load, as an additional DSM measure.

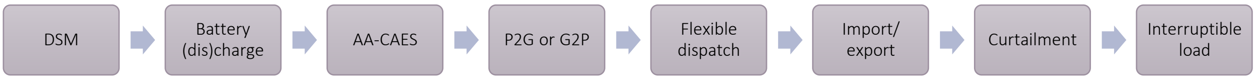

Figure 22: Flexibility merit order

3.5 Investment dynamics

The final theme in the framework concerns the investment behaviour. Most of the drivers mentioned in the framework exceed the model scope due to geographical scope (VRE investment feedback on the system) or the temporal scope of one year (expansion dynamics, capital stock inertia and aging and structural shift). Hence, rather than investment dynamics, this theme includes a cost analysis for the different storage technologies to compare the cost dynamics experienced. In order to do so, the following section sets forth the calculation for levelised cost of storage as well as a comment on the costs of any lost load. The relevant model inputs for the investment module can be found in Appendix III[13].

3.5.1 Levelised cost of storage

The following methodology for calculating the costs of storage is adapted from Zakeri & Syri (2015) and Lazard (2017). The average values reported in the former literature are adapted for the cost inputs, as summarised in Appendix III. Hence, it should be acknowledged that the costs come with significant uncertainty ranges and are primarily intended for identifying cost dynamics in the power system. Moreover, costs of storage facilities are to a large extent dependent on their application or *use case*, such as residential use, commercial use or installation near T&D nodes. Since the model does not differentiate between such different use cases, it was assumed that storage in the model concerns large-scale 'bulk' energy storage. Finally, the values proposed in the articles concern conventional CAES rather than AA-CAES. StoRE (2012) shows that capital costs of AA-CAES are reported in higher ranges. To account for this, the maximum capital cost reported in Zakeri & Syri (2015) is assumed rather than the average value.

Firstly, the total capital cost (TCC) of storage systems consists of three main components. The power conversion system (PCS) concerns the power module of the storage system, including electrical connections and cabling, and is described in €/kW. The concerning power rating is either the charging power or discharging power. In the model, the costs assume equal division between charging and

[13] Where required, an exchange rate between US$ and € was adapted on October 30th 2017, where the exchange rate was 1 US$ = €0.86.

discharging power since only total PCS values are provided[14]. The storage section includes all costs related to the physical storing of the energy, such as storage mediums, vessels and site excavation, described per unit of delivered energy €/kWh. In the model, the price for the storage medium is based on the largest stored reserve that occurs at any hour. Finally, the balance of plant (BOP) costs include all other assets required to set up a storage facility, such as project engineering, management or land acquisition. The TCC can thus be described as:

$$TCC[€/kW] = C_{PCS} + C_{storage} \times h + C_{BOP} \qquad (5)$$

Nevertheless, different storage technologies are characterised by distinctly different lifetimes. Hence, rather the TCC is annualised to allow better comparison between EES technologies. The annualised life cycle of cost components can be found through multiplying by the capital recovery factor (CRF):

$$CRF = \frac{i(1+i)^T}{(1+i)^T - 1} \qquad (6)$$

Where
i = interest rate [%]
T = lifetime [yr]

Moreover, the costs of different EES technologies are influenced by additional cost components during its lifetime, which are thus not incorporated in the capital costs. Firstly, these costs include the O&M costs, consisting of a fixed (€/kW) and a variable component for each discharging cycle (€/kWh). The variable component may also include any costs of the electricity or natural gas (in case of CAES) inputs required to charge the storage facility. Including the annualization factor, the O&M costs are described as:

$$C_{O\&M,a}\left[\frac{€}{kW}yr\right] = C_{O\&M,f} + (C_{O\&M,v} + CP + F) \times h \times n \qquad (7)$$

Where

$C_{O\&M,a}$ =	Annualised total O&M costs [€/kW-yr]
$C_{O\&M,f}$ =	Annual fixed O&M costs [€/kW-yr]
$C_{O\&M,v}$ =	Variable O&M costs [€/kWh]
CP =	Electricity charging price [€/kWh]
F =	Price of other fuel inputs, including emission costs [€/kWh]
h =	Discharge time [h]
n =	Annual number of discharging cycles

Furthermore, the costs of replacement concern any expenses required for replacing parts during the facility lifetime[15]. Especially in the case of batteries, this cost component is dependent on the amount of (dis)charging cycles, where increased cycling increases replacement requirements. However, Zakeri et al. (2015) provides replacement cost (C_r) indications using assumptions on the replacement lifetimes. Hence, the equation can be simplified to:

[14] E.g. if a 5 GW compressor is installed, the costs of PCS are multiplied with this value despite the notion that a different turbine power rating may be installed.

[15] Lazard (2017) describes this cost component as augmentation costs, which "represent the additional energy storage system (*ESS*) equipment needed to maintain the *Usable Energy* capability to cycle the unit according to the usage profile in the particular use case for the life of the system" (p. 5)

$$C_{R,a}\left[\frac{€}{kW}yr\right] = C_r \times CRF \quad (8)$$

Where

$C_{R,a}$ = Annualised replacement costs [€/kW-yr]

C_R = Total replacement cost [€/kW]

The lifetime costs should ideally include the disposal and/or recycling costs of the storage technology but Zakeri & Syri (2015) disregard this component due to a lack of data. Adding the different cost components, the annualised lifecycle costs is thus described by:

$$C_{lcc}[€/kW\ yr] = TCC_a + C_{O\&M,a} + C_{R,a} \quad (9)$$

The levelised lifecycle costs in terms of power is then converted to an energy dependent fraction by dividing by the annual operational hours. In the model, this occurs automatically based on the annual electricity output of the storage mediums. The remaining component is the final levelised cost of electricity (LCOE), as described by:

$$LCOE\ \left[\frac{€}{kWh}\right] = \frac{C_{lcc}}{n \times h} \quad (10)$$

Where

n = Annual discharge cycles

h = Discharge time [h]

Finally, the costs can also be made independent of the electricity charging price or fuel costs, leaving only the costs added by the storage technology. This is referred to as the levelised cost of storage (LCOS) and described by:

$$LCOS\ \left[\frac{€}{kWh}\right] = LCOE - \frac{CP}{\eta_{cycle}}$$

3.5.2 Value of lost load

In terms of interruptible load and load which is not met, an economic indicator of the costs is the so-called value of lost load (VoLL). This parameter defines the monetary implications (in €/kWh) of power outages and supply interruptions to retain a supply-demand equilibrium. Hence, it can be used as an indicator of the monetary payment to consumers that are required for them to lower their demand (Tol, 2007). Schröder & Kuckshinrichs (2015) show that the VoLL different significantly between user types and industrial sectors and furthermore depends strongly on the methodology for VoLL determination. Where the VoLL private consumers are reported mainly in the range of 5-25 €/kWh, this increases to ranges to over 250 €/kWh for industrial and commercial sectors (Schröder & Kuckshinrichs, 2015). For the Netherlands specifically, the VoLL for commercial end use is reported ranging between 0-50 €/kWh.

3.6 Summary

In conclusion of this research step, a power system model was created which utilises historical Dutch load curves to find residual load curves for different power system configurations. The model allows a variable level of VRE to be installed as well as a variable demand profile, in turn resulting in annual residual load curves. The input data were based on 2016 data regarding the Netherlands, but analyses were repeated using 2017 data. In terms of flexibility measures, the model includes three different storage types, which represent short, medium and long-term storage, interconnection, curtailment and flexible power plant dispatch. Additionally, a simplified representation of demand-side management was included, but more elaborate modelling is required to allow more accurate response to DSM measures. The model accommodates the subsequent research steps, since its main objective is providing the inputs for the spectral analysis. Its annual scope and 1-hour timeframe allow components of supply and demand to be analysed for a full year.

The model was shown to operate functionally and initial validation steps showed how the outcomes match a more elaborate model to a satisfactory extent. This suggests that the model is eligible to be used in a stand-alone fashion, but it should be recognised that the model is not a unit-dispatch model, nor does it include a cost-based merit order. It may therefore be used for supplementary scenario explorations, but should not be treated as a reflection of actual power system operations. Such models are highly detailed and complex in their operation, surpassing the aim of this research. The LCOS component of the model was included to indicate the dynamics that occur in electricity storage, but should be recognised as highly uncertain and case-specific.

4. Method Part II – Fourier analysis

The following section describes the methodological steps for performing the Fourier analyses. As aforementioned, the analyses are performed for 2016 data and repeated for 2017[16] to validate the results. First, the required computational steps are described, followed by the definition of the frequency bands and finally an elaboration on the inputs and outputs of the analyses. The actual code for performing the analyses can be found in Appendix VI.

4.1 Processing and computation

Performing a DFT involves a large number of calculations, causing it to require significant computation time. Hence, alternatively a Fast Fourier transform (FFT) is performed, which is an algorithm for greatly reducing computational time of the transformation (Klingenberg, 2005; DECE, no date). Although Excel provides an FFT function, the computation of the FFT is performed in MATLAB. Excel requires the number of samples to be set manually to 2^n and is limited by a maximum of 4096 samples, causing one full year of 8760 hourly data samples to be outside the computable range. The Excel function is further limited by high computational times[17]. To ensure the accessibility of the spreadsheet model, the MATLAB functionality is integrated into the Excel model using MATLAB's Spreadsheet Link. Hence, MATLAB automatically imports data for computation and exports the results back into Excel if required. Appendix VI contains both the MATLAB code for performing the FFT analysis as well as the commands used for importing and exporting data.

Despite the integrated FFT functionality, several steps were taken after the FFT produced its output. First of all, the output of an FFT initially consists of the *magnitude* of a signal rather than its amplitude. The magnitude is a complex number which describes both the amplitude and the phase of a signal[18]. It is therefore rather converted into the signal amplitude A using equation 1, where *abs* indicates the absolute value, M is the magnitude and N the number of data samples [Figure 23]. Dividing by N is required for scaling the magnitude to its actual value (Sek, no date). The phase can be derived from the imaginary part of the magnitude as shown in the MATLAB code.

$$A = \frac{\mathrm{Abs(M)}}{\mathrm{N}} \qquad (11)$$

Secondly, the results of an FFT have the tendency to show a large peak at f=0, which is referred to as the DC-value or DC-component (Sek, no date). This value merely indicates the mean of the signal and causes an undesired peak in the frequency spectrum at f=0. Hence, in order to process the FFT results properly, the signal value at f=0 is discarded. This can be achieved using the following formula, where *x(t)* denotes the input signal of the FFT.

$$x(t)_{No\ DC} = \mathrm{x(t)} - mean(x(t)) \qquad (12)$$

The FFT output is furthermore limited by a principle called the Nyquist criterion. This states that any frequencies above the Nyquist frequency can be considered redundant. Plotting the FFT results beyond the Nyquist limit will merely cause the signal in the frequency domain to mirror (Kerr, 2009). The Nyquist frequency is described by the equation below, where F_s is again the sampling frequency.

---

[16] Data were available from January through November, so any missing hourly data were supplemented with data from 2016 to still allow the Fourier analysis.

[17] Test runs ran for ~4 minutes for a dataset with 1028 samples and ~13 minutes with the maximum number of samples. In MATLAB, the computation time is several seconds.

[18] In the form of *a + b*i*, where i is the imaginary square root of -1.

$$F_{Nyq} = \frac{F_S}{2} \quad (13)$$

Another notion in the output of an FFT is that although it appears as if the x-axis holds specific frequencies, it rather shows small ranges of frequencies. This is the result of data discretisation by the FFT, which simplifies the full frequency range into small segments or *frequency bins*. Hence, if a peak on the axis is shown at frequency *f*, it actually shows the combined amplitude of all sinusoids within that frequency bin. Since the entire range of frequencies in the FFT output always equals the sampling frequency F_s (Kerr, 2009), the increment of a single frequency bin is described by:

$$F_{bin} = \frac{F_S}{N} \quad (14)$$

An effect that occurs as a result of the separation into frequency bins is called smearing or leakage. This effect entails that energy (i.e. amplitude) from a certain bin is leaked into neighbouring frequency bins, illustrated in Figure 23. Note that although the time domain shows an almost perfect sinus, the frequency peak 'leaks' its amplitude content to neighbouring bins which results in a peak that spans multiple frequency bins. This effect is to be recognised when interpreting frequency and phase spectra.

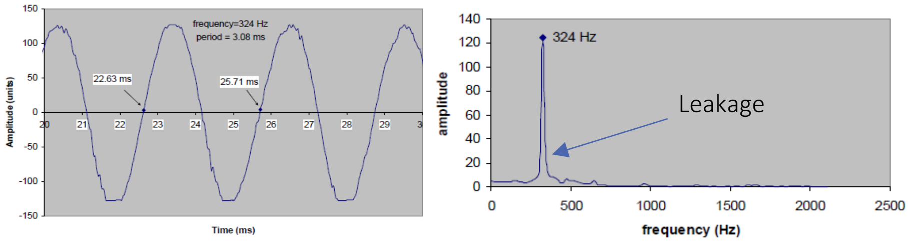

Figure 23: Leakage in the frequency spectrum (edited, from Klingenberg, 2005; p. 1)

Finally, the total volume of each individual fluctuation can be calculated. Since each fluctuation is a perfect sinus, the volume of a fluctuation is described by the area under the positive half of one full fluctuation. This can be used to compare the fluctuation volumes at different VRE generation mixes. In formula this becomes:

$$\mathrm{Vol} = \frac{A \times P}{\pi} \quad (15)$$

4.2 Frequency band definition

As discussed in the theory, to allow a signal to be separated into individual temporal components, specific frequency bands are to be defined. In the light of this research, the frequency bands are chosen in a way that they separate the expected temporal fluctuations in the power system. The cycling components of solar PV, wind and electricity demand at least include a seasonal cycle due to climate variations and a daily cycle due to weather conditions. Furthermore, the demand profile is expected to show potential cycles on a weekly timeframe, since demand varies for different days of the week.

Hence, the first frequency band is defined as the *'slow cycling'* component to reflect any annual fluctuations. Due to the separation of frequencies into bins, the frequency band spans sinusoids with a period of >2190 hours (or about a quarter of a year). The specific frequency range is given in Table 4.

The second frequency band contains all frequencies between slow and weekly fluctuations. Hence, it involves fluctuations that fluctuate on a timeframe of several weeks or months. This timeframe is the '*monthly cycling'* and contains any sinusoid with a period of 169-730 hours.

The third band is chosen to reflect the intraweekly variations and is called ‘*weekly cycling*’. It contains all the sinusoids with period between one day (24h) and a week (168h). Finally, the highest frequency band is the ‘*intradaily cycling*’, spanning the frequency range with fluctuations of equal to or less that one full day.

Table 4: Frequency bands for the inverse Fourier analysis

Cycling component	f_l [Hz]	f_u [Hz]	P [h]
Slow	3.17 E-08	1.27 E-07	2190-8760
Monthly	1.59 E-07	1.62 E-06	169-730
Weekly	1.65 E-06	1.13 E-05	25-168
(Intra)daily	1.13 E-05	1.85 E-04	1-24

4.3 Input signals and interpretation

Prior RE literature has applied a DFT or FFT over generation profiles, the residual load curve or power imbalance curves (Belderbos et al., 2017; Makarov et al., 2012; Verzijlbergh et al., 2015). Hence, the Fourier analysis is first performed for the VRE generation curves of solar PV and wind generation. Additionally, a spectral analysis was performed for the default demand curve. The resulting frequency spectra indicate on what timeframes and how strongly these individual signals fluctuate, providing initial insights on the different system fluctuations. Using the proposed frequency bands, the individual temporal components of the fluctuation in solar PV, wind and demand can be isolated and visualised. Comparing the individual fluctuation components of provides insight into possible complementarity between solar PV and wind, as well as showing on what timeframes they match the demand fluctuations.

Rather than describing the amplitude of the sinusoids in MWs, the amplitude is normalised to be independent of installed capacity, which allows a comparison between the amplitude of the different technologies and installation sizes. As a result, the y-axis of the frequency spectra shows the amplitude in % of the average generation. E.g. if the average hourly signal amplitude in the time domain is 1 MW[19], a sinusoid amplitude of 2 MW would show a peak of 200%. In turn this means that the sinusoid fluctuates between +200 and -200%. For additional basic explanation on interpreting DFTs, a generic example is annexed in appendix V.

Afterwards the Fourier analysis is performed for the residual load at different installed ratios of solar PV and wind, without any storage deployed. This allows the mismatch between supply and demand to be visualised in the frequency spectrum and in turn provides indications of optimal solar/wind-ratios for limiting fluctuations on different timeframes. The analysis is performed for different cases where solar PV and wind generate the amount energy equal to 100% of the annual electricity demand, which was by default set at 415 PJ or 115 TWh. Additionally, a scenario is regarded where 150% of the annual energy demand is generated to simulate installing VRE overcapacity. The required installed capacities are provided for different ratios of solar PV and wind in Table 5. For each case, the wind energy generation is divided equally between onshore and offshore wind in terms of installed power capacity.

[19] Which for example entails 10 MW installed solar PV capacity at a load factor of 10%.

Table 5: Installed capacities solar PV and wind to generate 100% of demand (415 PJ)

	Installed capacity [GW]		
Ratio solar PV - wind	Solar PV	Onshore wind	Offshore wind
Solar PV 25%, wind 75%	32.9	15.2	15.2
Solar PV 40%, wind 60%	52.6	12.1	12.1
Solar PV 50%, wind 50%	65.8	10.1	10.1
Solar PV 60%, wind 40%	79.0	8.1	8.1
Solar PV 75%, wind 25%	98.7	5.1	5.1
Solar PV 37.5%, wind 112.5%	49.3	22.7	22.7

The effect of introducing storage into the system can now quantified in terms of a change in the residual load frequency spectrum. Since the effect of introducing storage poses a *reduction* in fluctuation of the residual load spectrum, the frequency spectrum will be negative, or in other words a *difference spectrum*. From these difference spectra it can be concluded to which extent the measure reduces the system's power fluctuations. The effect of the flexibility measures is normalised to the total energy supplied over a year, to allow comparison between different sized storage facilities. Otherwise, a larger storage facility would naturally induce stronger reductions without means for comparison.

Additionally, the model allows any other signal from the model to be run through the Fourier analysis as long as the timeframe is 8760 hours. Hence, this provides the possibility of a spectral analysis for signals such as the (dis)charging behaviour of storage technologies, the level to which storage caverns are filled, the use of interconnection, curtailment levels or the deployment of DSM measures.

4.4 Summary

The previous section discussed the processing steps taken in the execution of the spectral analysis. The spectral analysis in combination with the power model allows any desired signal to be transformed into the frequency domain. It thus completes the methodology for the research and accommodates the answering of the research questions.

Firstly, several practicalities regarding the output of the FFT in MATLAB were discussed. The formulas were provided for scaling the axes to the correct and interpretable values as well as for discarding the undesired DC-component from the output signals. Besides that, the frequency bands were determined, which are required for performing the iFFT over sections of a frequency spectrum. The bands were determined based on own judgment to match the expected fluctuational behaviour of supply and demand curves. It was shown that both the MATLAB code as well as the processing steps functioned properly and thus allowed the spectral analysis. The input signals for the spectral analyses were then discussed, mainly consisting of generation, demand and residual load curves. Nonetheless, any other model variable consisting of 8760 consecutive hours can be run through the analyses as well. Finally, the effect of introducing storage into the system can be quantified in terms of a change in the residual load frequency spectrum.

5. Spectral analysis of VRE supply and demand

The following section shows the results of the Fourier spectral analyses over the 2016 generation profiles and demand profiles. First the frequency spectra are discussed for the demand, solar PV and wind power to map the individual power system fluctuations. Note that the Fourier analyses of the generation and demand profiles were repeated for the year 2017[20], as annexed in Appendix II. Subsequently, the individual temporal cycling components are identified and compared. Finally, the storage and power requirements are deduced from the analysis for different power system compositions.

5.1 Demand

Figure 24 shows the frequency spectrum of the electricity demand, including the phase for the high-amplitude fluctuations[21]. Note that the x-axis normally shows the frequency from f=0 Hz to the Nyquist frequency, but was adapted to indicate the period of the fluctuation. Furthermore, the amplitude is shown as a share of the hourly average to allow comparison between different frequency spectra. As aforementioned, an amplitude of 15% entails that the sinusoid fluctuates between -15% and +15% of the average hourly generation.

In terms of intradaily fluctuations, the strongest sinusoid is shown at a period of 24 hours. This is presumably due to electricity demand differences between day and night. The amplitude of the fluctuation varies at 16% of the average demand, and the phase is -60°. Secondly, a fluctuation is shown at P = 12 hours at an amplitude of 6% from the average. The phase of this intradaily fluctuation is 228°. Other than the described peaks, a variety of low-amplitude harmonics are shown, which cause the daily fluctuation to be shaped by a range of sinusoids.

In terms of intraweekly fluctuations, the largest peak is shown at P=168 hours, corresponding exactly to a fluctuation of a full week. The amplitude of the fluctuations deviates at 7% of the average at a phase of 245°. Additionally, a lower-amplitude sinusoid is present at P=84 hours which fluctuates at 4% of the average at a phase of 132°. The presence of these peaks suggests that the electricity demand differs per several days of the week.

Besides a small amount of noise, no significant monthly fluctuations are shown in the frequency spectrum. However, in the slow cycling band a dominant annual fluctuation is present with a period of 8760 hours, which thus reflects the differences in electricity demand per season. The phase of the annual fluctuation is 25° at variation 4% of the average. In conclusion, the variability of demand over time is well described by several sinusoids that fluctuate on a timeframe of a year, a week and intradaily.

[20] Data from January through November

[21] See Appendix VIII

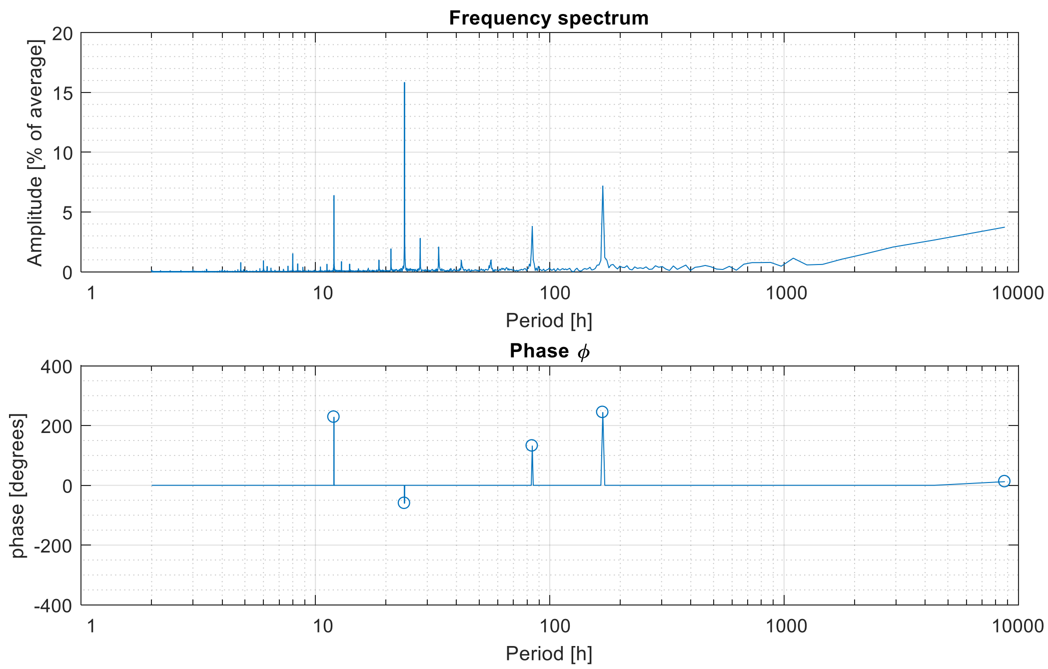

Figure 24: Default demand curve in the frequency spectrum (log)

5.2 Solar PV

The Fourier analysis was then performed over the generation curve of solar PV. Figure 25 again shows the frequency spectrum and the phase for the high-amplitude peaks[22].

It can be recognised that there are three dominant fluctuation components that determine the original waveform. Note that amplitude leakage from the fluctuation at period of 24 hours causes the phase spectrum to suggest multiple sinusoids are present. However, this can be attributed to one single fluctuation with P=24 hours, hence denoting the cycling between day and night. The amplitude of the sinusoid is shown to fluctuate strongly, deviating at over 150% of the average. The phase of the sinusoid is -45°, corresponding to the marked point in the phase spectrum. Furthermore, a second intradaily fluctuation is shown with a period of 12 hours, indicating a sinusoid with a variation of 60% and a phase of -84°.

Only one prominent sinusoid concerns slow cycling, fluctuating at a period of 8760 hours or one full year, with an amplitude of just over 30% of the average and a phase of -169°. It can be presumed that this sinusoid denotes the presence of seasonal fluctuations. Besides the three sinusoids, the frequency spectrum only depicts low-amplitude noise, suggesting that the variability of solar PV is only to a very small extent influenced by other periodical fluctuations. Concludingly, the variability of solar PV can to a large extent be described by three sinusoids, which fluctuate on the timeframe of a year, a day and semi-daily.

[22] See Appendix VIII

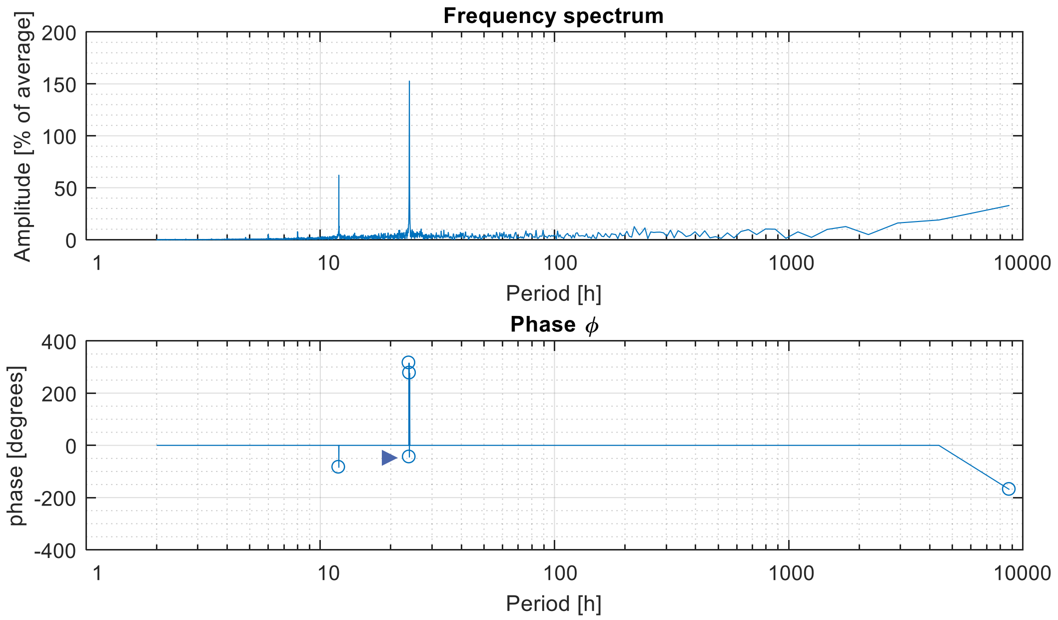

Figure 25: Solar PV in the frequency spectrum (log)

5.3 Wind power

Figure 26 shows the frequency spectrum for onshore wind energy generation. The first notion is the fact that wind power is much less regular than solar PV. Whereas solar PV is well-described by three fluctuating components, wind power shows a large number of sinusoids with similarly high amplitudes that determine the original waveform. This notion obsoletes the thresholding of the phase spectrum for improved legibility[23], since the signal remains noisy regardless of any threshold. As a result, visualising the phase spectrum provides little information in itself. Moreover, individual peaks in the frequency spectrum provide limited information about the actual fluctuations, since they are influenced by a large of number of cycling components. Nevertheless, several strong fluctuations can be identified. The frequency spectrum shows the largest fluctuation at a period of 400 hours with an amplitude of about 27% of the average and a phase of 255°. The second strongest fluctuation occurs at P = 1095 hours, deviating at 23% of the average at a 37° phase. Hence compared to solar PV, the strongest fluctuations in wind energy output occur on a relatively longer timeframe since the highest peaks in the spectrum occur at periods of a week up to a year. An annual fluctuation is also present for onshore wind power, deviating by 20% at a phase of -32°. Concludingly, the variability in onshore wind generation is to a large extent irregular, but the strongest fluctuations occur on longer timeframes of multiple weeks or months.

[23] Appendix VIII

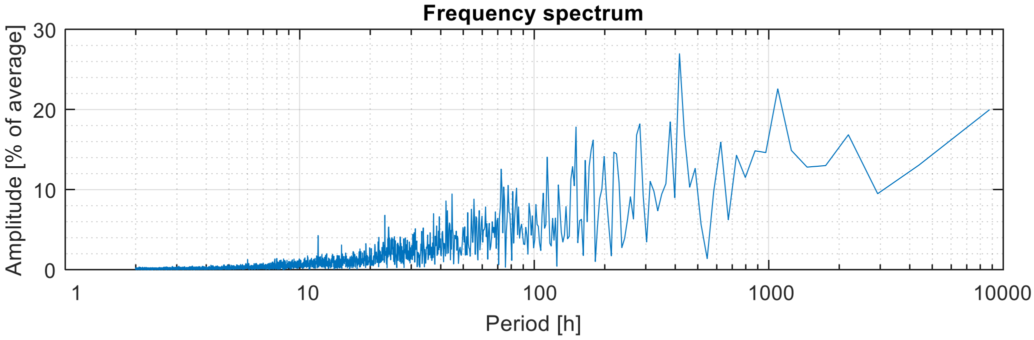

Figure 26: Onshore wind in the frequency spectrum (log)

The frequency spectrum for offshore wind production is similarly noisy as the onshore wind spectrum, as shown in Figure 27. The largest fluctuation is again shown at a period of 400 hours, yet at a lower deviation of 23%. The same trend of slightly lower amplitudes can be recognised for most individual sinusoids in the offshore spectrum as compared to onshore wind. This is shown in Figure 28, which depicts the difference between the onshore and offshore spectrum. Note how most fluctuations are higher for the onshore wind frequency spectrum, especially on longer timeframes. Also on timeframes of 12 and 24 hours, it is suggested that offshore wind is less prone to fluctuations. In conclusion, offshore wind generation fluctuates in a similar fashion as onshore wind but at lower relative amplitudes and to a lesser extent dominated by monthly cycling.

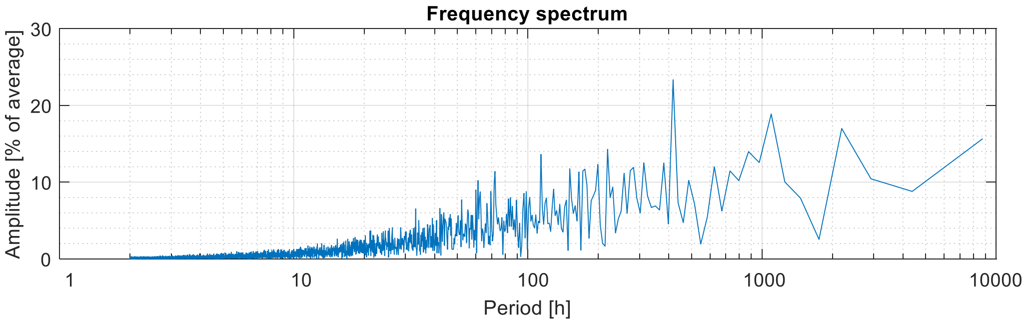

Figure 27: Offshore wind in the frequency spectrum (log)

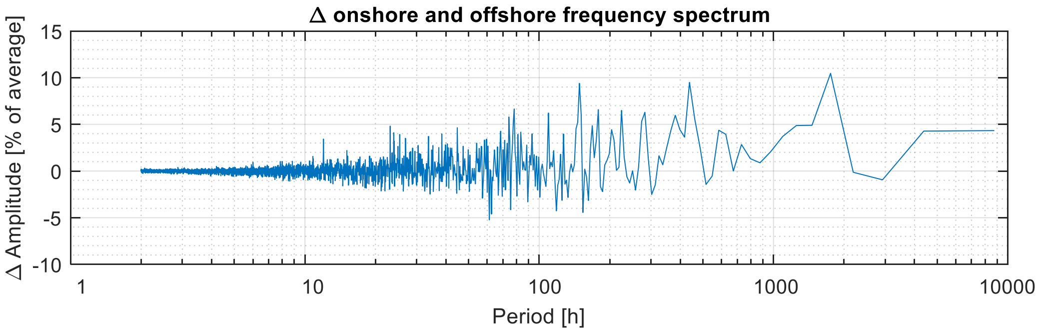

Figure 28: Difference between the frequency spectrum of onshore wind and offshore wind

5.4 Individual temporal components

Using the frequency spectra and the defined frequency bands, the individual temporal components of the signals can be derived. Following the described methodology, the results concern the output of the iFFT for certain frequency ranges, transformed back into the time domain. First of all, Figure 29 shows the amplitude deviation of the slow cycling components. The Fourier diagrams showed that all generation profiles were influenced by a relatively strong annual fluctuation, which is reflected in the figure[24]. The slow cycling component of solar PV deviates up to +30% from the average, whereas onshore and offshore wind deviate by 20% and 15% respectively. The demand curve shows a limited slow cycling component, varying by a maximum of about 4% of the hourly average hourly. The graph furthermore shows a significant phase shift between the slow cycling components of solar PV and the demand curve, being almost fully in anti-phase. Whereas the electricity demand is high from about November through March, solar PV generation reaches its peak during the summer months. On the other hand, both onshore and offshore wind appear to be only at a minimal phase shift compared to the slow cycling of the demand curve. Especially offshore wind fluctuates in almost perfect phase compared to the demand profile. Hence on this timeframe, wind power seems more effective in meeting demand and thus reducing system fluctuations.

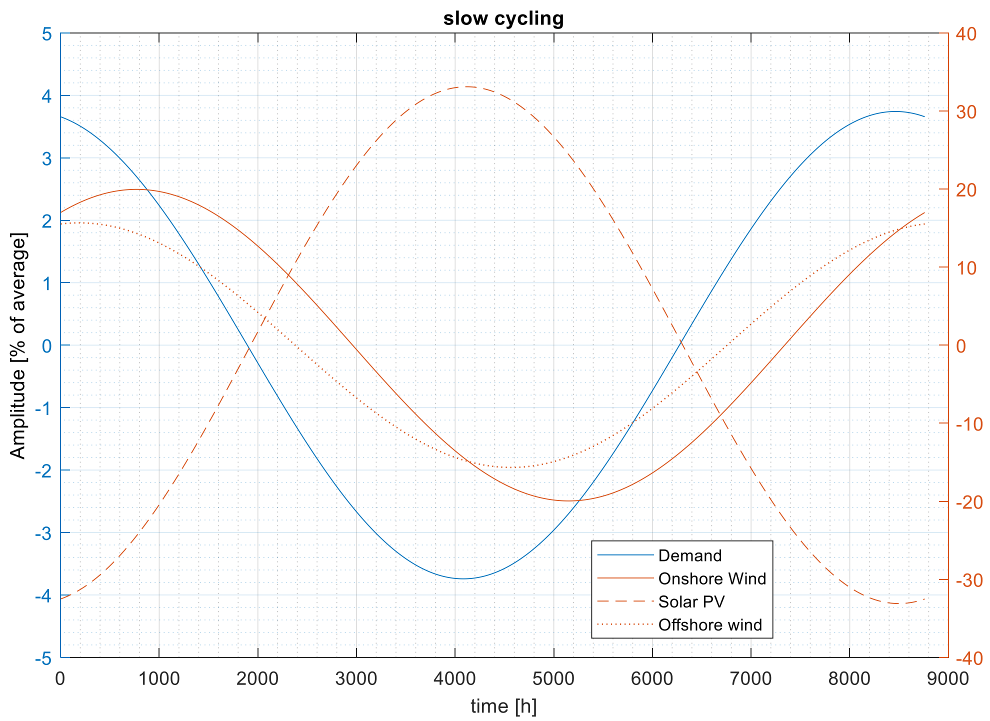

Figure 29: Slow cycling component of demand, solar PV and wind power

Nevertheless, Figure 29 also shows how the variations in wind power on a monthly timeframe occur at much higher relative amplitude (up to 75%) than its slow cycling variations. Similarly, the highest variations of solar PV vary up to a range of 40% of the mean. Hence, this indicates that especially wind power, and solar PV to a lesser extent, is dominated by its monthly fluctuations. So although the slow cycling components of wind and demand are almost in phase, the monthly fluctuations in wind power cause a monthly discrepancy. This can further be illustrated by summing the slow and monthly cycling components [Figure 31]. Since the profile of wind offshore is similar to wind onshore, it has been omitted for legibility of the figure. Note how the highest peaks of the onshore wind production

[24] Note that from here on, the y-axes in graphs are often biaxial

coincide with times of relatively high demand (1) but peaks of up to 70% also occur at moments of low demand (2). Similarly, (3) shows an instance where both solar PV and wind cycling experience a dip, whereas the demand component peaks.

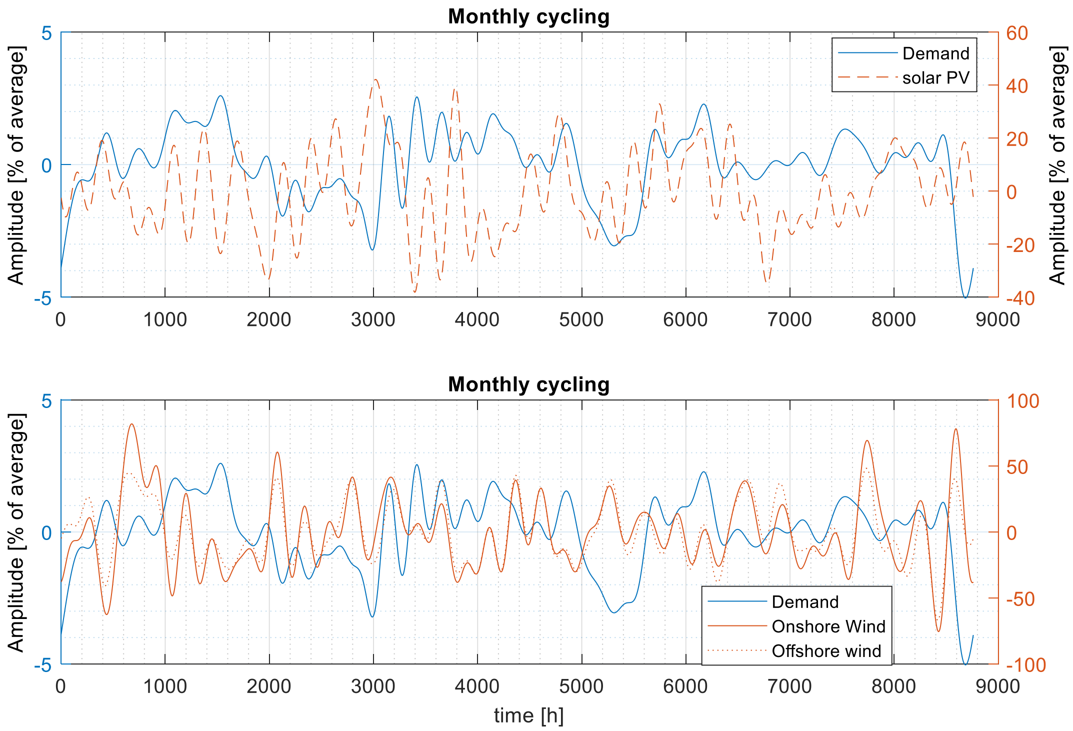

Figure 30: Monthly cycling component of demand, solar PV (top) and wind (bottom)

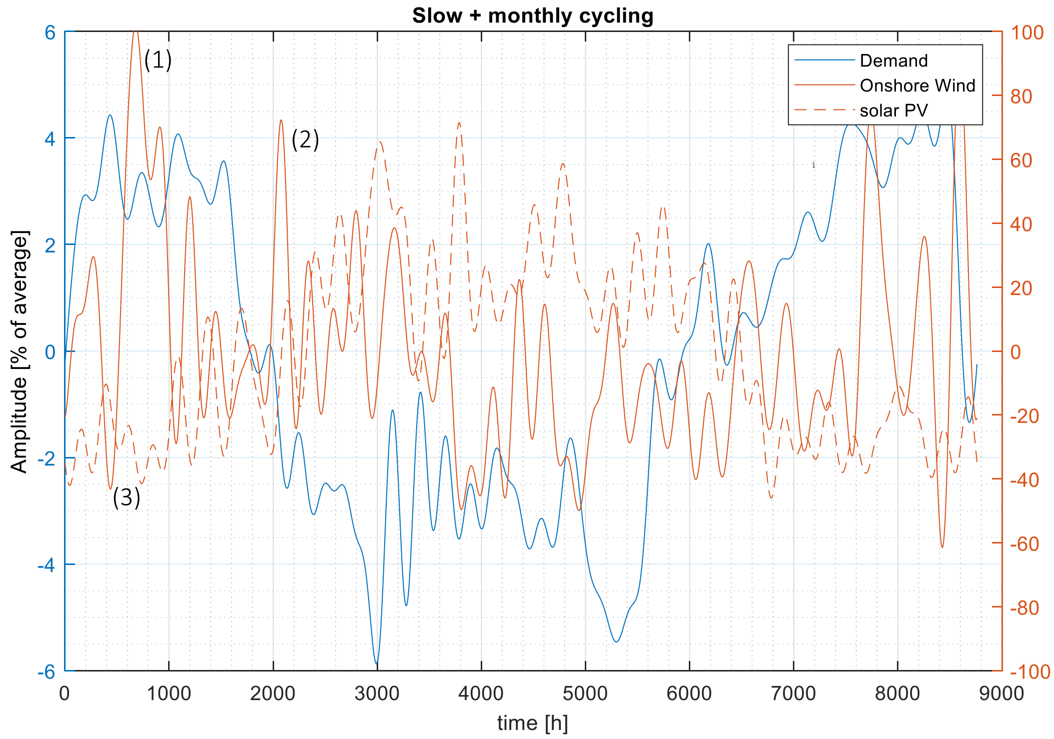

Figure 31: Slow + monthly cycling of demand, solar PV and onshore wind

For the weekly component of the demand profile, it can be recognised that a variation in demand occurs between weekdays and weekend days [Figure 32]. The graph shows the cycling behaviour for 5 weeks, where t=0 is a Friday at 12:00 am. Iteratively, two dips and subsequently five peaks can be recognised, which respectively reflect the weekend and the weekdays. Moreover, this effect appears to be slightly stronger in summer compared to the week in winter. Figure 34 furthermore shows how this fluctuation is reoccurring throughout the year to form 52 weeks. Both solar PV and wind generation show a noisy signal on the weekly timeframe, causing a discrepancy between the residual load both on weekdays and in weekends. Whereas wind shows similarly noisy fluctuations throughout the year, weekly solar PV fluctuations are stronger in summer.

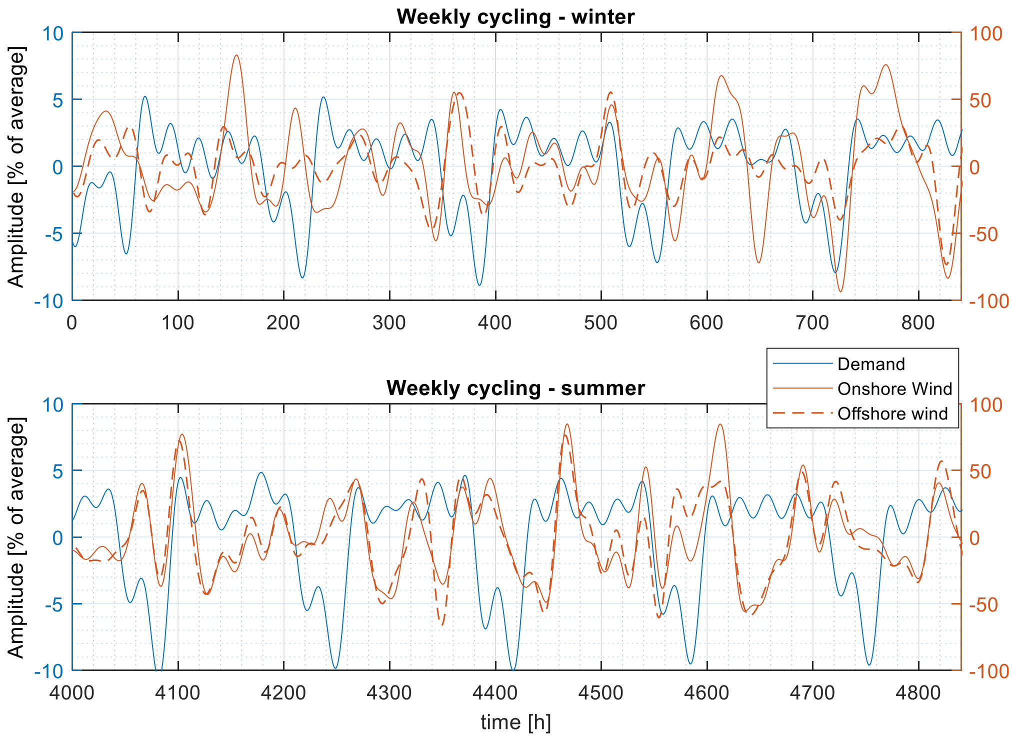

Figure 32: Weekly cycling component of demand and wind

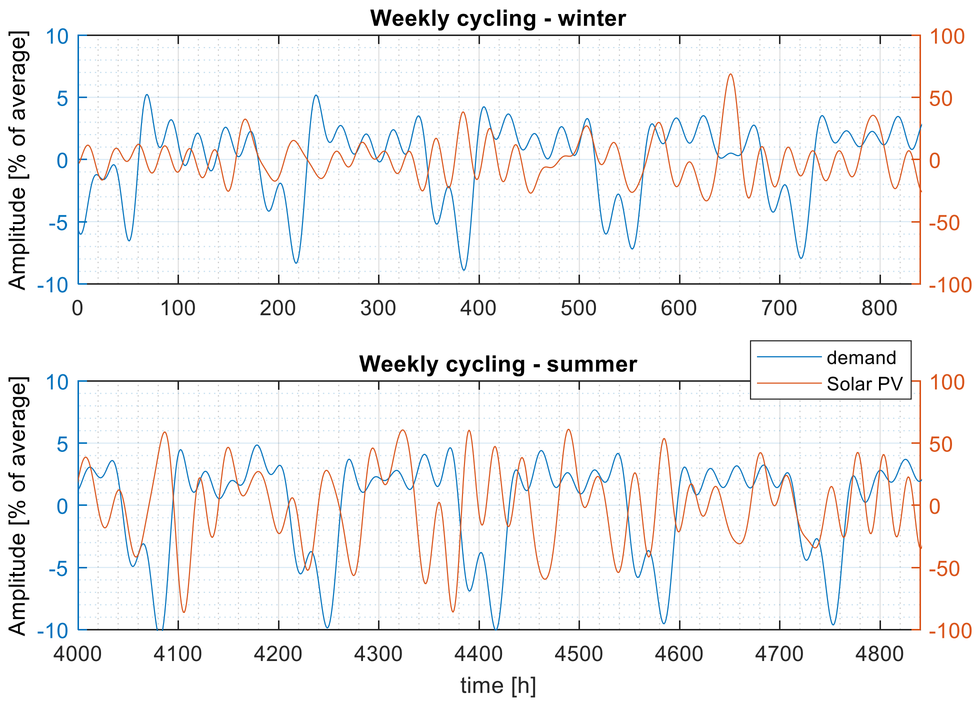

Figure 33: Weekly cycling component of demand and solar PV

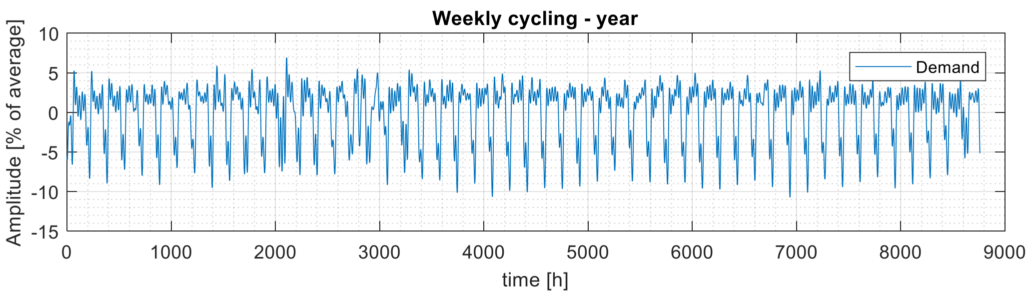

Figure 34: Annual weekly cycling component of demand

Finally, on an intradaily basis the fluctuation components of demand and solar PV are to a large extent in phase, as shown most clearly for a week in summer [Figure 35]. From the frequency spectra, it was deduced that the strongest intraday fluctuations occur at a phase of -60°and -45° for solar PV and demand respectively. Hence, the phase shift of the strongest intradaily fluctuation is only 15° and daily generation levels are to a certain extent complementary with the demand. Nevertheless, daily solar PV fluctuations are much lower in winter as compared to the summer, where fluctuations of nearly 400% of the average occur. Days even occur where the solar PV output fluctuates between -200 to 500% of the average. The figure furthermore shows how the demand strongly fluctuates on an intradaily basis. With variations between approximately -20 and +20% of the average, the demand is to the largest extent influenced by its daily fluctuations. These daily fluctuations are more explicit in winter, being characterised by additional evening peaks in the demand. Finally, wind power is again shown to be noisy throughout the year on a daily timeframe.

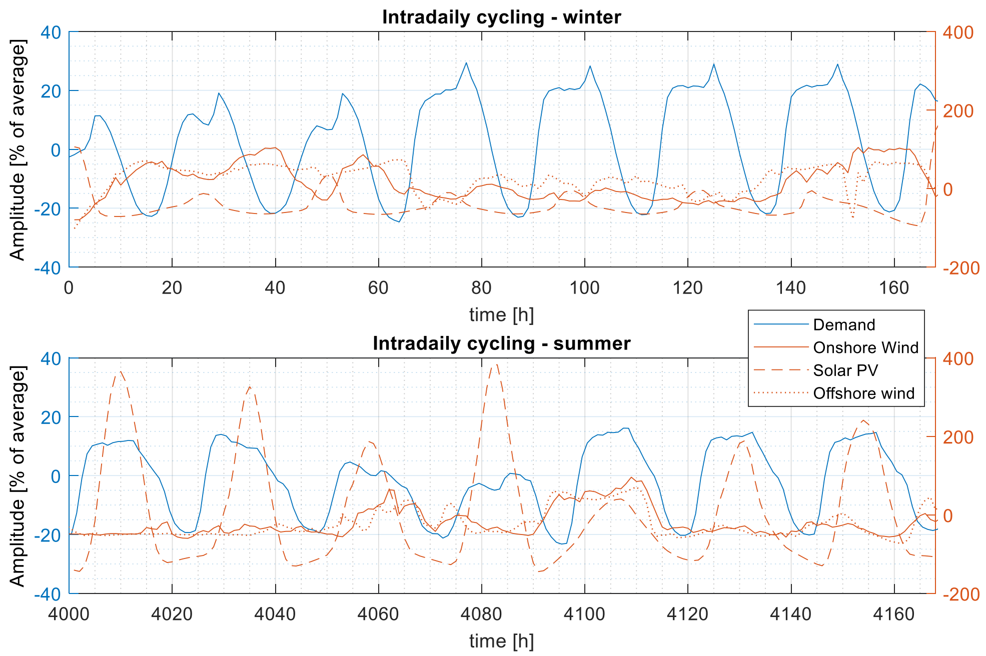

Figure 35: Intradaily cycling component of demand, solar PV and wind power

5.5 Residual load

Besides spectral analyses of individual signals, the frequency spectrum of the residual load can be used to visualise how the mismatch between supply and demand varies over time. The introduction of storage will in turn influence the residual load over time. Hence, any influence that storage has on the power system fluctuations can later be reflected in the frequency spectrum of the residual load. The resulting frequency spectra of the residual load are shown in Figure 36 for the different generation mixes[25] described in Table 5.

Firstly, it can be recognised that increasing the share of solar PV in the generation mix significantly induces a significant peak on both the 12-hour and 24-hour timeframe. At a solar PV share of 75%, the 24-hour fluctuation has an amplitude of approximately 13 GW. Although the frequency spectra of solar PV and demand indicated that the 24-hour fluctuation of solar PV and demand were in phase, the installed capacity of solar PV generates much more energy than demanded. Hence, a share of 75% solar PV causes large negative residual loads at peak hours, especially during summer. This peak is reduced to a mere 3 GW if 25% solar PV is installed. Additionally, increasing the solar PV share causes a higher residual load fluctuation at P=8760, since the slow cycling components of demand and solar PV were shown to be in anti-phase.

On the other hand, increasing the share of wind in the generation mix causes more fluctuating energy to be concentrated on a weekly and monthly cycling timeframe as was expected from the frequency spectra of wind generation. This is characterised in the frequency spectrum especially by a higher amplitude in the range of P=400 hours to P=2000 hours. It further induces a lower seasonal fluctuation, being limited to an amplitude of <1 GW. Since wind power was found to be dominated less by daily cycling components, the 12-hour and 24-hour peaks are also significantly lower at high wind shares.

[25] Note that the y-axis is changed for legibility in the bottom two generation mixes.

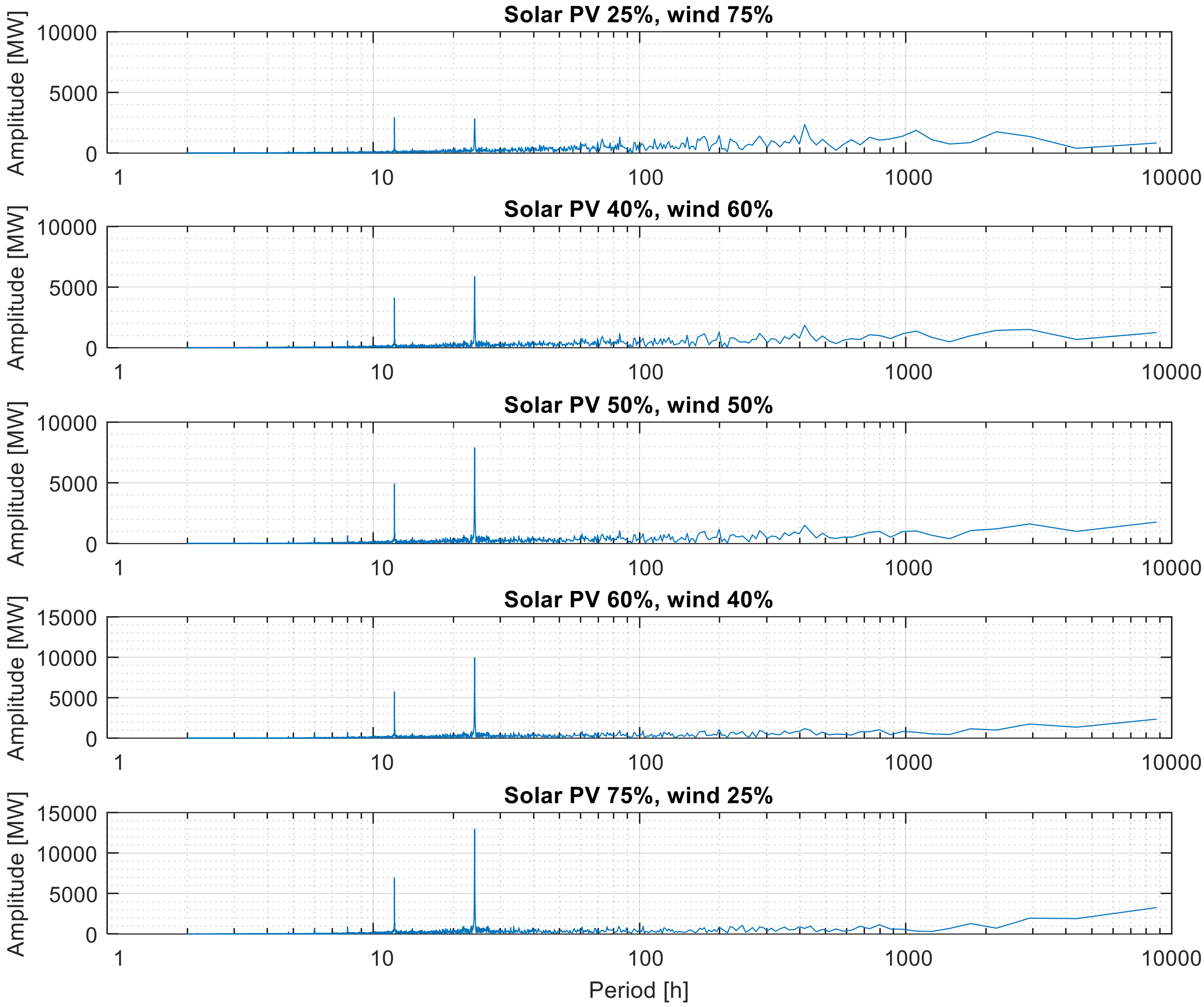

Figure 36: Frequency spectrum of residual load at different solar PV-wind ratios

5.6 Fluctuation volume and power requirements

Using the frequency spectra, the fluctuation volumes can be calculated for the different cycling components. Note again that this calculation disregards the phase ϕ of individual sinusoids. Thus, the figure significantly overestimates the actual storage requirements and should be interpreted as a comparison between different compositions of solar PV and wind rather than storage requirements in absolute numbers. From Figure 37, it can be deduced that the most suitable ratio between solar PV and wind energy seems to be a generation of 25% and 75% respectively if the 6 GW interconnection is assumed to be perfectly responsive. Increasing the share of solar PV adds significant fluctuation volumes on a slow cycling timeframe, whereas increasing the share of wind would result in significantly increased monthly fluctuation volumes. Linking this to climate conditions, this suggests that a higher solar PV share makes the seasonal generation discrepancy increasingly large whereas higher levels of wind occasionally cause wind fronts to induce higher storage requirements.

Figure 38 shows the fluctuation volume for the case that no interconnection is allowed. Besides the fact that naturally the volumes increase on all timeframes, it can be noted that a 40/60 ratio between solar PV and wind becomes slightly more favourable. Since in the real-life situation, interconnection will neither occur all hours of the year nor none at all, the suggestion that arises from these figures is that the optimal share of solar PV in the generation mix lies somewhere between 25-40%.

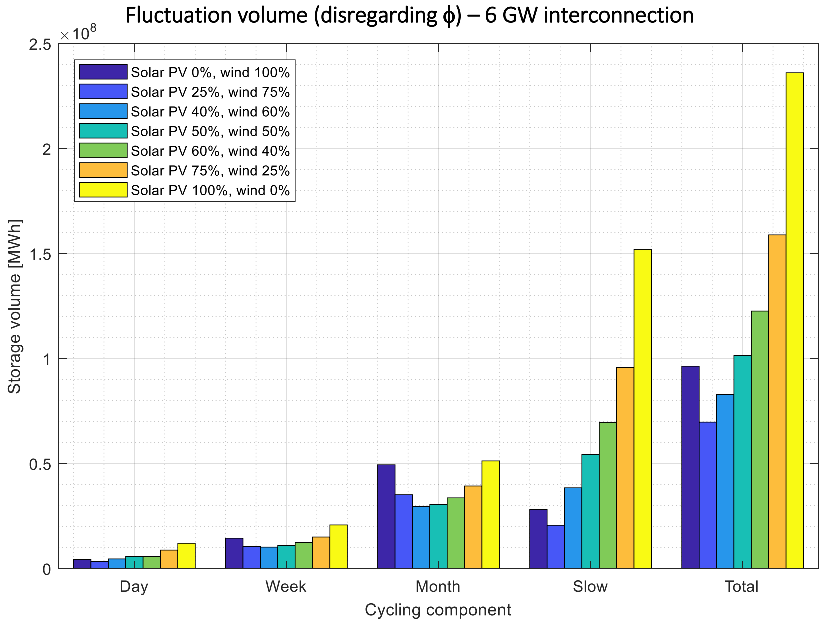

Figure 37: Maximum required storage volumes per cycling component (with interconnection)

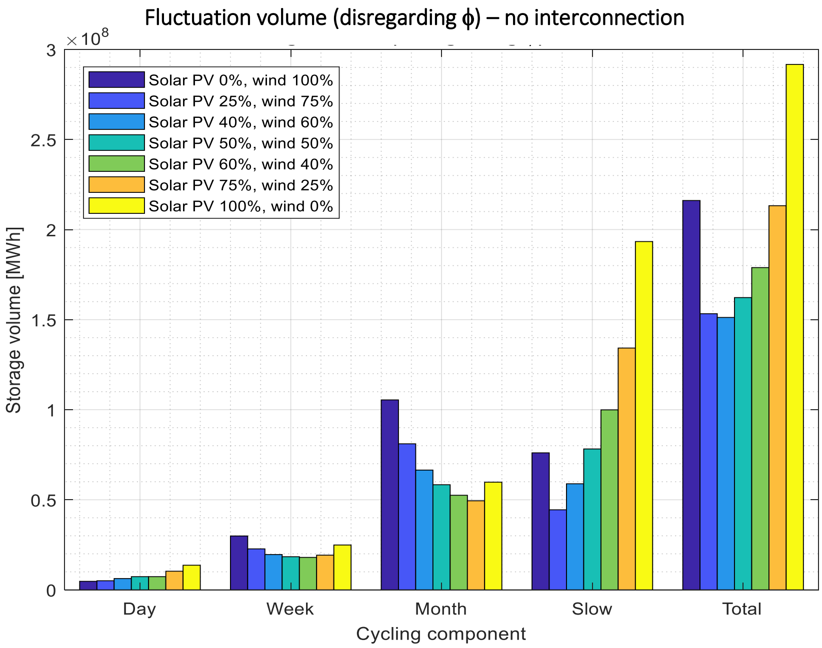

Figure 38: Maximum storage volumes per cycling component (no interconnection)

Apart from the storage capacity, different ratios of solar PV and wind have implications for the required power capacity of both absorbing surpluses as well as supplying deficits. This can be well explained using load duration curves, which indicate how many hours per year the surplus or deficit reaches a certain level. Since the power system requires an equilibrium all hours of the year, even a single occurrence of high surplus or deficit requires ample system flexibility. Figure 39 and Figure 40 respectively show the duration curve for the annual deficit and surplus of electricity, assuming different VRE ratios generate 100% of the annual demand. Additionally, the analysis is repeated for the case that VRE generates 150% of the annual demand, as annexed in appendix XII.

Figure 39 shows how increasing the share of solar PV causes a higher generation deficit to occur during more hours of the year. This means that apprehending a lower share of PV in the generation mix results in fewer hours which require another means of electricity generation. Notably, the largest experienced deficit is almost independent of the generation mix. All four curves have a maximum deficit of just below 18 GW, caused by a single instance when demand is relatively high but both solar PV and wind generation are near zero. As a result, increasing the installed capacity to generate 150% annual demand does not affect the maximum deficit experienced. Hence, a combination of electricity imports, storage medium discharging, interrupting load or flexible generation needs to be able to provide 18 GW of power capacity at least once. Considering that the import capacity is 6 GW, at least 12 GW is required from energy storage capacity, demand-side measures or back-up generation.

Furthermore, the duration curve of the surplus shows that increasing the amount of PV causes a reduction in the number of hours which experience a generation surplus. However, the level of surplus during these hours increases significantly due to the large diurnal peaks of solar PV generation. As a result, the maximum occurring surplus at a PV share of 75% is over 60 GW, whereas it reaches just over 30 GW at a 25% solar PV share. Increasing the installed VRE capacity to generate 150% of the annual demand raises the maximum to 100 GW and 55 GW for the respective generation mixes. This entails that in order deal with the oversupply of electricity, the system requires the ability to store, export or curtail at these power capacities.

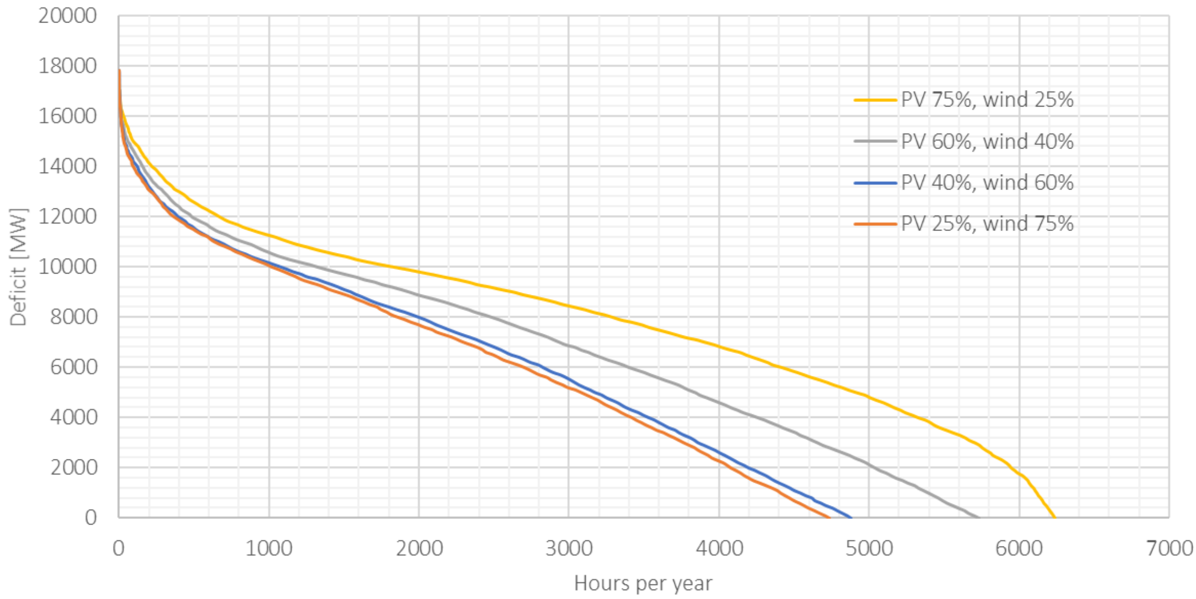

Figure 39: Load duration curve of annual generation deficit at different installed capacities

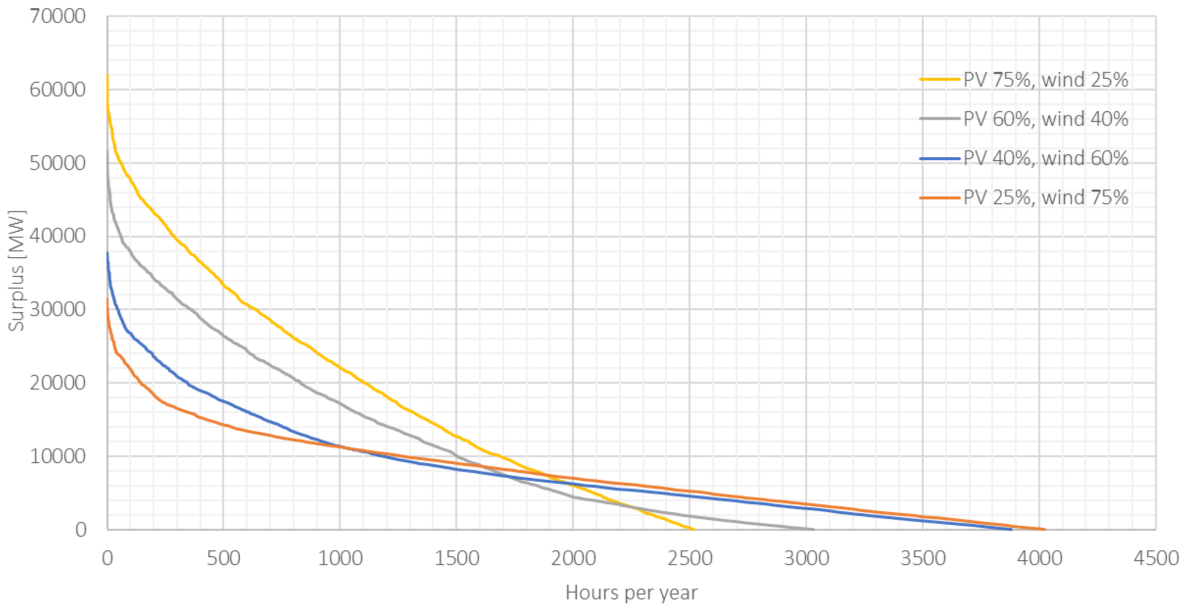

Figure 40: Load duration curve of annual generation surplus at different installed capacities

5.7 Summary

Several concluding notions arise from the spectral analysis of the supply and demand curves. Firstly, in terms of the variability in demand, diurnal fluctuations are the strongest and form a daily usage pattern. The weekly fluctuations suggest lower demand in weekends and the seasonal fluctuation shows how demand is higher in winter. Furthermore, additional evening peak demands occur in winter. For solar PV, the generation is well-described by three sinusoids that fluctuate at period of 12, 24 and 8760 hours, where the diurnal cycling is dominant. On this particular timeframe, fluctuations of up to 700% of the average generation occur, requiring high flexibility to accommodate the ramping. Wind power, on the other hand, especially experiences strong fluctuations on longer-term timeframes, thus requiring both ample power and energy capacity to abate the fluctuations. It was further shown that slow cycling components of wind power are in phase with demand fluctuations, but its noisy generation profile causes a weekly and monthly mismatch between supply and demand. This was also reflected in the frequency spectrum of the residual load, where high wind penetration induced large monthly fluctuations. Finally, it was shown that the fluctuations in offshore wind production are lower than in onshore wind production.

Subsequently, it was noted that the optimal ratio for reducing fluctuation volumes lies somewhere between a 25/75 and 40/60 solar PV-to-wind ratio, depending on the interconnection availability. This ratio appears to align with prior research on solar-wind optimisation, reporting a 26-74% ratio as the optimal configuration for Europe (Zappa & van den Broek, 2017). Additionally, duration curves of the surpluses and deficits showed wind power causes the least intensive power requirements. Increasing the share of solar PV causes a higher generation deficit to occur during more hours of the year as well as higher surpluses. Hence, this provides an indication that the optimal generation mix apprehends a relatively low share of solar PV. Nonetheless, the maximum deficit experienced was independent of the generation mix as it concerned an instance of almost no VRE generation and relatively high demand.

6. Spectral analysis of flexibility measures

Introducing flexibility measures into the system affects the residual load over time. Hence, by subsequently implementing measures, the residual load fluctuations are increasingly reduced. Thus, the effect of each measure can be visualised as a change in the frequency spectrum of the residual load[26]. This section subsequently discusses the frequency spectra of storage technologies and other flexibility measures. It further includes a section regarding the related cost dynamics that are observed when deploying storage technologies. In doing so, a step-wise approach is apprehended in answering the research questions.

6.1 Storage (EES)

6.1.1 Battery energy storage

A first step of increasing flexibility may entail day-and-night storage to reduce the discrepancy that occurs on a daily timeframe. Since batteries are generally considered to provide such short-term storage, one can evaluate the effect of introducing batteries in the model. Figure 41 shows the residual load in the frequency spectrum at a share of 25% solar PV and 75% wind, both with and without battery energy storage. The effect of BES is normalised to the amount of energy supplied over a full year, which allows different storage types to be compared independent of storage size.

It can be seen that the effect of merely installing batteries predominantly affects short term fluctuations, being limited to noisy fluctuation reductions of <50 MW/TWh of delivered energy. Only on a 12-hour cycling timeframe, the reducing effect is stronger at about 150 MW/TWh. Yet, a battery capacity of 1 GW with 5 GWh of storage only induces a total battery discharge of 1.16 TWh annually. Hence, even a large amount of battery storage has a limited potential in reducing fluctuations on any timeframe. The reason that the effect of BES remains so limited is that the dominant share of wind in the generation mix reduces the discharge cycling of the batteries. Since the batteries' energy content is low, increased daily residual loads allows the battery to be discharged and recharged more often, increasing its effectiveness in diurnal fluctuation reduction.

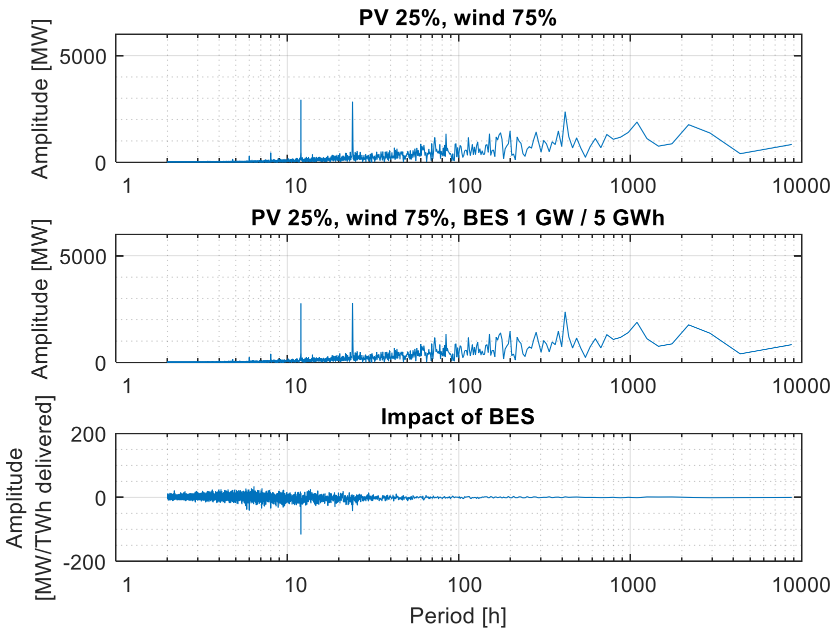

Figure 41: Effect of BES on the residual load frequency spectrum

[26] I.e. the difference between the residual load spectrum with and without a measure

This relation between the discharging behaviour and the generation mix can furthermore be made insightful by running the hourly battery discharge through the spectral analysis. This differs from the figure above in the sense that it does not incorporate reduction of surpluses. Figure 42 shows how increased solar PV generation induces a harmonic discharge pattern with higher amplitudes on a daily timeframe[27]. This indicates that the discharge of the batteries is increasingly dominated by a daily cycle. At higher wind penetration, a limited effect is observed on weekly and monthly timeframes which indicates that the batteries poorly supply the deficits induced on these timeframes. Similarly, it can be recognised that at high PV penetration, BES is poorly able to supply the deficits on a seasonal timeframe.

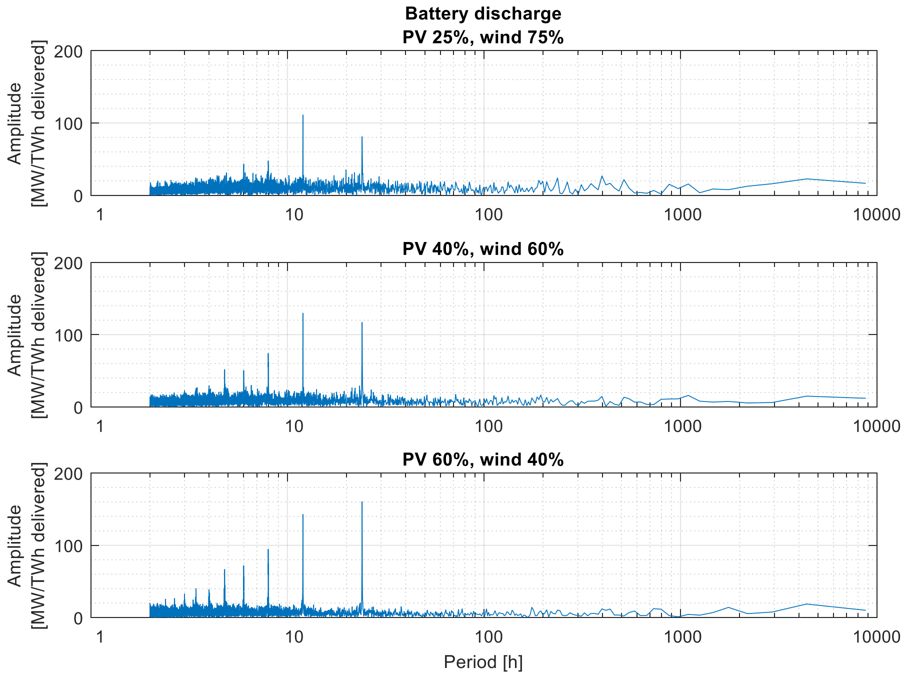

Figure 42: Hourly BES discharge in the frequency spectrum at different generation mixes

6.1.2 Compressed air energy storage

The effect of an AA-CAES installation can be analysed in a similar fashion, where the installed (de)compression capacities and energy capacity can now be varied freely. Assuming all Dutch energy storage capacity is utilised, an analysis can be made to what extent different compression and decompression capacities pose effective power capacity.

Figure 43 shows the number of hours at which a CAES facility is discharged[28] with different compression capacities, at VRE generation of 25% solar PV and 75% wind. First of all, assuming unlimited discharge capacity, the maximum occurring discharge is 17 GW which corresponds to the largest occurring deficit of around 17 GW. Nonetheless, it can be recognised that discharging above a level of 6-8 GW occurs only occurs around 200 hours per year. This suggests that any discharge capacity above this threshold is operated only rarely. Furthermore, the model shows that the effect of CAES is in many instances limited by its storage capacity rather than its power capacity [e.g. Figure 44]. Additionally, it is shown that increasing the compression capacity above 5 GW induces limited additional decompression.

[27] Note that the amplitude of the discharge cycles is normalised to the total annual amount of discharge
[28] Assuming discharge is not limited by turbine capacity.

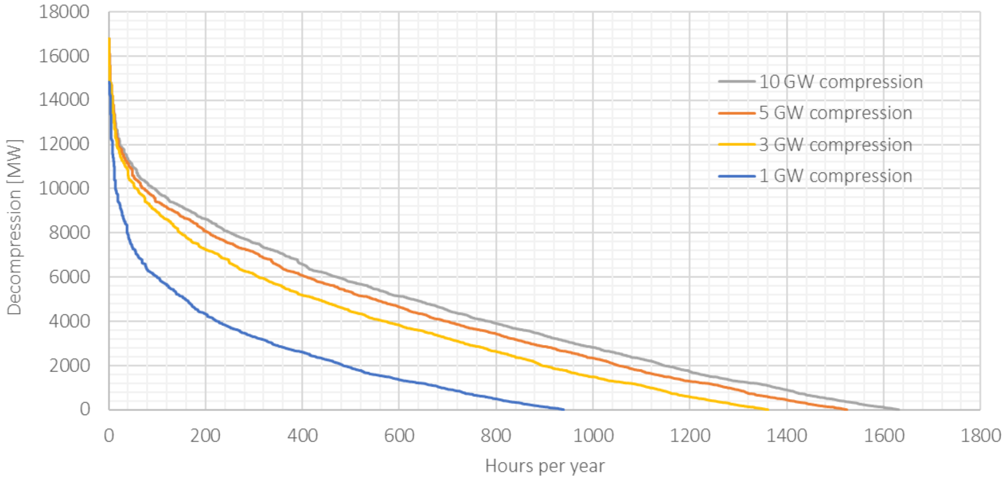

Figure 43: Duration curve of CAES decompression (solar PV 25%, wind 75%)

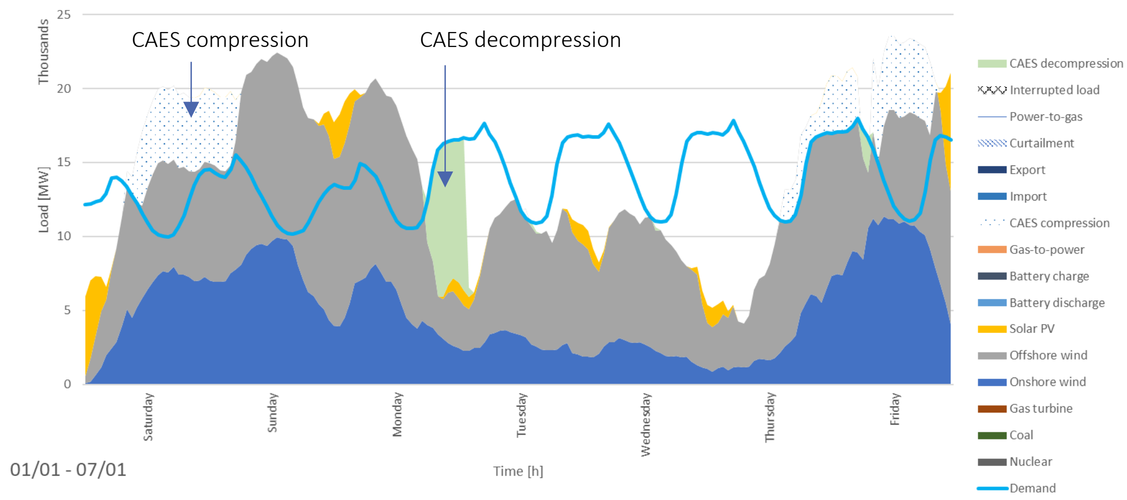

Figure 44: Instance where CAES is limited by storage capacity

The reducing effect of different compression capacities on the residual load was then run through the spectral analysis, as shown in Figure 45. The decompression capacity was set at 8 GW, or a discharge time of about 9 hours. For a compression capacity of 1, 3 and 5 GW, the respective amount of delivered energy was 2.60 TWh, 5.29 TWh and 6.36 TWh. Yet as shown in Figure 45, the reducing effect per delivered unit of energy remains almost constant at the assumed capacities. From the spectrum, it can be deduced that a CAES capacity predominantly reduces the fluctuations on a 12- and 24-hour timeframe. The achieved reduction lies around 150 MW/TWh of annually delivered energy. Furthermore, some level of fluctuation reduction occurs on a weekly timeframe, but these remain limited to amplitude of <50 MW/TWh. Nonetheless, due to the larger energy capacity, CAES seems more capable of storing larger sections of the weekly fluctuations induced by wind power than BES.

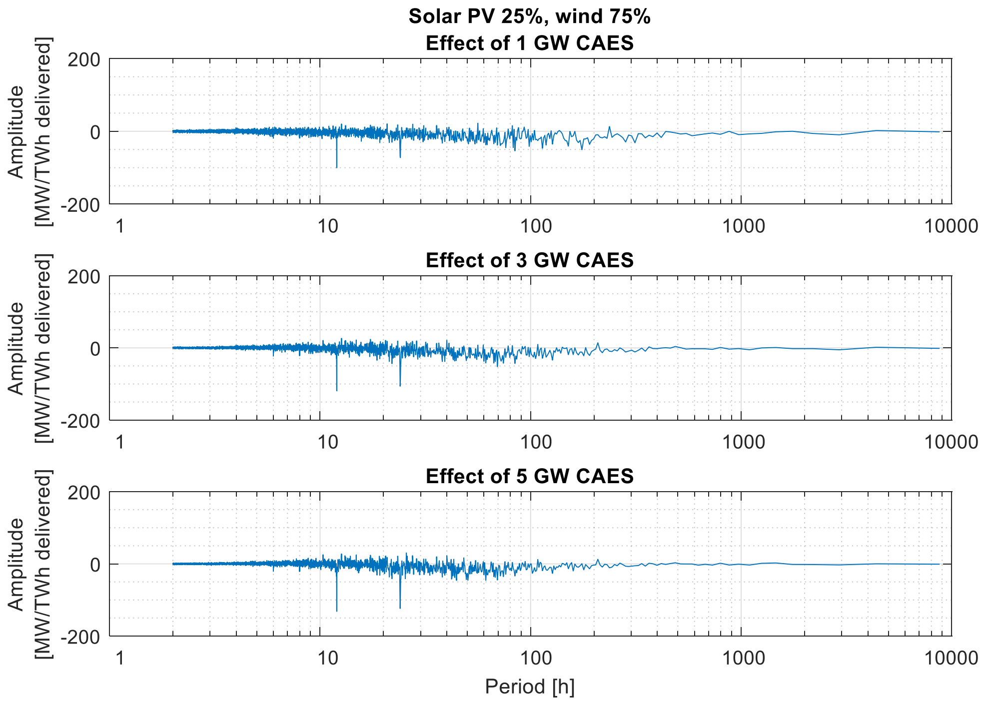

Figure 45: Difference frequency spectrum of CAES (discharge time = 9 h)

6.1.3 Power-to-gas storage

Thirdly, P2G storage can be deployed, where contrarily to CAES, the storage capacity for P2G is in practice inexhaustible due to the 556 TWh of available caverns. As a result, the P2G capacity can be theoretically increased to such an extent that all annual electricity surpluses are converted into gas without being constrained by the storage capacity. Figure 47 shows how different P2G and G2P capacities influence the total gas storage requirements for P2G storage [see also Appendix XIII]. In case of 25% solar PV generation and assuming a non-constraining turbine capacity, the duration curve of the gas-to-power discharge is shown in Figure 46. Up to an installed capacity of 20 GW, increasing the capacity induces additional gas-to-power conversion. Above this threshold, the number of hours which require >20 GW of charging power are too rare to induce significant additional gas-to-power discharge. Additionally, a discharge capacity of around 6-8 GW only operated a limited number of hours annually.

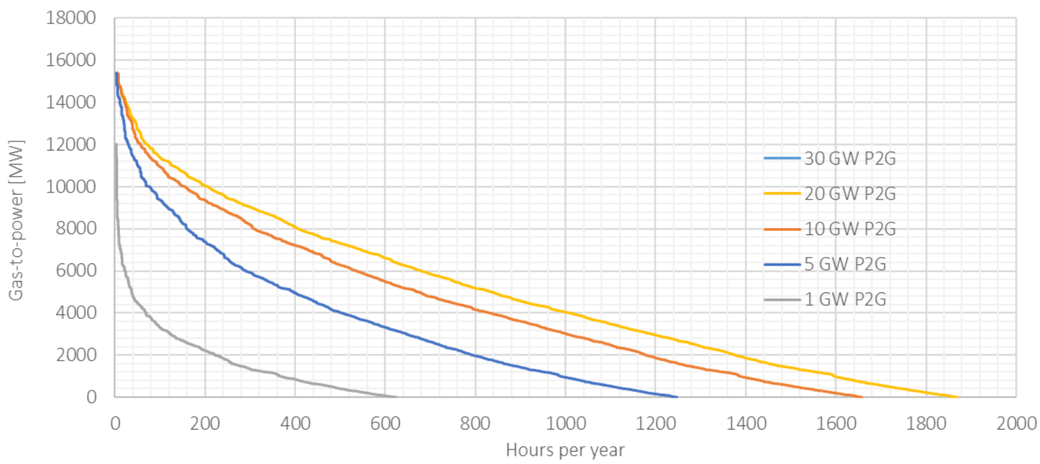

Figure 46: Duration curve of G2P at different P2G capacities and 25% PV and 75% wind

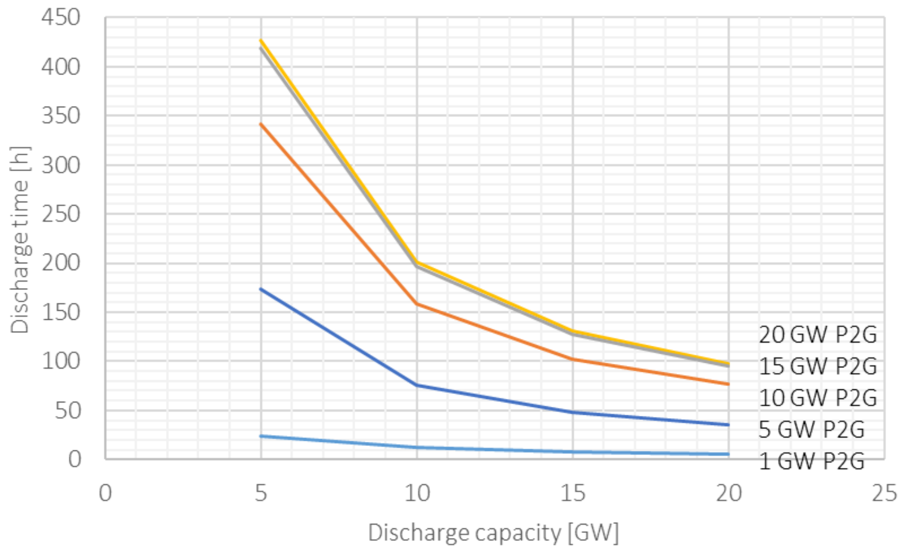

Figure 47: P2G storage requirement at different capacities (in discharge time)

Figure 48 shows the fluctuation reduction induced by different installed capacities power-to-gas. It is assumed that P2G occurs in a P2P form, where all H_2 is used for electricity generation. The figure shows how the P2G storage has a strongly reducing effect on long cycling timeframes. Hence, P2G is shown to be able to reduce fluctuations on these timeframes to a larger extent than both BES or CAES. This is primarily due to the notion that the storage volume of P2G is not a constraining factor and large surpluses can be stored on all timeframes. Furthermore, a significant reduction is also present on a 12- and 24-hour timeframe.

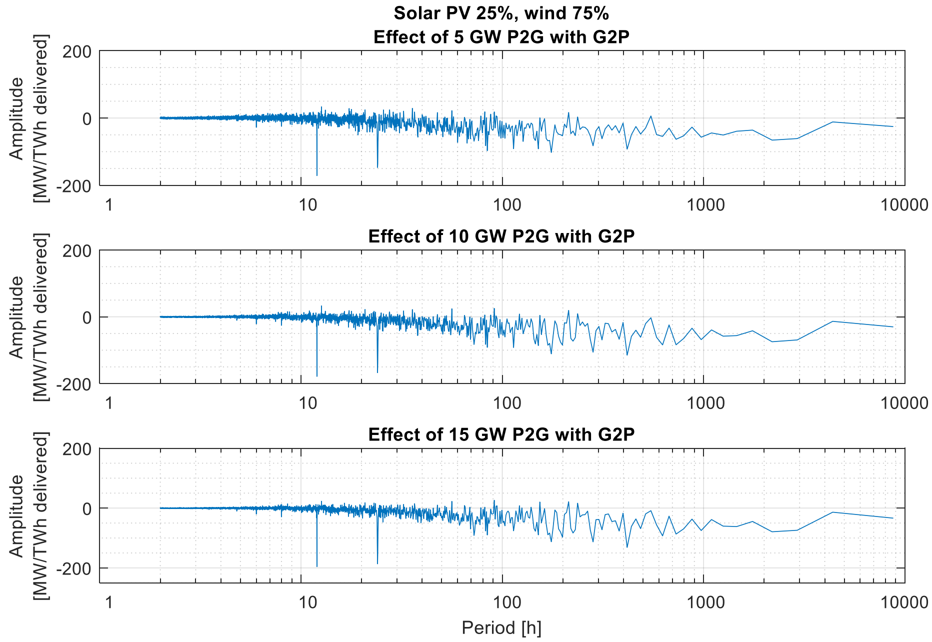

Figure 48: Difference frequency spectrum of P2G with G2P

Nonetheless, due to the low cycle-efficiency of P2G with P2P properties, the reducing effect is mainly attributable to surplus reduction rather than the supplying of deficits. Figure 49 shows the effect of gas-to-power isolated in the frequency spectrum, which thus denotes to what extent P2G supplies electricity deficits. It can be recognised that the peaks are significantly lower than the negative peaks in Figure 48, especially on a diurnal timeframe. Still, the figure shows that P2G is quite well able to reduce deficits on monthly and seasonal timeframes.

It is acknowledged that alternatively, the H_2 may well be sold to another market rather than being used to generate electricity. The frequency spectrum of the generation of H_2 is the same shape as the gas-to-power fluctuation, only with larger amplitudes because of the efficiency losses included in H_2 combustion.

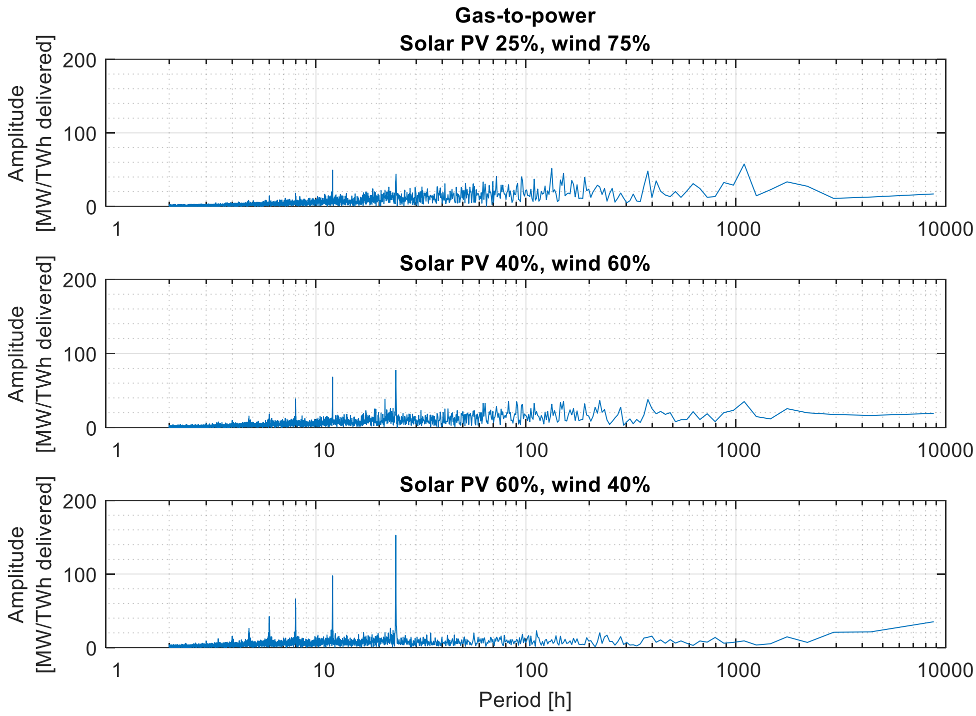

Figure 49: Gas-to-power in the frequency spectrum

6.2 Comparison between storage types

Comparing the effect of each storage type in the frequency spectrum[29], it can be clearly identified how they apply to energy shifting over different timeframes. Figure 50 compares the different storage types per unit of delivered energy, which shows a distinction between short term effects of BES, medium term effects of CAES and the longer-term effects of P2G storage. If looking at the effect per unit of delivered energy, it is concluded that P2G reduces the fluctuations on all timeframes most effectively. This is the result of P2G not being limited by its storage capacity, thus having the capacity to capture all surpluses.

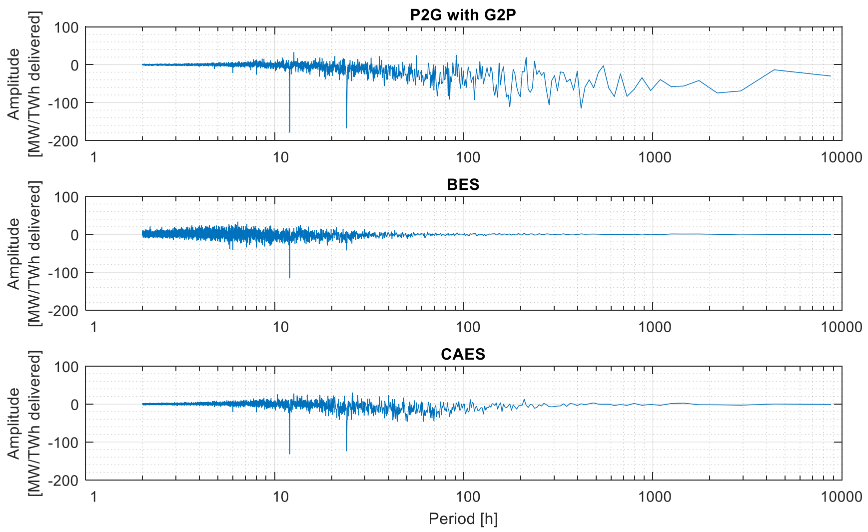

Figure 50: Fluctuation reduction potential per energy output (PV 25%, wind 75%)

A notable difference between the spectra is furthermore that the <12-hour reducing noise experienced in BES is not reflected in the frequency spectrum of P2G or CAES. The argued reason for this is a dynamic between the small storage section of BES and high surpluses induced by solar PV. Figure 51 shows how 1 GW of BES causes a 'dent' in the surplus of solar PV, shifting the residual load by several hours but not affecting the maximum surplus. On the other hand, 1 GW of CAES is shown to affect the full diurnal fluctuation of solar PV, thus rather affecting the 12- or 24-hour cycling timeframe.

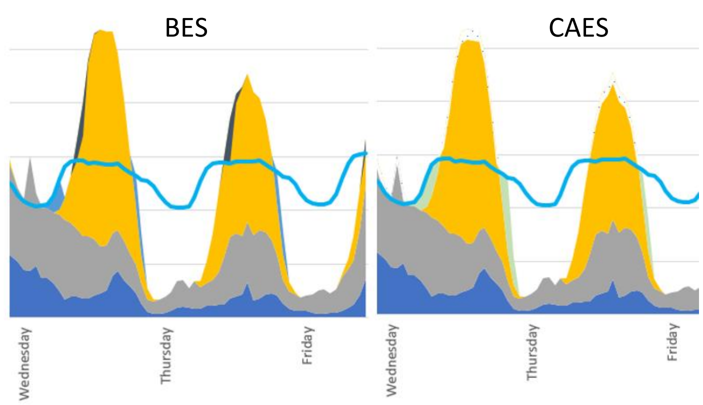

Figure 51: Effect of 1 GW charging capacity for a day in summer

[29] The frequency spectra show only minor changes with installed capacity, since the scale is normalised to energy output. Nonetheless, this case specifically concerns 1 GW BES, 5 GW CAES and 10 GW P2G.

In a similar fashion, the effect of storage can be identified per unit of installed capacity. Although the shape of the reducing effect stays the same, this influences the relative effect of different storage technogies. Figure 52 shows that per GW, BES and CAES pose a similar reduciton potential on a 12-hour timeframe. The effect of P2G is lower per installed GW, which is the result of the low full-cycle efficiency induced by the inclusion of G2P combustion.

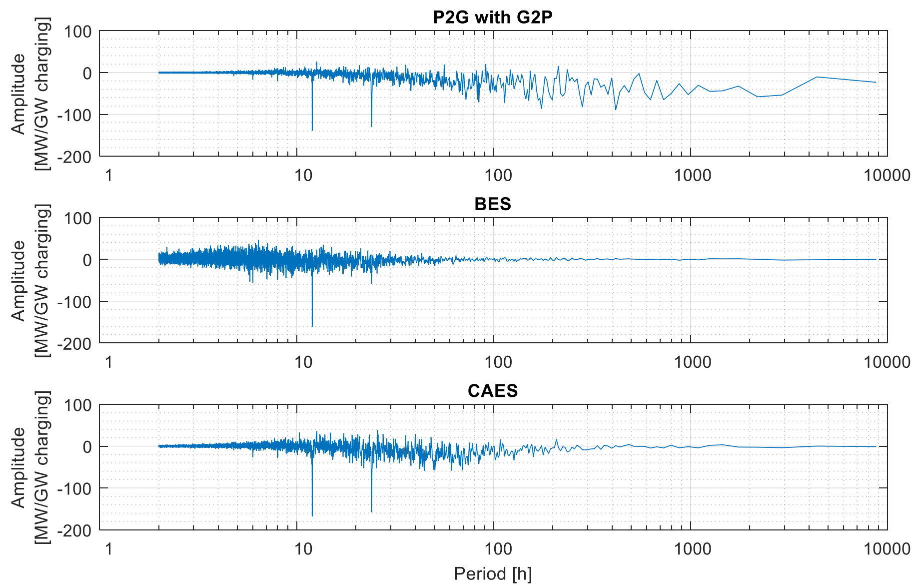

Figure 52: Fluctuation reduction potential per installed charging capacity (PV 25%, wind 75%)

6.3 Other flexibility measures

Besides the effect of individual storage measures, the spectral analysis can be used to identify to what extent residual load fluctuations can be reduced if storage technologies are combined with other flexibility measures. In other words, the frequency spectra can be used to make insightful to what extent the supply-demand balance can be achieved using flexibility measures. This allows a step-wise approach to identifying VRE integration potential. This section sets forth initial steps in such spectral analysis, which can be used as grounds for more elaborate analyses.

6.3.1 Interconnection and curtailment

After the storage technologies have been implemented, remaining options include exporting or curtailing surplus and importing energy to reduce deficits. Figure 53 shows the amount of import, export and curtailment for different storage combinations[30] and Appendix XI repeats this for other VRE generation mixes.

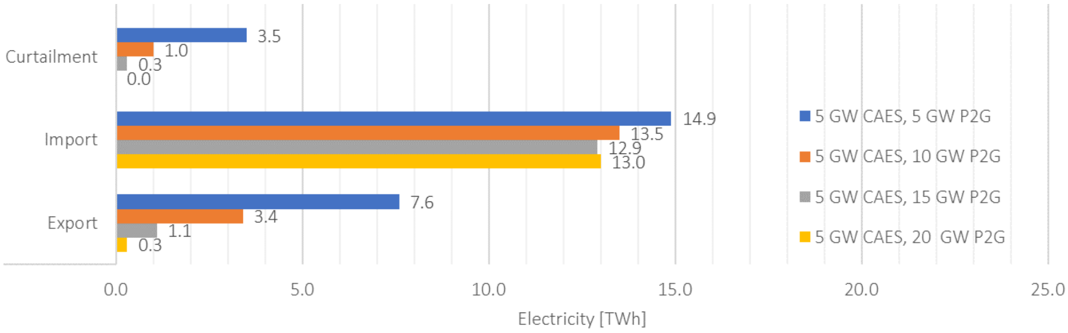

Figure 53: Curtailment and interconnection at 25% PV and 75% wind

Figure 54 then depicts the remaining frequency spectrum of the residual load after the implementation of EES in combination with curtailment and interconnection, both with and without G2P. Note that since curtailment of surpluses is allowed, any remaining residual load merely indicates electricity deficits. The top figure indicates that the residual load fluctuation is now dominated by a 12-hour fluctuation as well as strong influences on monthly and seasonal timeframes. Although the short-term fluctuations that were dominant in the original frequency spectrum are to a large extent reduced, there is still a strong diurnal deficit is present. This may suggest additional value can be posed by demand-side options, for reducing supply-demand discrepancies on a daily timeframe. Additionally, the longer-term fluctuations are to a lesser extent reduced by the storage technologies, thus indicating that this cycling component is less easily reduced. Moreover, as was shown earlier, the inclusion of G2P shows a relatively limited effect on the frequency spectrum.

[30] Note this analysis excluded battery storage whereas it is included in the frequency spectrum of Figure 54.

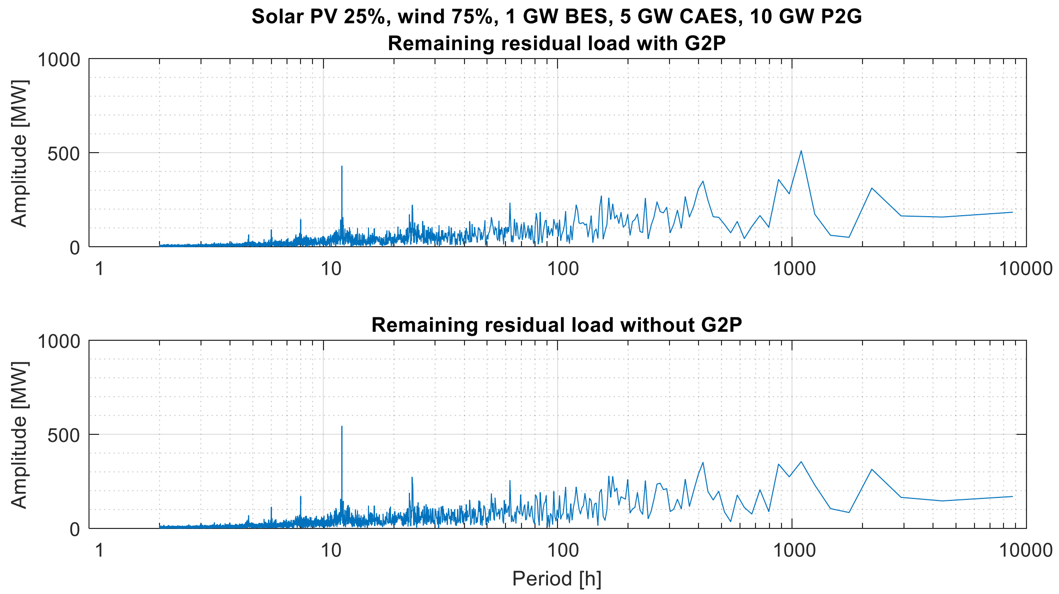

Figure 54: Remaining frequency spectrum with EES, curtailment and interconnection

6.3.2 Demand-side management

Although modelled in a simplified fashion, the power model can be used to give indications of the additional effect of DSM in reducing the remaining residual load. Figure 55 shows the spectrum again for the case that 5% of the load follows VRE generation (assuming no G2P). Comparing it to the case without any DSM measures, it can be identified that some fluctuation reduction occurs on a 12-hour timeframe[31]. This provides first indications of diurnal supply-matching capabilities of DSM.

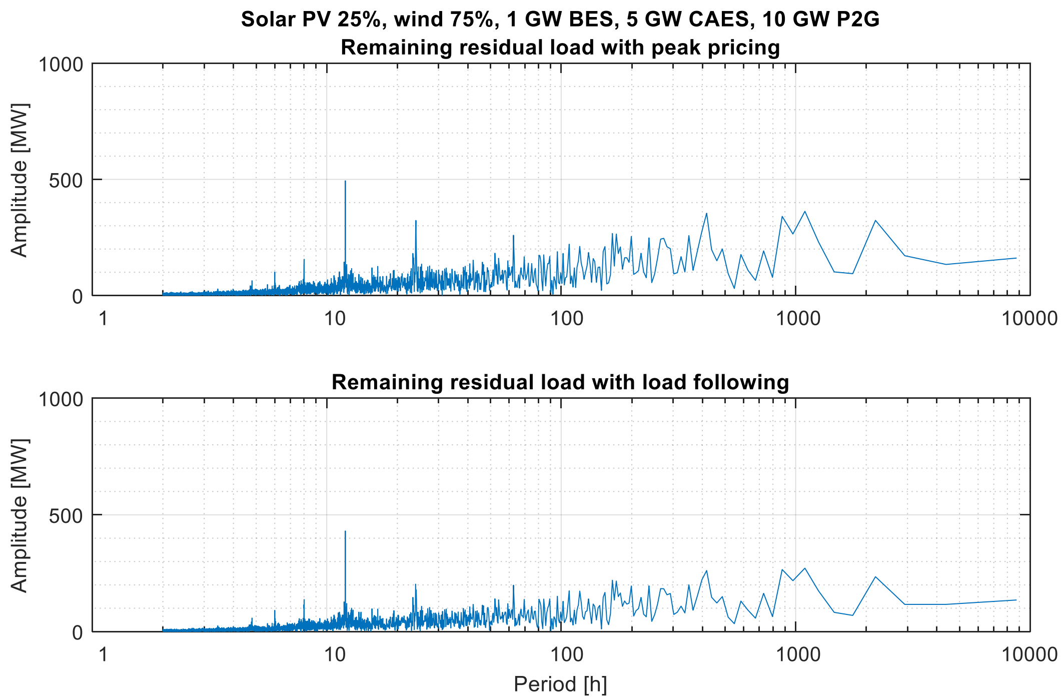

Figure 55: Remaining frequency spectrum with 5% peak pricing and load following

[31] This could alternatively be made more insightful using a difference spectrum as applied to the different storage technologies.

6.3.3 Overgeneration

Figure 56 repeats the spectral analysis for the case that VRE generates 150% of the annual demand at the same ratio of 25% solar PV and 75% wind. Overgeneration could make up for the storage-induced energy losses. The figure shows that overgeneration has a significant potential to reduce the annual fluctuations even further, especially if G2P is deployed. Even without G2P electricity generation, the fluctuations on a diurnal timescale are reduced significantly. Although the increased generation causes significantly larger surpluses, curtailment allows these surpluses to be neutralised. Notably, the remaining residual load is mostly dominated by the monthly fluctuations as well a strong seasonal fluctuation. Nonetheless, the highest deficit that is experienced in this case is still 10.1 GW, even assuming G2P is possible. This indicates that even at 150% overgeneration, instances occur when storage caverns are depleted too much to supply the required level of electricity.

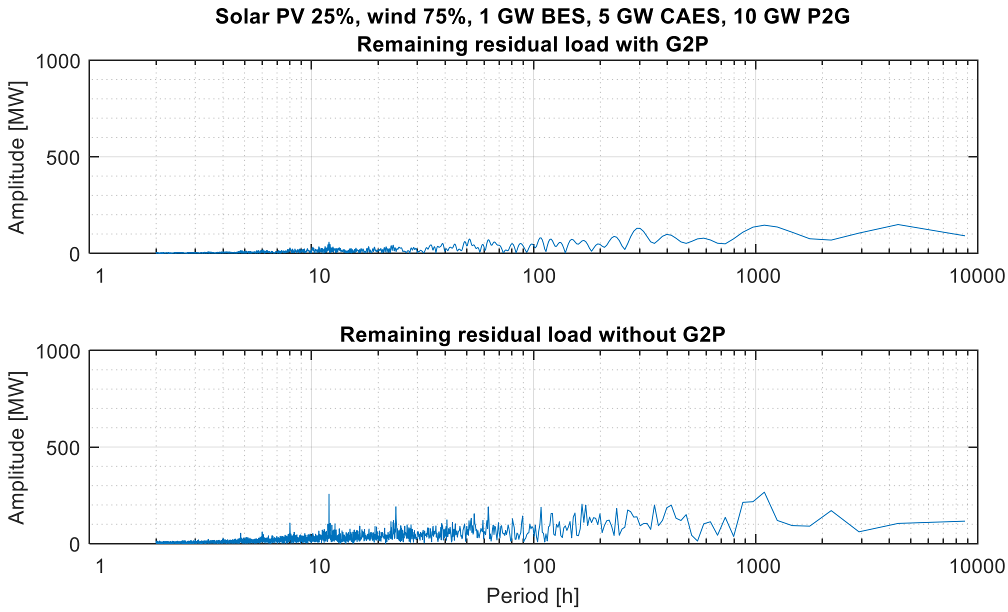

Figure 56: Remaining frequency spectrum with EES, curtailment and interconnection at VRE overgeneration

6.4 Cost dynamics

Besides the spectral analyses, the analysis induces practical limits in terms of economical operation of storage technologies. This gives an additional explanation to the limits of storage deployment and VRE integration.

First of all, the positive effect of increased discharge cycling of batteries is reflected in the LCOS of BES. The LCOS is shown for different VRE configurations in Figure 57, resulting from RESPECT model runs. A first notion is that the LCOS increases with additionally installed battery capacity. This is the result of the fact that for each battery installed, some of the surpluses have already been stored and less storable energy is available. Hence, the amount of full load hours decreases for each battery installed causing a reduced business case. Secondly, the price of batteries becomes increasingly cheaper with an increased solar PV share in the generation mix. As shown in the duration curves, a higher solar PV share induces more hours of deficit, which allows increased discharge cycling of the storage technologies.

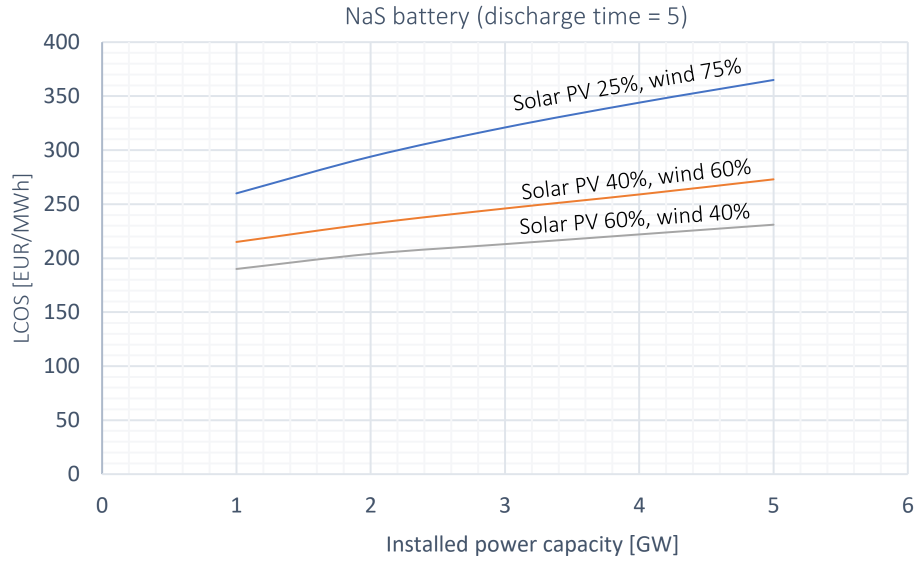

Figure 57: NaS battery cost per generation mix and installed capacity

This dynamic can be further represented by plotting the LCOS against the level of annual operation Figure 58 & Appendix XV]. The LCOS is clearly shown to decrease with increased operational hours of the batteries[32]. Additionally, the LCOS of BES is strongly dependent on the apprehended E2P ratio since this determines the cost of the storage section. Theoretically, the LCOS is lowest if a small storage section is apprehended and increases with larger storage sections. Although the E2P ratio of a single battery is to a large extent fixed, literature reports batteries with E2P ratios between 1-10. As shown in Figure 58, a discharge time of 5 hours with the maximum level of operation leads to an LCOS of approximately 70 €/MWh. With a discharge time of 1 hour, this price is already reached at around 1800 annual discharge hours.

The notion that arises from the figure is that CAES is a cheaper option, even if high E2P values are assumed for the CAES storage. If the default BES E2P value of 5 hours is assumed, a CAES storage cavern with a discharge time of 50 hours would still pose a cheaper storage option. Alternatively, if a low E2P ratio of 1 h is assumed for BES, a CAES storage cavern with an E2P of <9 hours would be a cheaper storage option. Together with the fact that CAES has a much larger storage volume (up to 69

[32] Maximum discharge operation indicates 4380 hours of the year, assuming that the other 4380 hours are required for charging.

GWh in salt caverns) and thus allows the time-shifting of large energy volumes, it is suggested that batteries are not the most effective storage option for flexibility on a >1-hour timeframe. This naturally does not entail BES may have valuable application in grid stability operation, such as frequency regulation or voltage control.

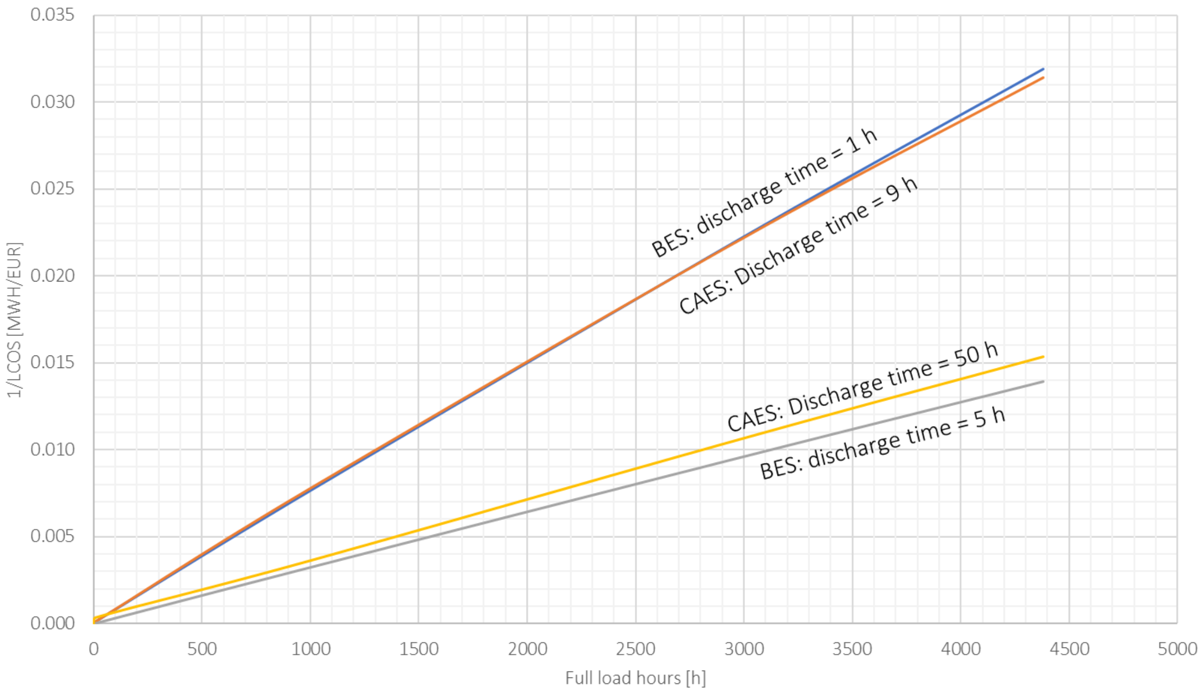

Figure 58: Comparison of LCOS for BES and CAES at different discharge times

At the same time, the electricity delivered by P2G storage is relatively even more expensive. Figure 59 shows how CAES remains a cheaper option even if a large E2P ratio of 30 is apprehended. Since the LCOS of P2G is minimally dependent on the E2P ratio [Appendix XV], this entails that CAES is almost all cases cheaper in operation. The high LCOS of P2G with G2P is mainly the result of high capital investment costs per installed power capacity. The cost analysis suggests that using P2G in a P2P cycle may not be economically attractive and other uses of the renewable H_2 may be rather explored first. Nonetheless, the assumed costs include the costs of a combustion turbine. Since the hydrogen may well be used in existing combustion turbines, the costs may be in lower ranges.

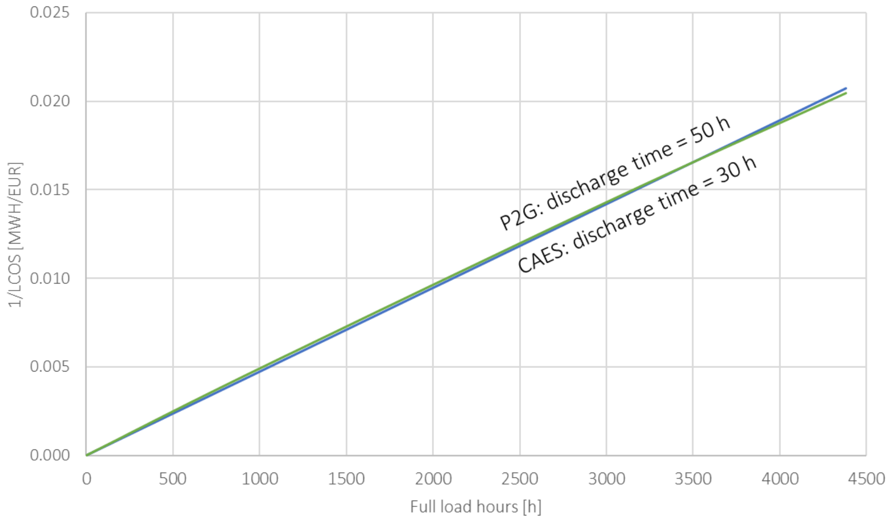

Figure 59: Discharge times at which the LCOS for CAES and P2G is equal

6.5 Summary

In conclusion, it was shown that the effect of different flexibility measures can be reflected in the frequency spectrum. There appeared to be a clear distinction between the timeframes on which different storage technologies acted. BES mainly reduces the 12-hour cycling component but also noisily affects <12-hour fluctuations. Additionally, BES effectiveness increases with increased solar PV penetration due to more periodical discharging, a dynamic that is furthermore reflected in a reduced LCOS. For CAES, indications were provided that 5 GW charging and 6-8 GW discharging are effective capacities. Furthermore, the frequency spectra indicated a reducing effect on a predominantly diurnal timeframe. Yet, a reducing effect was also visible on timeframes of multiple days up to a week. CAES is furthermore a cheaper option, even if a very large storage section would be assumed. Finally, P2G shows a reducing effect on all timeframes, which is primarily attributable to reducing surpluses. If only the G2P effect is isolated, the effect remains present on monthly and seasonal timeframes. Due to it slow efficiency, however, the reducing effect per unit of installed capacity is relatively low. In terms of costs, the LCOS of P2G is much higher than CAES at common E2P ratios, suggesting that the inclusion of G2P may not be economically attractive.

Further results showed that after introduction of storage, interconnection and curtailment, the residual load fluctuation is especially dominated by a 12-hour fluctuation and monthly fluctuations. These fluctuations can be reduced significantly by overgeneration of VRE, especially if G2P is deployed. Hence, it is shown how the spectral analysis can be used to iteratively determine which fluctuations drive the residual load. Finally, the effect of the modelled DSM measures is shown to be noticeable in the frequency spectrum, but requires more elaborate modelling to represent them more accurately.

In terms of costs, the relation between different storage components and the level of operation was derived. This provides substantiation for the fact that the costs of storage technologies are harmed by reduced discharge levels. Additionally, it showed that at common E2P ratios, CAES is in almost all instances the cheapest option per delivered unit of energy. Only if batteries are operated with a small storage section, the LCOS of battery storage becomes similarly low.

7. Discussion

The following section discusses the methodology and the research results. First, several methodological limitations are discussed, followed by the interpretation and implications of the main findings. In the subsequent sections, the research questions are answered, practical recommendations are given for applying the results and suggestions are made for further research.

First of all, the power system model is naturally a simplified representation of the real-life situation and should thus be interpreted as such. As a result, the model results are not eligible to make claims regarding actual power system operation, power plant dispatch or power markets. Rather, as a stand-alone model, it provides a tool for broad scenario exploration, the mapping of system fluctuations and the identification of general power system dynamics. The power model was furthermore shown to operate functionally and provide usable inputs for the Fourier analysis. It was supplemented with an embedded tool for performing spectral Fourier analyses which was proven to provide the means for executing Fourier analyses. An important simplification in the model is the lack of spatial distribution of VRE sources causing the pooling effect to be disregarded in the analysis. Yet since historical country-wide generation figures were used as model inputs, the data reflect actual power system configurations to a decent extent.

A limitation of the research scope is furthermore the notion that the energy system was only regarded in terms of the power system. Hence, no integral analyses were performed for the heat or fuel demand in other sectors. Especially since power-to-gas storage is acknowledged to have potential in sectors outside the power system, this underestimates the potential value of this type of storage. Nonetheless, the research provides the foundation for a more holistic analysis of mapping energy system fluctuations.

In the methodology for the spectral analysis, the inverse Fourier analysis was performed using frequency bands based on the researcher's judgment. The fact that clear seasonal, weekly and daily supply and demand patterns resulted from the inverse Fourier analyses proved that the choice of these frequency bands was to a large extent justified. Only the 'monthly' cycling component resulted in limited information due to the fact that wind power fluctuated on many timeframes within this frequency band. Hence, an inverse transformation did not result in a clear visualisation of the fluctuational behaviour on this timeframe. It may be argued that separating this frequency band into smaller segments would allow more detailed representation of the fluctuations of wind, but the noisy nature of wind power fluctuations will remain regardless.

A negative practicality of the spectral analysis is furthermore the notion that the phase information for wind power generation provided little information due to the many present cycling components. Whereas solar PV showed three peaks with their corresponding phase, wind power is much less dominated by a few cycling components. As a result, the phase spectrum was not only illegible, but offered little information in itself. Nonetheless, the phase information was required for the inverse Fourier transformations.

The results of the spectral analyses in this research firstly mapped the fluctuations of power demand and VRE generation for solar PV, onshore wind and offshore wind. This provided evidence for successful use of frequency spectra to visualise the different cycling components that influence supply-demand matching of electricity. Firstly, the demand was mainly shown to be dominated by its diurnal fluctuations, forming a daily usage pattern. In winter, an additional evening peak occurred on a daily timeframe. Additionally, a dominant weekly cycling component induces a higher electricity demand during weekdays as compared to weekends. Finally, a seasonal fluctuation was present where a higher demand occurs in winter, yet less dominant than the weekly and diurnal cycling. Solar PV was then shown to be well-described by three sinusoids, with a period of 12, 24 and 8760 hours. Through inverse Fourier transformation, it was furthermore shown that the seasonal fluctuation of solar PV and demand fluctuate in anti-phase. The wind's seasonal fluctuation was more in phase, but strong monthly fluctuations cause discrepancies on the longer timeframes. Although no single timeframe dominated the wind power generation, most dominant fluctuating components had a cycling timeframe of several hundred to several thousand hours. Additionally, it was shown that onshore and offshore wind have a similar noisy fluctuation pattern but offshore wind fluctuations are weaker and slightly less dominated by monthly fluctuations.

The spectral analysis was then performed to make the fluctuations in residual load visible in an insightful manner for different ratios between solar PV and wind generation. It was shown that a solar PV share ratio of 25-40% induced the lowest fluctuation volumes. Similarly, increased wind power in the generation mix lowers the number or hours where a deficit occurs as well as the magnitude of the deficits. Naturally, the number of hours where a surplus occurs therefore becomes higher with increased wind penetration, but again at lower magnitudes. Full reliance on solar PV can induce surpluses of over 60 GW, or even higher when overgeneration occurs.

The highest experienced deficit was shown to be independent of the generation mix, since it entails an instance of high demand and almost no VRE generation. This suggests that regardless of the generation mix, an instance may occur where all storage mediums are depleted. In turn, this notion may vow for the importance of single-instant solutions such as interruptible load, as deploying back-up generation for such a low level of operation quickly becomes economically inefficient. Nonetheless, the instances of no VRE generation assume linear scaling of the model's VRE generation data to installed capacity. This means that if the input data include an instance of no VRE generation, increasing the installed capacity of VRE in the model will not affect this instance. In reality, increasing the installed VRE capacity to high levels may induce pooling effects, where some point sources generate electricity when others do not.

Subsequently, the residual load spectra were used to visualise the effect of flexibility measures on different cycling timeframes. This poses valuable information in the sense that it allows the measures to be matched to the specific timeframe on which flexibility is required. E.g. if a spectrum shows that the residual load fluctuates heavily on a diurnal timeframe, spectral analyses can be used to identify the most applicable flexibility option. After deploying the most suitable measure, the residual load that remains can again be reflected in the frequency spectrum and so forth. Thus, a step-wise approach to reaching full VRE reliance can be taken by iteratively representing the residual load in the frequency spectrum.

The spectral analyses showed a clear distinction between the timeframes on which different storage technologies acted. BES was shown to influence the <12-hour cycling components of the residual load. Per unit of energy delivered, the effect of batteries on these timeframes is significant but in absolute numbers the batteries' energy content is too low to shift significant energy volumes. Yet, increasing the solar PV share positively influences the effect of BES in the frequency spectrum due to increased daily discharging. Batteries are thus ineffective in shifting wind power fluctuation, but can to a larger extent form a synergy with high levels of solar PV. This is well-explained by looking at the frequency spectra, where wind power induces monthly fluctuations but BES had none or little effect on these timeframes. As a result, the LCOS of batteries is harmed by limited discharging cycles induced by large wind fronts. This exposes a consideration on the choice for either wind or solar PV where increased wind generation is beneficial for limiting the level of fluctuation experienced in a system whereas solar PV poses synergetic characteristics with battery storage. Simultaneously, the model showed how the LCOS decreases with every additional battery installed.

The difference spectrum of CAES indicated a reducing effect on both diurnal cycling as well as on cycling timeframes up to several days. Even at high wind penetration, this reducing effect remains prominent, making it more suitable for abating some of the longer-term fluctuations induced by wind. It provides indications that storage facilities with capacities and an E2P ratio similar to CAES have the potential to provide significant flexibility. It was however found that the available storage capacity of 69 GWh was in many instances a limiting factor at higher power capacities. This vows for the value of research into alternative storage facilities with similar discharge capabilities as CAES, such as underground hydro-storage. Furthermore, indications were supplied that the effective installed capacities of CAES lie around 5 GW of charging and 6-8 GW of discharging (i.e. a discharge time of 8-11 hours). Yet, more elaborate cost analyses are required to determine the actual economically viable capacities.

Finally, P2G is the only storage type that showed fluctuation reduction potential on monthly and seasonal cycling timeframes. Especially the capturing of surpluses occurs on all timeframes, due to the practically unlimited storage capacity. Of the total available capacity, it was shown that up to 1.2 TWh of storage capacity is utilised if high installed capacities are assumed. Additionally, indications were provided regarding the effective P2G and G2P capacities. The LCOS of P2G was shown to be significantly higher than CAES or BES, even if the latter storage types apprehend large storage sections.

Results regarding other flexibility measures showed that overgeneration does pose significant additional potential for reducing the residual load fluctuations to near zero, especially in combination with G2P. Yet, the monthly cycling is shown to remain a dominant cycling component if overgeneration of VRE occurs. Furthermore, overgeneration naturally entails very high levels of installed VRE capacity. Interconnection and curtailment are concluded to have a significant role in reducing the requirements for storage options, since high VRE levels induce large surpluses. An assumption was however that the interconnection was modelled to be available whenever required, whereas neighbouring countries may not always have the reserves to supply at the maximum power capacities. DSM was modelled in a highly simplified fashion, causing the spectral analysis to only be a first indication of the potential effects.

Finally, an initial analysis of the cost dynamics for deploying storage was performed. This was used for further substantiating the practical limits and potential for deploying different EES technologies for flexibility purposes. The general relation between E2P ratios, level of operation and the levelised cost of storage was derived. From these figures, one can identify the number of hours of discharge that is required to reach a certain levelised cost of storage. Moreover, it provides this information for storage sections of different sizes per technology. The costs of storage technologies are however highly uncertain and case-specific, so the values are especially to be interpreted as denoting the general LCOS dynamics.

8. Conclusions

This research asked the question to what extent electricity storage and other flexibility measures can accommodate the residual load fluctuations induced by high levels of VRE. More specifically, this research investigated a new approach to explicating power system fluctuations and their response to flexibility measures per individual cycling component. The research results can thus be used to draw several conclusions regarding both the application of spectral analyses in renewable energy research as well as VRE integration strategies.

First it was concluded that Fourier analyses can be applied to map the fluctuation of VRE generation and demand in frequency and phase spectra. The demand pattern of electricity usage as well as generation profiles can thus be insightfully visualised. Additionally, the frequency spectra could be transformed to identify complementarity between different cycling components. The individual time-varying fluctuations of VRE supply and demand were thus depicted comprehensively, answering the question on what timeframes VRE generation and demand fluctuate. The same principle was successfully applied to visualising the residual load per individual cycling timeframe. Concludingly, the research successfully investigated an alternative approach to analysing supply-demand matching potential for VRE.

Moreover, it was concluded that frequency spectra can be used to visualise how flexibility measure affect different cycling timeframes of the residual load. It was shown that BES affects residual load fluctuations on hourly timeframes, whereas CAES also affects cycling components up to several weeks. P2G storage affects the cycling components with diurnal, monthly and seasonal periods, but its LCOS and low full-cycling efficiencies suggest it has higher value in cross-sectoral application. The effect of flexibility measures for enhancing VRE integration could now be described per individual cycling timeframe rather than in general terms. As a result, this allows the deployment of flexibility measures to be tailored to match the exact fluctuations experienced in a power system. The same methodology furthermore lends itself for similar application in other sectors where cyclical behaviour is concerned.

In terms of costs, increased wind penetration reduces the effectiveness and increases costs of deploying storage technologies. The increased discharge cycles induced by high levels of solar PV are beneficial for the LCOS. Additionally, storage technologies tend to reduce their own business case due to saturation of the captured surpluses. These dynamics were explained by deriving the sensitivity of storage technologies to the level of operation as well as to the size of the storage section.

In final conclusion, the spectral analyses suggest that although flexibility does provide a high level of fluctuation relief, in practice it struggles to accommodate full reliance on VRE sources. On the one hand, a high share of wind power generation minimises fluctuation magnitudes and power requirements but reduces effectiveness of storage technologies. Additionally, its monthly cycling components are poorly abated through storage deployment. On the other hand, the strong diurnal fluctuation induced by solar PV would require high charging power for storage technologies or large amounts of VRE curtailment. Additionally, its seasonal fluctuation is in anti-phase with the demand fluctuation. As a result, single instance of high supply or deficit occur despite the deployment of flexibility measures. Back-up generation is economically inefficient in supplying single instant solutions, which vows for alternative solutions such as interruptible loads or other DSM measures.

9. Recommendations

This section formulates recommendations for both applying the results in practice as well as the proposed methodology. It furthermore recommends how further research can build on the results and proposes fields of interest.

The simplified power model has the potential to act as quick tool to be used in policy design, supporting more elaborate power system models. It was shown to operate in a stand-alone fashion and thus provides a foundation for utilisation in scenario. Since power models are often complex, detailed and time-consuming, this model provides an alternative for exploring supply-demand matching in quick scenarios. Moreover, its modularity and customisable nature allows expansion to other sectors, energy carriers or flexibility measures and allows it to be specified to other regions or years. This was for example shown by specifying the inputs for the year 2017. In doing so, it provides a starting point for further modelling research into the effects of VRE integration.

The incorporation of the DFT allows the model to insightfully visualise causal relations in a complex system. Such an accessible representation has application potential for didactic purposes in the field of renewable energy. They may e.g. be used to explain the complex dynamics in a power system to policy-makers or stakeholders in other fields in a comprehensive way. Moreover, it provides a generally applicable methodology for comprehensively explaining system with complex cycling behaviour. This allows policy measures to be tailored to cycling behaviour of signals in a more effective manner.

In more general terms, policy-makers and other relevant stakeholders can benefit from the insights into the underlying factors influencing VRE integration, as it exposes both opportunities and limitations to VRE integration. By more explicitly formulating the relation between flexibility and VRE integration, the results can be valuable in guiding VRE integration strategies. Additionally, this research provides a comprehensive summary of literature regarding VRE integration. Finally, it is acknowledged that insight into the effects of high VRE shares is valued in advance of the actual installation process of large VRE capacities[33], e.g. due to the long lead times that come with installing wind power.

From the research, several recommendations for future research on the topic of VRE integration and spectral analyses could be identified. First of all, further research should build on the results by performing more elaborate spectral analyses of flexibility measures besides EES. This could for example entail a more detailed representation of the different DSM measures and a subsequent spectral analysis of their effect. By reflecting flexibility measures in more detail, the frequency spectrum poses more accurate information on their reducing effect on different cycling timeframes. More accurate frequency spectra in turn allow flexibility measures to be tailored to match the specific residual load fluctuations.

It is furthermore recommended that further spectral analysis research is performed in a more integral view of the energy system. The methodology lends itself for application to other supply and demand sectors besides merely the power system. Applying it in a cross-sectoral fashion can map different energy flows in the system and explicitly formulate the influence of an increasing renewable energy system. Moreover, since P2G storage is expected to have significant cross-sectoral application potential, an integral view of the energy system could provide better indications of the value of P2G. This research acts as a foundation for more integral research since both the model and the spectral analysis can be built upon in further research. As stated, the model allows extension to other sectors and any signal from the model can be run through the Fourier analysis as long as the timeframe is 8760 hours.

[33] Personal communication with the Netherlands Wind Energy Association (NWEA), September 1st. *The Dutch wind sector association promoting and steering the implementation of wind power.*

Furthermore, an assessment is recommended for determining the optimal level of VRE in the system, rather than merely analysing full VRE reliance. Such an assessment could include a more elaborate economic assessment of the flexibility measures for abating fluctuations. This shifts the question towards identifying the perfect balance is between VRE generation, flexibility measures but also operation of conventional plants. The proposed spectral analyses can in this case aid in identifying an optimal flexibility portfolio. Additionally, spectral analyses can be used to visualise operational patterns of conventional plants at power system configurations with different levels of VRE integration.

Supplementary research could combine spatial distribution of VRE with spectral analyses to analyse whether generation curves of different VRE point sources are complementary or alternating. Since the problematic instances of supply-demand matching occur because of an instance of close to zero VRE generation, spreading of VRE resources may pose significant benefits. Abating single instances of high deficit is essential in allowing VRE reliance. Spectral analyses may pose a comprehensive method of visualising how different point sources of VRE generation can be optimised to reduce fluctuations.

Finally, follow-up research could perform the Fourier analyses over shorter periods, such as on a 24-hour timeframe, to represent the diurnal effect of short-term flexibility measures in greater detail. Especially the effect of DSM, electrification and BES may well be represented on a shorter timeframe. It is recommended that such analyses apprehend a <1-hour timeframe. This inclusion could thus suggest spectral analyses for use in power system stability analyses as well.

10. Literature

1. ANVS (2017). Kerncentrale Borssele (EPZ). *Autoriteit Nucleaire Veiligheid en Stralingsbescherming (ANVS),* The Hague, The Netherlands. Consulted November 8th, at: <https://www.autoriteitnvs.nl/onderwerpen/kerncentrale-borssele-epz>

2. Belderbos, A., Virag, A., D'haeseleer, W. & Delarue, E. (2017). Considerations on the need for electricity storage requirements: power versus energy. *Energy Conversion and Management* Vol. 143, p. 137-149

3. Berenschot (2017). Electrification in the Dutch process industry. In-depth study of promising transition pathways and innovation opportunities for electrification in the Dutch process industry. *Berenschot Groep B.V.*, Utrecht, The Netherlands

4. Bergaentzlé, C. Clastres, C. & Khalfallah, H., (2014). Demand-side management and European environmental and energy goals: an optimal complementary approach. *Energy Policy*, Vol. 67, p.858-869

5. Blanco, H. & Faaij, A. (2018). A review at the role of storage in energy systems with a focus on Power to Gas and long-term storage. *Renewable and Sustainable Energy Reviews* Vol. 81, p. 1049-1086

6. CBS (2017a). Windenergie; elektriciteitsproductie, capaciteit en windaanbod per maand. *Centraal Bureau voor de Statisiek (CBS) Statline*, Den Haag, The Netherlands

7. CBS (2017b). Hernieuwbare elektriciteit; productie en vermogen. *Centraal Bureau voor de Statisiek (CBS) Statline*, Den Haag, The Netherlands

8. CBS (2017c). Motorvoertuigenpark; inwoners, type, regio, 1 januari. *Centraal Bureau voor de Statisiek (CBS) Statline*, Den Haag, The Netherlands

9. Das, T. & McCalley, J. (2012). Educational Chapter - Compressed Air Energy Storage. *Iowa State University Ames*, Iowa, USA

10. De Boer, H.S., Grond, L., Moll, H. & Benders, R. (2014). The application of power-to-gas, pumped hydro storage and compressed air energy storage in an electricity system at different wind power penetration levels. *Energy* Vol. 72, p. 360-370

11. DECE (no date). FFT tutorial. *University of Rhode Island*, Department of Electrical and Computer Engineering (DECE). Consulted October 11th, at: <https://www.researchgate.net/file.PostFileLoader.html?id=5923adad48954c4d3440d709&assetKey=AS%3A497020986236928%401495510445504>

12. DG ENER (2013). The Future Role and Challenges of Energy Storage (STORE). *European Commission Directorate-General for Energy (DG ENER),* Brussels, Belgium*.* Consulted October 9th, at: <https://ec.europa.eu/energy/intelligent/projects/en/projects/store>

13. Elzenga, H. & Ros, J. (2014). De Rol van de Elektrische Warmtepomp in een Klimaatneutrale Woningvoorraad. *Planbureau voor de Leefomgeving (PBL),* The Hague, The Netherlands

14. ENEA Consulting (2016). The potential of power-to-gas. Technology review and economic assessment. *ENEA Consulting,* Paris, France

15. Energiebusiness (2017). Gemiddelde jaaropbrengst zonnepanelen 2016. Consulted on November 2nd, at: <http://www.energiebusiness.nl/2017/01/17/gemiddelde-jaaropbrengst-zonnepanelen-2016/>

16. ENTSO-E (2016a). Transparency platform: Generation - Actual Generation per Production Type 2016. *European Network of Transmission System Operators (ENTSO-E).*

17. ENTSO-E (2016b). Power statistics – Monthly Hourly Load Values 2016. *European Network of Transmission System Operators (ENTSO-E).* Consulted on September 11th, at: <https://www.entsoe.eu/data/statistics/Pages/default.aspx>

18. ENTSO-E (2017a). Knowledge base: Actual Generation per Production Type. *European Network of Transmission System Operators (ENTSO-E).* Consulted on November 13th, at: <https://transparency.entsoe.eu/content/static_content/Static%20content/knowledge%20base/knowledge%20base.html>

19. ENTSO-E (2017b). Transparency platform: Generation - Actual Generation per Production Type 2017. *European Network of Transmission System Operators (ENTSO-E).*

20. ENTSO-E (2017c). Power statistics – Monthly Hourly Load Values 2017. *European Network of Transmission System Operators (ENTSO-E)*. Consulted on September 11th, at: <https://www.entsoe.eu/data/statistics/Pages/default.aspx>

21. ESMAP (2015). Bringing Variable Renewable Energy up to scale. Options for Grid Integration Using Natural Gas and Energy Storage. *Energy Sector Management Assistance Program (ESMAP),* Washington, USA

22. Esterl, T., Kaser, S., Stifter, M., Kamphuis, R., Galus, M., Renting, M., Rijneveld, A., Targosz, R., Widergren, S., Nordstrom, L., Brodén, D. & Galsworthy, S. (2016). IEA DSM Task 17: Valuation Analysis of Residential Demand Side Flexibility – Demand Flexibility in Households and Buildings. *International Energy Agency Demand Side Management (IEA DSM)*

23. Eurelectric (2010). Integrating intermittent renewables sources into the EU electricity system by 2020: challenges and solutions. *Eurelectric,* Brussels, Belgium

24. Frontier Economics (2015). Scenarios for the Dutch electricity supply system. A Report Prepared for the Dutch Ministry of Economic Affairs. *Frontier Economics Ltd.,* London, UK

25. Gardner & Haynes (2007). Overview of Compressed Air Energy Storage. *Boise state University, Office of Energy Research, Policy and Campus Sustainability,* Boise, USA

26. Gelazanskas, L. & Gamage, K. (2014). Demand side management in smart grid: A review and proposals for future direction. *Sustainable Cities and Society* Vol. 11, p. 22-30

27. Gracceva, F. & Zeniewski, P. (2014). A systemic approach to assessing energy security in a low-carbon EU energy system. *Applied Energy* Vol. 123, p. 335-348

28. Hilston, J. (2017). “Model Validation and Verification”. Lecture given in the course Performance Modelling. The university of Edinburgh School of Informatics, 16th March 2017, Edinburgh, Scotland

29. IEA (2011). Technology Roadmap - Smart Grids. *International Energy Agency (IEA)*, Paris, France

30. IEA (2012). Energy Technology Perspectives 2012 Pathways to a Clean Energy System. *International Energy Agency (IEA)*, Paris, France

31. IEA (2014). The Power of Transformation. Wind, Sun and the Economics of Flexible Power Systems. *International Energy Agency (IEA)*, Paris, France

32. IEA DSM (no date). Demand-side bidding. Task VIII Brochure. *International Energy Agency Demand Side Management (IEA DSM)*

33. IEC (2011). Electrical Energy Storage – White Paper. *International Electrotechnical Commission (IEC),* Geneva, Switzerland

34. IRENA (2012). Renewable Energy Technologies: Cost Analysis Series - Volume 1: Power Sector Issue 5/5: Biomass for Power Generation – working paper. *The International Renewable Energy Agency (IRENA),* Abu Dhabi, United Arab Emirates

35. IRENA (2013). Smart Grids and Renewables: A Guide for Effective Deployment – working paper. *The International Renewable Energy Agency (IRENA),* Abu Dhabi, United Arab Emirates

36. IRENA (2015a). Battery Storage for Renewables: Market Status and Technology Outlook. *The International Renewable Energy Agency (IRENA),* Abu Dhabi, United Arab Emirates

37. IRENA (2015b). Renewable Energy Integration in Power Grids: Technology Brief. *The International Renewable Energy Agency (IRENA),* Abu Dhabi, United Arab Emirates

38. IRENA (2016). The Power to Change: Solar and Wind Cost Reduction Potential to 2025. *The International Renewable Energy Agency (IRENA),* Abu Dhabi, United Arab Emirates

39. IRENA (2017). Planning for the renewable future Long-term modelling and tools to expand variable renewable power in emerging economies. *The International Renewable Energy Agency (IRENA),* Abu Dhabi, United Arab Emirates

40. Kakran, S. & Chanana, S. (2018). Smart operations of smart grids integrated with distributed generation: A review. *Renewable and Sustainable Energy Reviews* Vol. 81, p. 524–535

41. Kerr, D. (2009). The Fourier Analysis Tool in Microsoft Excel. Issue 1. Consulted October 11th, at: <http://dougkerr.net/Pumpkin/articles/Excel_Fourier.pdf>

42. Kirby. 2006. Demand Response for Power System Reliability. *Oak Ridge National Laboratory.* Oak Ridge, USA

43. Klingenberg, L. (2005). Frequency Domain Using Excel. *San Francisco State University School of Engineering,* San Francisco, USA

44. Kool, R (2011). Load Management with Demand-Side Management, an overview. Workshop Johannesbrug: IEA Demand Side Management. *International Energy Agency (IEA)*, Paris, France

45. Lazard (2017). Lazard's Levelized Cost of Storage Analysis – Version 3.0. *Lazard*

46. Love, J., Smith, A., Watson, S., Oikonomou, E., Summerfield, E., Gleeson, C., Biddulph, P., Chiu, L., Wingfield, J., Martin, C., Stone, A. & Lowe, R. (2017). The addition of heat pump electricity load profiles to GB electricity demand: Evidence from a heat pump field trial. *Applied Energy* Vol. 204, p. 332-342.

47. Lunter, G. & Van Wayenburg, B. (2003). Het idee van Fourier. From book: *Speeltuin van de wiskunde*. De Smit, B. & Top, T. (red.) © 2003, Veen Magazines

48. Luo, X., Wang, J., Dooner, M. & Clarke, J. (2015). Overview of current development in electrical energy storage technologies and the application potential in power system operation. *Applied Energy* Vol. 137, p. 511-536

49. Makarov, Y., Kinter-Meyer, M., Du, P., Jin, C & Illian, H. (2012). Sizing energy storage to accommodate high penetration of variable energy resources. *IEEE Transactions on sustainable Energy* Vol. 3.1, p. 34-40.

50. Mathworks (2017). Documentation: Fft – fast fourier transform. Consulted October 11th, from: http://nl.mathworks.com/help/matlab/ref/fft.html

51. Milieucentraal (2017). Hoe werken zonnepanelen. *Milieu Centraal*, Utrecht, The Netherlands. Consulted on November 2nd, at: <https://www.milieucentraal.nl/energie-besparen/zonnepanelen/hoe-werken-zonnepanelen/>

52. Morin, D. (2009). Fourier Analysis. Version 1. Consulted on September 18th, at: <http://www.people.fas.harvard.edu/~djmorin/waves/Fourier.pdf>

53. Movares (2013). Laadstrategie Elektrisch Wegvervoer. *Movares Nederlands B.V.,* Utrecht, The Netherlands

54. Movares (2014). Demand response – kansenverdeling onder enkele MJA sectoren. *Movares Nederland B.V.,* Utrecht, The Netherlands

55. Music, M., Merzic, A., Redzic, E. & Aganovic, D. (2013). Complementary Use of Solar Energy in Hybrid Systems Consisting of a Photovoltaic Power Plant and a Wind Power Plant. *Recent Advances in Energy and Environmental Management*

56. NEA (2011). Technical and Economic Aspects of Load Following with Nuclear Power Plants. *Nuclear Energy Agency (NEA) - Organisation for Economic Co-Operation and Development (OECD),* Paris, France

57. Netbeheer Nederland (2017). Rekenmodellen. *Netbeheer Nederland,* Den Haag, The Netherlands. Consulted on September 11th, at: <http://www.netbeheernederland.nl/dossiers/rekenmodellen-21/documenten>

58. NETL (2012). Impact of Load Following on Power Plant Cost and Performance: Literature Review and Industry Interviews. *US Department of Energy (DOE) - National Energy Technology Laboratory (NETL)*, USA

59. NIST (2016). Time and Frequency from A to Z, P. *National Institute of Standards and Technology (NIST),* Gaithersburg, USA. Consulted on November 7th, at: <https://www.nist.gov/time-and-frequency-services/p>

61. NTI Audio (2017). Let’s Clear Up Some Things About FFT… Part 1 of 2: The basics. *NTI Audio,* Schaan, Liechtenstein. Consulted November 10th, at: <http://www.nti-audio.com/en/news/let%E2%80%99s-clear-up-some-things-about-fft%E2%80%A6-1.aspx>

62. Pierie, F., van Someren, C., & van Noppen, M. (2015). Het energieopslaglabelprincipe: een methode voor het vergelijken van het volledige spectrum van opslagsystemen. *Netbeheer Nederland,* Den Haag, The Netherlands

63. Pietzcker, R., Ueckerdt, F., Carrara, S., de Boer, H.S., Després, J., Fujimori, S., Johnson, N., Kitous, A., Scholz, Y., Sullivan, P. & Luderer, G. (2017). System integration of wind and solar power in integrated assessment models: a cross-model evaluation of new approaches. *Energy Economy,* Vol. 64, p. 583–599

64. Quintel (2017). Energy Transition Model. *Quintel Intelligence B.V>,* Amsterdam, The Netherlands. Consulted on October 18th, at: <https://energytransitionmodel.com/?locale=en>

65. REN21 (2017). Renewables 2017 Global Status Report. *Renewable Energy Policy Network for the 21st Century (REN21),* Paris, France

66. RvO (2014). Status rapportage warmtepompen - technologie en markt in Nederland. *Rijksdienst voor Ondernemend Nederland (RvO)*, Utrecht, The Netherlands

67. RvO (2017). Elektrisch vervoer in Nederland - Highlights 2016. *Rijksdienst voor Ondernemend Nederland (RvO)*, Utrecht, The Netherlands

68. Sargent, R. (2007). Verification and Validation of Simulation Models. *Proceedings of the 2007 Winter Simulation Conference,*

69. Schoots, K., Hekkenberg, M. & Hammingh, P. (2016). Nationale Energieverkenning 2016. ECN-O--16-035. *Energieonderzoek Centrum Nederland (ECN),* Petten, The Netherlands

70. Schröder, T. & Kuckshinrichs, W. (2015). Value of Lost load: An Efficient Economic Indicator for Power Supply Security? A Literature Review. *Frontiers in Energy Research* Vol. 3, art. 55

71. Sek, M. (no date). Frequency Analysis, Fast Fourier Transform, Frequency Spectrum. *Victoria University*, Victoria, Australia

72. Spees, K., & Lave, L. (2007). Impacts of responsive load in PJM: load shifting and real-time pricing. *The Energy Journal*, p. 101-121.

73. Spees, K., & Lave, L. (2008). Demand Response and Electricity Market Efficiency. *The Electricity Journal*, Vol. 20, Issue 3, p. 69-85.

74. Staats, M., De Boer-Meulman, P. & Van Sark,W. (2017). Experimental determination of demand side management potential of wet appliances in the Netherlands. *Sustainable Energy Grids and Networks,* Vol. 9, p. 80-94

75. StoRE (2012). Facilitating energy storage to allow high penetration of intermittent renewable energy D2.1 Report summarizing the status, Role and Costs of Energy Storage Technologies. *stoRE-project*

76. Stötzer, M., Hauer, I., Richter, M. & Styczynski, Z. (2015) Potential of demand side integration to maximize use of renewable energy sources in Germany. *Applied Energy* Vol. 146, p. 344-352

77. TenneT (2015). Transportmogelijkheden 2016. *TenneT TSO B.V.,* Arnhem, The Netherlands

78. TNO (no date). Electrification of Chemical Industry. An Opportunity for The Chemical and Electricity Sector. *Nederlandse Organisatie voor Toegepast Natuurwetenschappelijk Onderzoek (TNO),* The Hague, The Netherlands

79. Tol, R. (2007). The Value of Lost Load – working paper. *The Economic and Social Research Institute (ESRI),* No. 214, Dublin, Ireland

80. UK Power Networks (2014). Impact of Electric Vehicle and Heat Pump loads on network demand profiles. *UK Power Networks*, London, United Kingom

81. Van den broek, M. (2015). “Energy systems modelling”. Lecture given in the course Energy Systems Modelling, The university of Utrecht, 2015, Utrecht, The Netherlands

82. Verzijlbergh, R., de Vries, L. & Herder, P. (2015). Routekaart Energieopslag 2030: Systeemintegratie en de rol van energieopslag. *DNV GL – KEMA Nederland B.V.,* Arnhem, The Netherlands

83. Vlap, H., Holstein, J., Van der Steen, A. & Grond, L. (2015). Technische uitgangspunten en resultaten demonstratieproject P2G. *DNV GL– KEMA Nederland B.V.,* Arnhem, The Netherlands

84. Wimmler, C., Hejazi, G., Oliveira Fernandes, E., Moreira, C. & Connors, S. (2017). Impacts of Load Shifting on Renewable Energy Integration. *Energy Procedia*, Vol. 107, p. 248-252

85. World Energy Council (2016a). World Energy Perspectives. Renewables integration. Variable Renewables Integration in Energy Systems: How to get it right. *World Energy Council,* London, UK

86. World Energy Council (2016b). World Energy Resources. E-storage: Shifting from cost to value. Wind and solar applications. *World Energy Council,* London, UK

87. Zakeri, B. & Syri, S. (2015). Electrical energy storage systems: A comparative life cycle cost analysis. *Renewable and Sustainable Energy Reviews*, Vol. 42, p. 569-596

88. Zappa, W. & Van den Broek, M. (2017). Optimal distribution of variable renewable power generation capacity across Europe.

11. Appendix

Appendix I: Model characterisation

Figure 60 shows the simulation model characterisation, which was used to guide the modelling process[34]. The choices for certain categories in are supported in Table 6.

Type of dimension	CATEGORIES				
Discipline	bottom up	hybrid			top down
Discipline	technogical	hybrid			economic
Sector scope	electricity sector	energy system in a specific sector (e.g. households)		energy system of all sectors (i.e. transport/industry/households/conversion sector)	whole economy including energy
Geographical scope	local region	country		world region	world
Geographical scope	one region				multiple regions
Purpose	optimisation	optimisation with simulation elements		simulation with optimisation elements	simulation
Purpose	prescriptive				descriptive
Purpose	backcasting				forecasting
Conceptual model	physical relations	micro-economic relations			macro-economic relations
Conceptual model	fixed equilibrium	partial equilibrium		general equilibrium	non-equilibrium
Conceptual model	rational	rational combined with behaviour			behaviour
Conceptual model	individual persons/firms/institutes				central (invisible) actor
Conceptual model	energy flows				monetary flows
Formal model	linear				non-linear
Dynamics	static	static comparative		recursive dynamic (step-wise)	dynamic (in one go)
Foresightedness	myopic				perfect foresight
Time step	15 minutes	1 hour	1 year	5 years	10 years
Time horizon	1 week	1 year			30-100 years
Certainty	deterministic	a few stochastic parameters			stochastic
Exogenous to the model	techno-economic parameters				price elasticities
Data sources	statistics	techno-economic parameters (e.g. based on commercial, demo, pilot, or lab data)	econometric estimates	based on calibration	scenario assumptions (drivers)

Figure 60: Model characterisation

[34] Based on Lecture: Van den broek, M. (2015). "Energy systems modelling". *Given in the course Energy Systems Modelling, The university of Utrecht, 2015, Utrecht, The Netherlands*

Table 6: Elucidation to model characterisation

Dimension	Category
Discipline	The model is top-down since there are no components modelled to an individual level, such as demand sectors, generators or actors. Although bottom-up modelling would provide a more reliable system simulation, a top-down approach was chosen due to increased model simplicity and time restrictions. Furthermore, the discipline is purely technological since the model does not incorporate economic drivers.
Sector scope	The model concerns the electricity system. Again, the economy is disregarded and no electricity market is included.
Geographical scope	The scope is The Netherlands, so country-wide.
Purpose	The model is a simulation model with an indicative cost optimisation function. It is prescriptive because the model outcome 'prescribes' the composition of the energy system (i.e. how much energy is generated using what technology). Furthermore, the model is backcasting since it assumes certain hypothetical scenarios in the future in order to define implications for the current situation.
Conceptual model	The model mainly focuses on physical relations between energy supply and energy demand (i.e. energy flows). However, due to the simplified representation of the system it has some macro-economic features where sectors are represented as a single component. The model is based on a fixed equilibrium, where the supply and demand of energy are always in balance. No behavioural aspects of certain actors are included in the model, causing the decision-making to be purely rational.
Dynamics	The dynamics in the model are not static, since the battery storage over time is a recursive process. However, the model run takes place 'in one go' rather than iteratively running each time step.
Foresightedness	There is no foresightedness in the model; decisions are made merely based on the current time-step. Hence, the model is myopic.
Time step	The time step is 1 hour, which can be cumulated into days, weeks, months and years.
Time horizon	The time horizon is 1 complete year. More specifically, the time horizon is 8760 hours from 12:00 January 1st 2016 to 12:00 December 31st 2016.
Certainty	The model is deterministic since it is merely the result of its input parameters. Hence, there is no degree of randomness in the model outcomes.
Exogenous parameters	See Appendix II for an overview.
Data sources	The data sources include a combination of (historical) statistics, techno-economic parameters and scenario assumptions.
Endogenous parameters	See Appendix II for an overview.

Appendix II: Frequency spectra of VRE generation and demand for 2017

The graphs shown represent the Fourier analyses performed over the 2017 Dutch generation and load curves from ENTSO-E (2017b; 2017c). Since the 2017 ran only up to mid-November, any missing hours at the end of the year were set to the 2016 values. The phase spectrum with threshold is again only shown for solar PV and the demand.

Solar PV

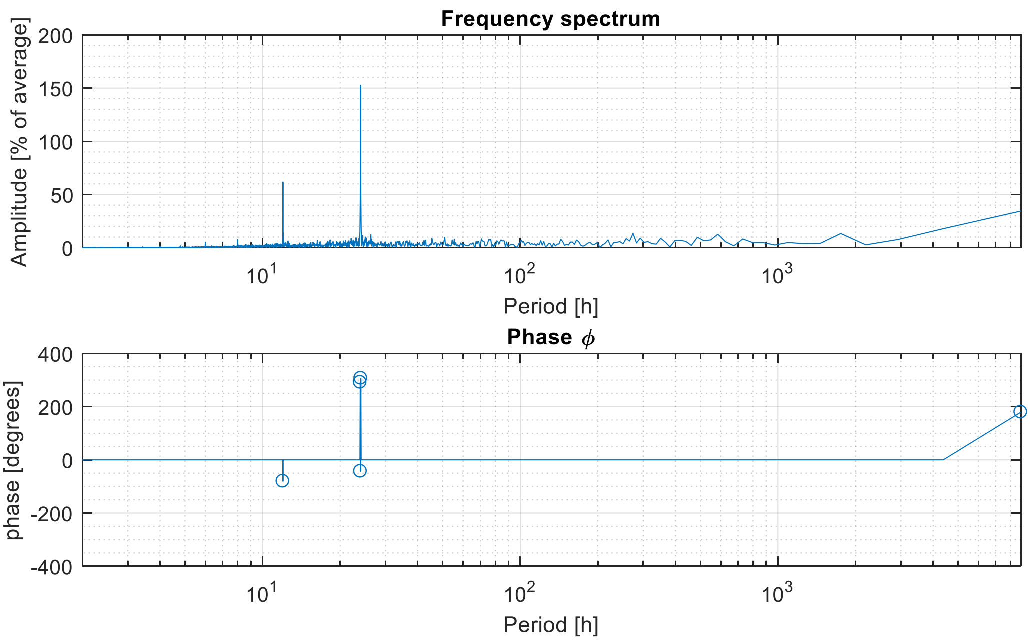

Default demand profile

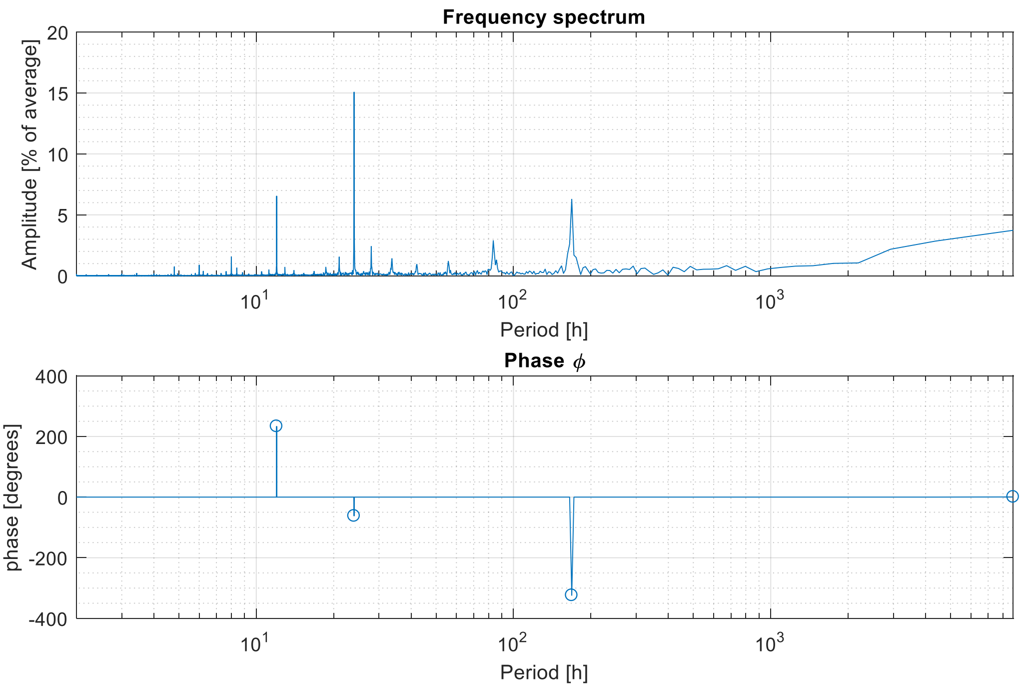

Onshore wind

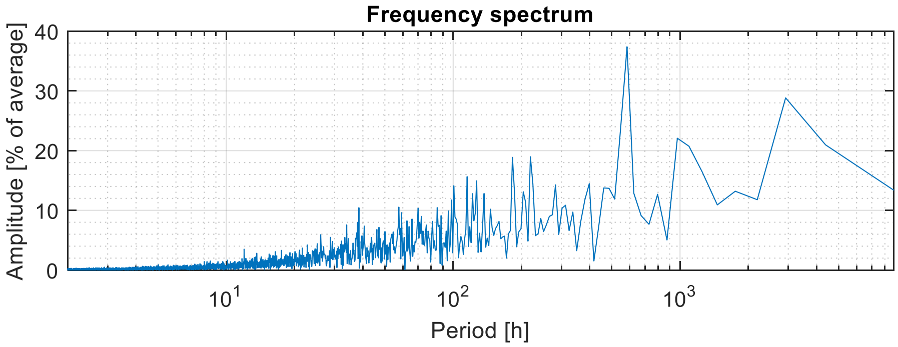

Offshore wind

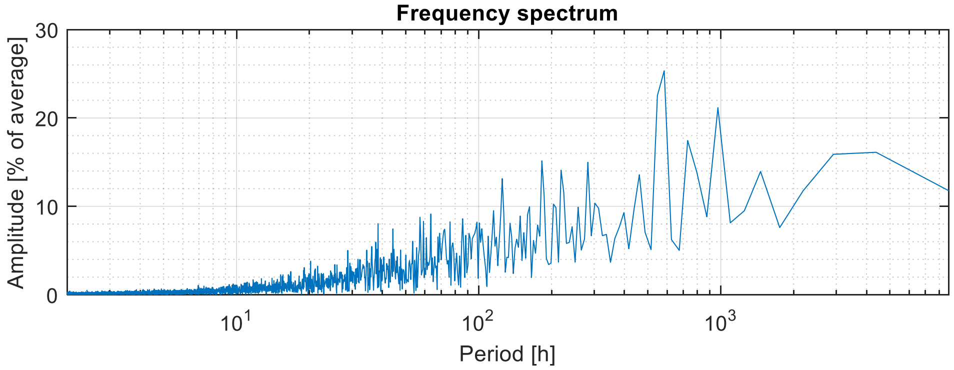

Appendix III: Cost components of EES technologies

The following appendix includes the cost components and other relevant parameters for the investment module. The costs are the average values as adapted from Zakeri & Syri (2015), expect for CAES where the maximum TCC is adapted to account for the fact that AA-CAES is considered.

Cost component		PCS+BOP [€/kW]	Storage section [€/kWh]	$O\&M_f$ [€/kW-yr]	$O\&M_v$ [€/MWh]	C_r[b] [€/kW]	T [yr]
CAES[a]		1014	40	3.9	3.1	-	30
BES	Pb-acid	465	618	3.4	0.37	172	15
	NaS	366	298	3.6	1.8	180	15
	Li-ion	463	795	6.9	2.1	369	15
P2G[a,c]		1548	3.7	35	-	-	20

[a] Values for subterranean storage

[b] Assuming cycle frequencies of 365-500 per year

[c] Power-to-H_2 used in a small to medium gas turbine

Parameter	Value	Unit
Electricity price	40[a]	€/MWh
Natural gas price	25	€/MWh
Emission price	20	€/MWh
Discount rate	8	%
AA-CAES gas input	0[b]	kWh/kWh
Emission factor natural gas	0.4	Tonne CO_2/MWh
Emission factor coal	0.8	Tonne CO_2/MWh

[a] Based on Frontier Economics (2015). Lazard (2017) apprehends 34 $/MWh and Zakeri & Syri (2015) propose 50 €/MWh.

[b] For conventional CAES 0.33 kWh/kWh is reported in Gardner & Haynes (2007)

Appendix IV: Power system framework

The themes and drivers of the framework for modelling power systems as proposed in Pietzcker et al. (2017). The checkbox indicates whether the driver has been incorporated in the RESPECT model.

Table 7: Power system framework (Pietzcker et al., 2017; p.10)

Theme	Driver	In model?
Investment dynamics	Investment into dispatchable technologies differentiated by load	☒
	Investment into VRE (incl. feedback on the system)	☐
	Expansion dynamics	☐
	Capital stock inertia and vintaging	☐
	Structural shift of generation capacity mix	☐
	Love of variety	☐
Power system operation	Dispatch[b]	☐
	Flexibility and ramping	☒
	Capacity adequacy	☒
	Curtailment	☒
Temporal matching of VRE and demand	Wind/solar complementarity	☒
	Demand profile evolution	☒
Storage	Short-term storage	☒
	Seasonal storage	☒
	Demand response (incl. electric vehicles and V2G)	☒
Grid	General transmission and distribution grid	☒
	Grid expansion linked to VRE[a]	☒
	Pooling effect from expansion	☐

[a] Represented through the possibility of increasing import/export capacities or VRE capacities.

[b] Although dispatch is partly included, the framework implies dispatch according to a cost-based merit order. Hence, this driver is not included as such.

Appendix V: Interpreting a Fourier transformation

This example illustrates a simple Fourier transformation over a periodical signal, as adapted from Mathworks (2017). Firstly, a waveform is generated in order to see how the DFT reflects the content of a signal. Assumed is a waveform made up of two cumulated sinusoids: a 50 Hz sinusoid with an amplitude 0.7 and a 120 Hz sinusoid with an amplitude of 1. Furthermore, the following signal properties apply where x(t) describes the signal in the time domain. It can be recognised that formula x(t) contains both frequencies as well as the amplitudes. Plotting x(t) in the time domain results in a periodic waveform, of which Figure 61 shows a short section.

Sampling frequency	$F_s = 1000$
Sampling period	$P_s = 1/Fs$
Signal length	$N = 1500$
Time vector	$t = (0{:}N\text{-}1)*T_s$
Signal	$x\,(t) = 0.7*\sin(2*pi*50*t) + 1*\sin(2*pi*120*t);$

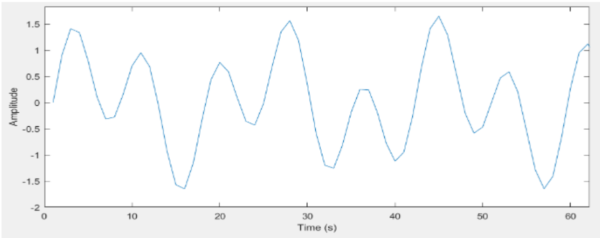

Figure 61: Cut-out of a waveform in the time domain

Now that a waveform is present, the DFT can be used to retrieve which sinusoids determined the shape of the waveform. The resulting frequency spectrum is presented in Figure 62. Note that rather than time, the frequency is plotted on the x-axis. In the plot, two peaks are shown with a certain frequency and amplitude. Hence, these suggest that the waveform can be separated into two sinusoids. Moreover, a peak is shown at both 50 Hz and 120 Hz, corresponding to the frequencies are prescribed for the initial waveform. Furthermore, the amplitude of each peak corresponds with the prescribed amplitudes of 0.7 and 1. Hence, the DFT shows exactly what sinusoidal signals determine the waveform. Although this example uses a simple waveform, the same principle applies to complex and distorted signals. In such a case, the plot shows many peaks of different amplitudes.

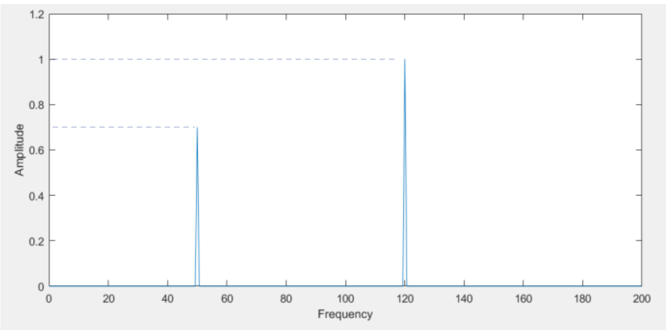

Figure 62: Cut-out of a waveform in the frequency domain

If an iDFT would be performed over the DFT output signal, the resulting waveform would be identical to Figure 61. Alternatively, the frequency domain can be divided into two frequency bands by dividing the spectrum at e.g. 80 Hz. Isolating one frequency band is done by setting all other frequencies in the other band to an amplitude of 0. Performing an iDFT over each isolated frequency band would then result in two separate sinusoids shown in the time domain, being the initially described sinuses.

Appendix VI: FFT MATLAB and Excel codes

MATLAB code

In the following code, 'A' indicates the variable exported from Excel. These variables can e.g. consist of generation, demand or residual load curves, reflected as an 8760 x 1 matrix. The code is then run to operate the Fourier analysis over the variable.

```
%General parameters
time=linspace(0,8760,8760);
f=1/3600; %frequency is 1 sample per hour, thus 1/3600 per second
N=length(A);
freq=(1:(N/2))*f/N; %The frequency for graphs until the Nyquist frequency
freq2=(1:N)*f/N;
Period=1/freq;
A_noDC=A-mean(A); %This cuts the 0 Hz DC component

%FFT execution
X=fft(A_noDC);
X_mag=abs(X);
X_amp=X_mag/N; %Normalises the magnitude into amplitude
X_ampsingle=X_amp(2:N/2+1); %Limits the plot to the Nyquist frequency
X_ampsingle(2:end-1)=2*X_ampsingle(2:end-1);

%Phase information extraction
X2=X;
      thres_phase=max(abs(X)/threshold); %An optional phase threshold
      X2(abs(X)<thres_phase)=0;
      phase=atan2(imag(X2),real(X2))*180/pi;
      phase_single=phase(2:N/2+1);
      phase_single(2:end-1)=2*phase_single(2:end-1);
      idxmax=find(phase_single>0);
      idxmin=find(phase_single<0);

%Plots of the frequency and phase spectrum
figure('visible','on')
subplot(2,1,1)
      semilogx(Period,X_ampsingle);
      curtick = get(gca, 'XTick'); %shows log units on x-axis
      set(gca, 'XTickLabel', cellstr(num2str(curtick(:))));
      grid on
      grid minor
      title('Frequency spectrum')
      xlabel({Period [h]'});
      ylabel({'Amplitude [MW]'});

subplot(2,1,2)
      semilogx(Period,phase_single,'-o','MarkerIndices',[idxmin;idxmax]);
      curtick = get(gca, 'XTick');
      set(gca, 'XTickLabel', cellstr(num2str(curtick(:))));
      grid on
      grid minor
      title('Phase \phi')
      ylim([-400 400]);
      xlabel({Period [h]'});
      ylabel({'phase [degrees]'});

%iFFT for different cycling components
figure('visible','on')
subplot(4,1,1)
      X_slow(1:3)=X(1:3);
```

```
        X_slow(3:8760)=0;
        A_slow=real(ifft(X_slow));
        plot(time,A_slow);
        title('Slow cycling')
        ylabel('amp [MW]')
        A_slow2=A_slow;
        A_slow2(A_slow2<0)=0;

subplot(4,1,2)
        X_month(4:52)=X(4:52);
        X_month(1:3)=0;
        X_month(41:8760)=0;
        A_month=real(ifft(X_month));
        plot(time,A_month);
        title('Monthly cycling')
        ylabel('amp [MW]')
        A_month2=A_month;
        A_month2(A_month2<0)=0;

subplot(4,1,3)
        X_week(53:361)=X(53:361);
        X_week(1:52)=0;
        X_week(362:8760)=0;
        A_week=real(ifft(X_week));
        plot(time,A_week);
        title('Weekly cycling')
        ylabel('amp [MW]')
        A_week2=A_week;
        A_week2(A_week2<0)=0;

subplot(4,1,4)
        X_day(362:8760)=X(362:8760);
        X_day(1:361)=0;
        A_day=real(ifft(X_day));
        plot(time,A_day);
        yyaxis left
        title('Intradaily cycling')
        xlabel('time [h]');
        ylabel('amp [MW]')
        A_day2=A_day;
        A_day2(A_day2<0)=0;


%Other plots:
%Reconstructs the signal from individual cycling components
figure('visible','on')
A_rec=(A_day(1:8760)+A_week(1:8760)+A_slow(1:8760)+A_month(1:8760))+mean(A)
;
        plot(time,A_rec);
        title('reconstructed signal');
        ylim([0 inf]);

%Plots the original input signal
figure('visible','on');
plot(time,A_noDC+mean(A)); %plots original signal
        title('Original signal');
        xlabel({'time [h]'});
        ylabel({'Amplitude [MW]'});
```

```
%Extracts the storage volumes
St=[X_ampsingle(1:4380) Period(1:4380) PI];
ST=prod(St,2);
Int_slow=sum(ST(1:3));
Int_month=sum(ST(4:52));
Int_week=sum(ST(53:361));
Int_day=sum(ST(362:4380));
Int_tot=Int_day + Int_week + Int_month + Int_slow;
```

Excel commands

The following Spreadsheet Link commands import and export the data form Excel to MATLAB and vice versa if written in a spreadsheet destination cell.

```
=MLPutMatrix("A";[range of cells]) %exports matrix into variable 'A'
=MLGetMatrix("phase_single";[target cell]) %imports phase
=MLGetMatrix("X_ampsingle";[target cell]) %imports amplitude
```

Appendix VII: Offshore wind correction

The graph below shows the uncorrected hourly generation of offshore wind, adapted from ENTSO-E (2016). It can be recognised that the curve shows a (polynomial) growth over time, which suggests that additional capacity was installed throughout the year. This is confirmed in CBS (2017) which reports installed offshore wind capacities of 357 MW for January, 657 MW for February until May and 957 MW for June through December. However, the graph suggests that the installation of capacity is not a stepwise process but occurs gradually. Hence, to correct for the installed capacity, the generation curve is used to make an estimation of the installed capacity development. The green line shows the moving trend of maximum generation levels which was assumed to be proportional to the installed capacity, or max generation ∝ installed capacity.

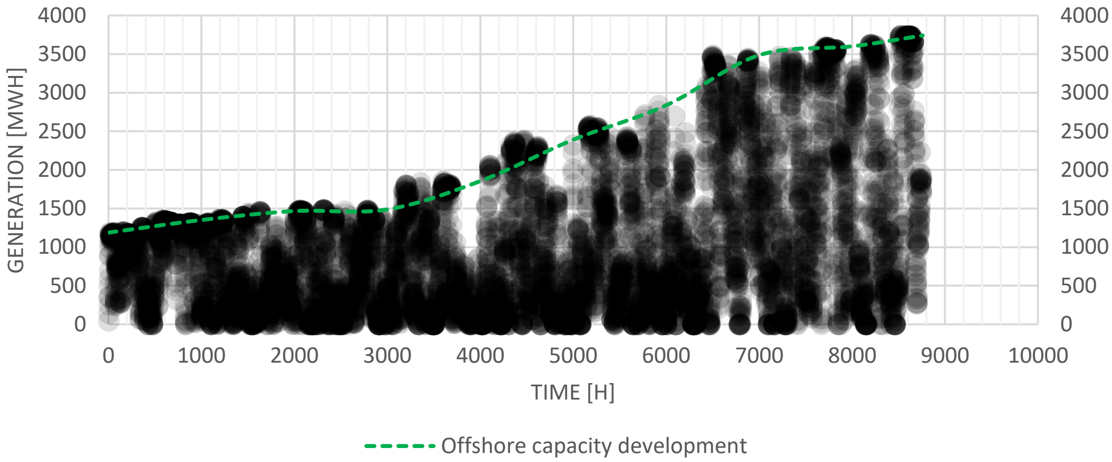

Normalising to the installed capacity at t=1, the corrected generation curve is the one shown below. It can be recognised that the annual generation shows a more balanced development. Although the cumulated annual generation is altered, these data are only used to derive the hourly *share* of wind power generation.

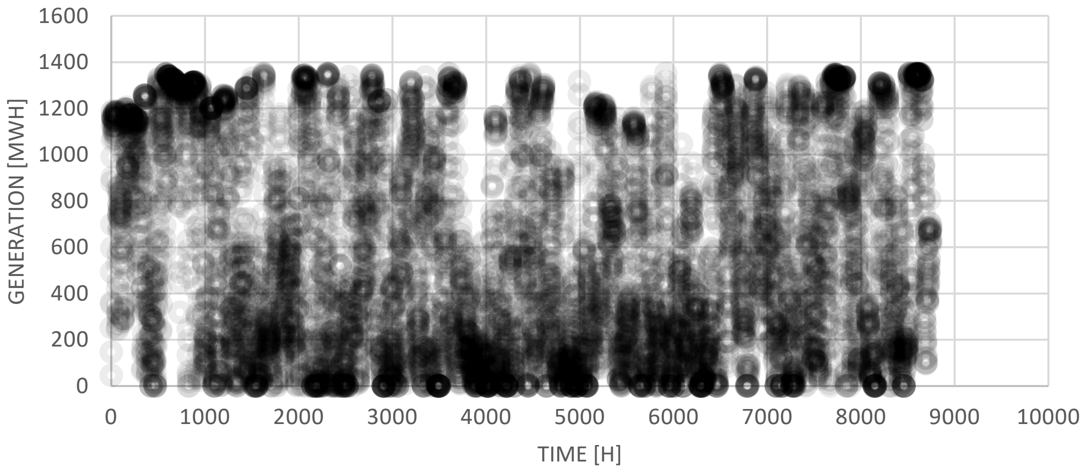

Appendix VIII: Phase thresholding in the Fourier analysis

In addition to the processing steps described in the theory, thresholding is applied to the phase spectrum to increase the legibility. Since the FFT provides information on amplitude and phase for each single frequency bin, it may occur that the information becomes illegible whenever a noisy signal is processed. A way of improving the legibility, is by removing low-amplitude noise from the FFT results. In other words, low-amplitude signals are filtered out in order to retain only the information for dominant system fluctuations. This can be achieved by setting an amplitude threshold value, below which any signal amplitude is set to 0. As a result, phase spectrum only depicts the high-amplitude sinusoids. It should be noted that, although it aids in improved visualisations of the FFT results, care is taken not to discard any valuable information since the phase information is required for the iFFT calculations. Figure 63 shows an example of a phase spectrum with low and high thresholding levels. In the lower figure, the low threshold causes the phase to be shown for nearly every frequency bin, even if its amplitude is very small. In the upper figure, any sinusoid with an amplitude below 20% of the highest amplitude is filtered out, which results in a comprehensive phase spectrum with information on merely the high-amplitude fluctuations.

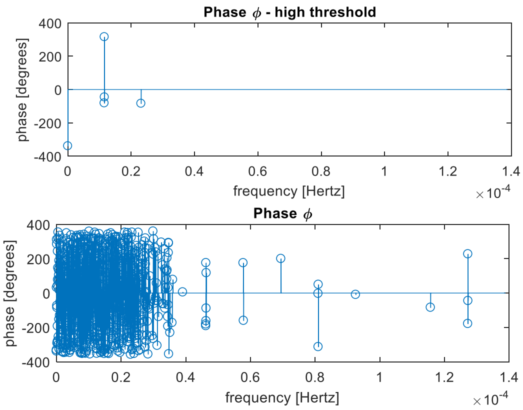

Figure 63: Effect of thresholding

Appendix IX: Elaboration on the different types of battery

As stated, the data are adapted from ESMAP (2015), IEC (2011), World Energy Council (2016b), Pierie et al. (2015), Verzijlbergh et al. (2015) and Luo et al. (2015).

Lithium-ion
Lithium-ion (Li-ion) batteries utilise an anode made of graphitic carbon and a cathode made from a lithium metal oxide. They are most widely used in electric transport due to their high energy density. Furthermore, their efficiencies are between 80-92% and their self-discharge rates are low. The rated power of batteries in series can be cumulated into multiple MWs. Drawbacks of Li-ion batteries are that the lifecycle reduces with depth of discharge (DoD)[35], the requirement of a special charging circuit and the tendency to become instable due to its temperature.

Lead-acid
Most commonly used is the lead-acid battery, with an anode of PbO_2 and an anode of Pb. The batteries have a similarly fast response time and low self-discharge rates. Its efficiency is generally somewhat lower than Li-ion batteries (65-90%) but specific investment costs are lower. They are well applicable to energy back-up supply, energy management and can be sized to utility scale application. The DoD is again a limiting factor in the battery lifecycle.

Sodium-sulphur
Thirdly, the sodium-sulphur (NaS) battery uses molten sodium and molten sulphur for an electrochemical reaction at high temperatures (>300 degrees C). Its efficiency (~90%) and energy density are relatively high whereas the self-discharge rate is almost negligible. Downsides are high current costs as well the requirement of a system to regulate the temperatures. Nevertheless, NaS batteries are considered promising in combination with wind and solar power.

Nickel-cadmium
Less commercialised is the nickel-cadmium (NiCd) battery, which uses (toxic) heavy metals to form electrodes of nickel hydroxide and metallic cadmium. Efficiencies range between 72-78% and their E2P ratio is relatively low (7-15 minutes). Utility-scale NiCd application is acknowledged to be unlikely. Batteries similar to NiCd are being developed, such as nickel-metal Hybride (NiMH) and nickel chloride (ZEBRA) batteries. These have improved characteristics and a more promising application potential.

Flow and hybrid batteries
As stated, flow (or *redox flow*) batteries use chemicals dissolved in liquids rather than solid electrolytes. The Vanadium Redox Flow battery (VRB) is the most developed flow battery, using one vanadium electrolyte in combination with a reversible fuel cell. It has applications in hourly load regulation, power security and even longer-term energy storage. It thus has the potential for supporting VRE generation. Efficiencies are in the range of 70-80% and response times are very quick. The downside is the high cost due to the immaturity of the technology. Besides the VRB, hybrid flow batteries exist such as the zinc bromine (ZnBr) and polysulfide bromine (PSB) battery. However, these are only in the earlier stages of demonstration.

[35] 100% of the energy capacity minus the amount of charge

Appendix X: Model verification and validation

Two indicators of whether a model operates correctly are verification and validation.

Verification

Firstly, verification concerns the question whether the internal functions of the computer program operate correctly. Amongst the techniques for increasing verification are debugging, third-party reviews, clear documentation, degeneracy testing[36] or consistency checks[37]. The verification of simulation model becomes more difficult with increasing model complexity, since the chance of modelling errors increases.

One consistency check that iteratively allowed model verification is the notion that the model always aims for an equilibrium between supply and demand. Hence, whenever the model stored, exported or curtailed energy below the demand profile, this indicated a fault in the model calculations. Similarly, if back-up generation or electricity import occurred while demand was already met, the calculations were reviewed and adapted. This mechanism was furthermore used to perform degeneracy tests. Another notion that aided in verifying the calculations is the fact that energy inputs are always equal to the energy outputs plus efficiency losses. Through manual recalculation, it was checked whether this criterion was met for the different generation and storage technologies.

In terms of the MATLAB code, no bugs were encountered by MATLAB during any of the code runs apart from common warnings regarding typos and missing variables. Nonetheless, several steps were taken to verify the essential part of the code which determines the frequency and phase spectra. First of all, to ensure that the FFT produced the correct output, initial results were compared to the automatic Excel FFT function. Besides that, the official MATLAB documentation as well as peer-reviewed literature provided elaborate examples of FFT analyses in MATLAB, which were closely followed during the coding process. Additionally, the MATLAB online community provided a large database of examples which aided in troubleshooting and reliable coding. The code component for extracting the frequency and phase spectrum was uploaded to the online MATLAB community, which allowed anonymous third-parties to review and comment on the code. It was concluded by reviewers that the code appeared to be written correctly.

[36] I.e. checking whether the model still functions properly using extreme inputs.

[37] Lecture: Hilston, J. (2017). “Model Validation and Verification”. Given in the course Performance Modelling. *The university of Edinburgh School of Informatics, 16th March 2017, Edinburgh, Scotland*

Validation

Validation concerns the notion whether the model succeeds in fulfilling its intended purpose accurately enough (Sargent, 2007). If a model aims to represent a certain system, there should be evidence that despite the assumptions made, the model produces outcomes that match the actual system to a satisfactory extent. The best tool for model validation is hence comparison to real-life data from the system that was simulated, both concerning model inputs as well as the outcomes produced. However, real-life data are often unavailable as models tend to be predictive or hypothetical in their assumptions. In that case, comparison to more elaborate models of the same system can provide an alternative source of validation[37]. Furthermore, critical reviews by the model creators, users and independent third-party experts can increase the level of validation (Sargent, 2007).

It should firstly be stated that the acquisition of model inputs occurred in an iterative process of data validation, where cross-checking peer-reviewed data sources ensured a selection of reliable data. Nonetheless, the VRE generation data required several processing steps and are stated to possible not include small-scale units (ENTSO-E, 2017a). Since these data make up the basis for the spectral analysis, it was double-checked with data from the national statistics agency whether the chosen data source provided accurate generation statistics. Firstly, the wind generation data from ENTSO-E (2016a) were checked against monthly generation data from Statistics Netherlands (CBS, 2017a). Figure 64 shows the hourly ENTSO-E data cumulated into months plotted against the CBS data. It can be recognised that both onshore and offshore generation wind match the CBS data closely so it can be concluded that the hourly ENTSO-E data are valid. Since the offshore data matched the CBS data, the CBS data were used as well for scaling the generation data back to the installed capacity in the first month.

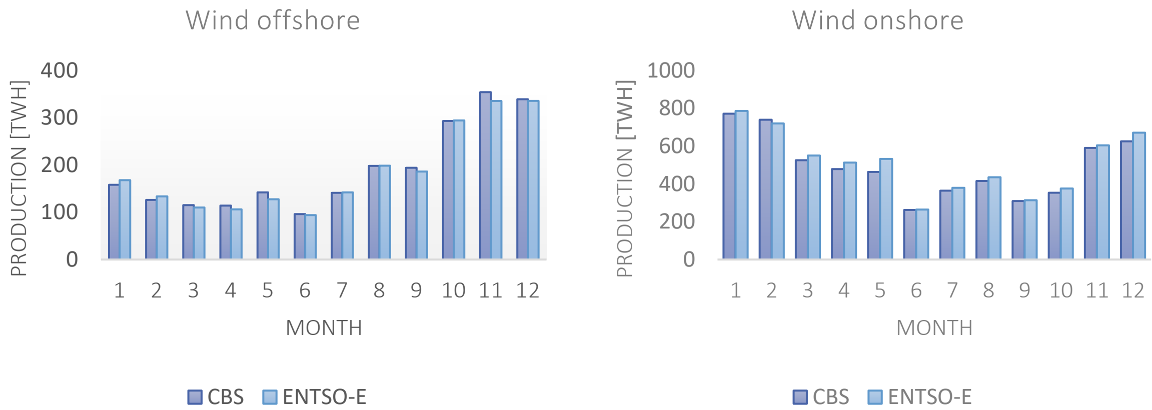

Figure 64: Comparison of 2016 wind generation in ENTSO-E and CBS

For solar PV, no monthly generation data were available in CBS (2017a) to validate the input data. Alternatively, a comparison is made to a measured monthly distribution of annual PV generation for the Netherlands (Milieucentraal, 2017; Energiebusiness, 2017). The result is shown in Figure 65, where no significant differences between the ENTSO-E distribution and the measured data.

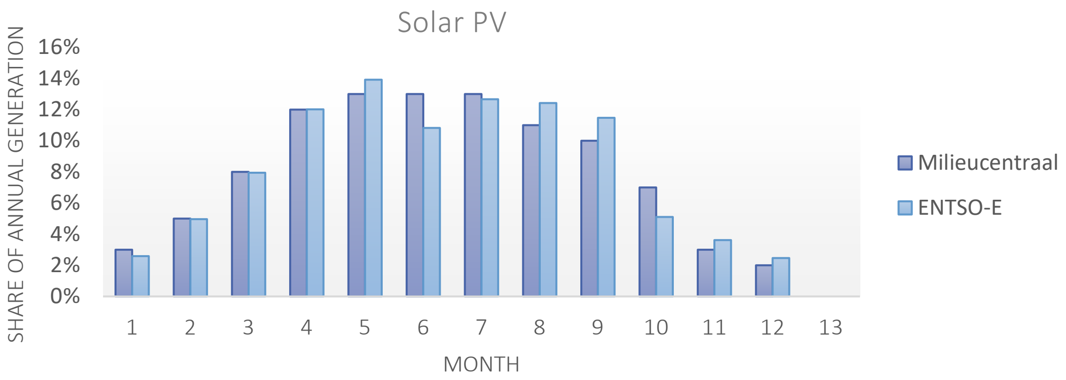

Figure 65: Comparison of solar PV distribution in ENTSO-E to measurement data (Milieucentraal, 2017; Energiebusiness, 2017)

Finally, to provide additional validation, the Fourier analyses were repeated using 2017 data from ENTSO-E (2017b; 2017c). By executing the analysis for multiple years, it was checked to what extent the results of the Fourier analysis are year-specific or whether they can be generalised in describing the system fluctuations.

As stated, comparison to more elaborate models can aid in validating model functionality. Netbeheer Nederland (2017) provides an overview of the available Dutch power system models, including a characterisation of their functionalities. Based on an analysis of this characterisation, the model that provided the best means of validation was found to be the Energy Transition Model (ETM), by Quintel (2017). Several characteristics of the ETM caused it to be comparable to the model in this research:

1) It has a wide array of customisable demand- and supply-side settings
2) It allows a variety of flexibility options to be incorporated
3) It allows a flexibility merit order to be manually chosen
4) It creates hourly generation curves for an entire year
5) It is open for public usage

Three scenarios were developed to check the whether the output of the RESPECT and the ETM correspond. The input of each scenario consists of certain levels of installed electricity generation capacity in combination with certain flexibility measures. Since RESPECT is an oversimplified representation, an exact match between output variables is not required. Rather, the values should be in similar ranges to indicate that the general decision dynamics within the model are realistic. Scenario 1 aims to check whether the prescribed fossil generation merit order gives valid results as well as whether the energy storage in EV batteries functions properly. The second scenario checks whether energy surplus is dealt with similarly in terms of P2G, import/export and curtailment. The third scenario does the same for battery storage. Since no CAES representation is possible in the ETM, this storage technology was not included in the validation process.

Table 8: Input data for validation scenarios

Input parameter		1	2	3
Installed capacity onshore wind	[GW]	9	12	0
Installed capacity offshore wind	[GW]	9	30	0
Installed capacity solar PV	[GW]	9	8	40
Installed capacity SCPC	[GW]	4	0	0
Installed capacity GT	[GW]	4	9.6	9.6
Installed capacity NPP (3^{rd} gen.)	[GW]	1.65	1.65	1.65
Battery energy capacity	[GWh]	0	0	150[a]
Installed P2G capacity	[GW]	0	1.85	0
Import capacity	[GW]	0	6	6
Electric car share	[%]	50	1	1
EV battery availability	[%]	50	0	0
Electric heat pump share	[%]	50	2	2

[a] In the ETM, this means 100% of the households are equipped with a 20 kWh battery.

[b] A combination of different coal and gas plants utilised for biomass and green gas combustion

The resulting generation profile of the first three validation scenarios is shown in Figure 66. It can be seen that the annual generation profiles correspond quite closely. For the VRE generation technologies, this is the result of the fact that the same installed capacity and load factor were used. For the fossil technologies, it appears that the assumptions on the deployment of SCPC, NGCC and NPP are valid to a large extent. Only the gas turbine seems to produce about 10-20 PJ more within the ETM. A share of this difference is explained by the fact that RESPECT appears to generate slightly more wind power than the ETM, which is presumably the result of electrical losses included in the ETM. Furthermore, the SCPC generates more energy in RESPECT. One reason may be that the SCPC is assumed to be flexible and have a minimum load of 25%, whereas the ETM assumes lower flexibility parameters. In terms of dealing with energy surplus, similar amounts of energy were stored, curtailed and exported in both models.

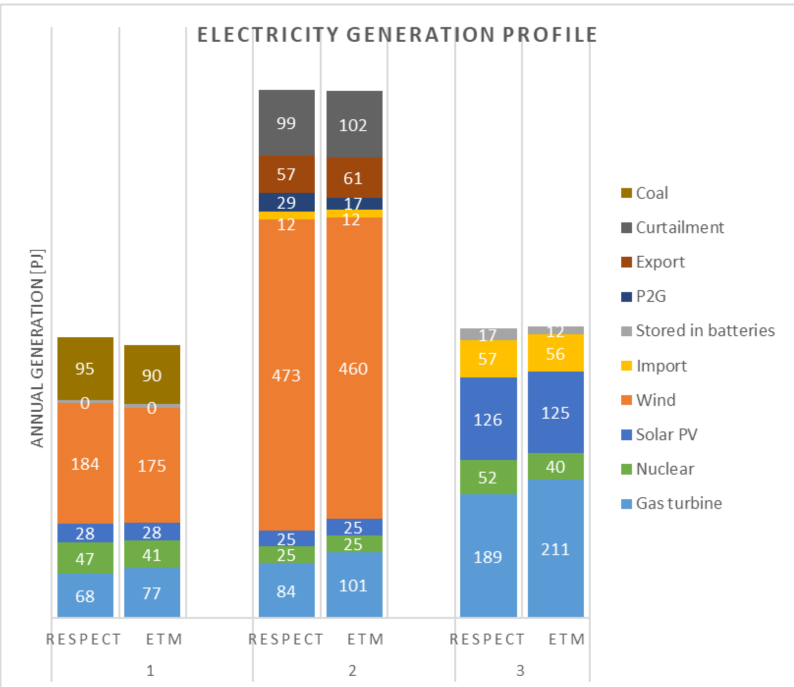

Figure 66: Validation scenario results

Appendix XI: Curtailment, import and export at different installed P2G capacities (with G2P) and generation mixes

Based on model runs in RESPECT. The amount of interconnection assumed to be 6 GW and the VRE generated is equal to the annual demand of 415 PJ.

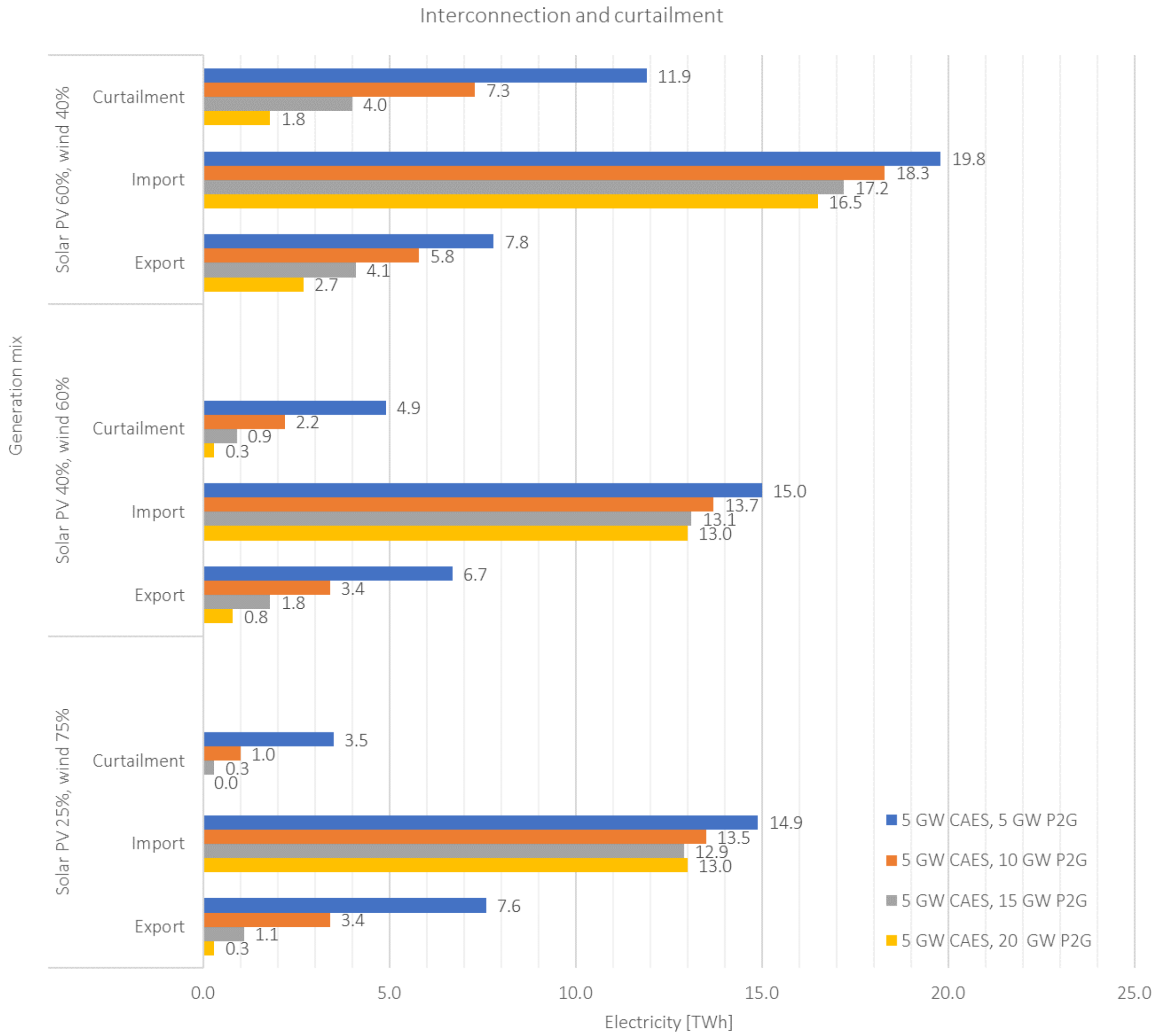

Appendix XII: Duration curves of surplus and deficit at 150% demand generation (622.5 PJ)

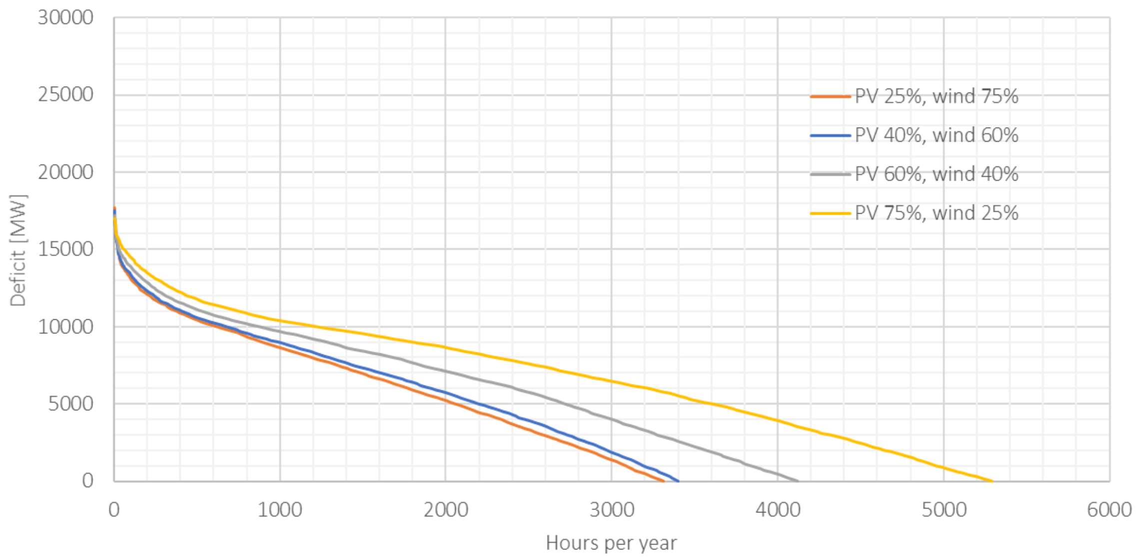

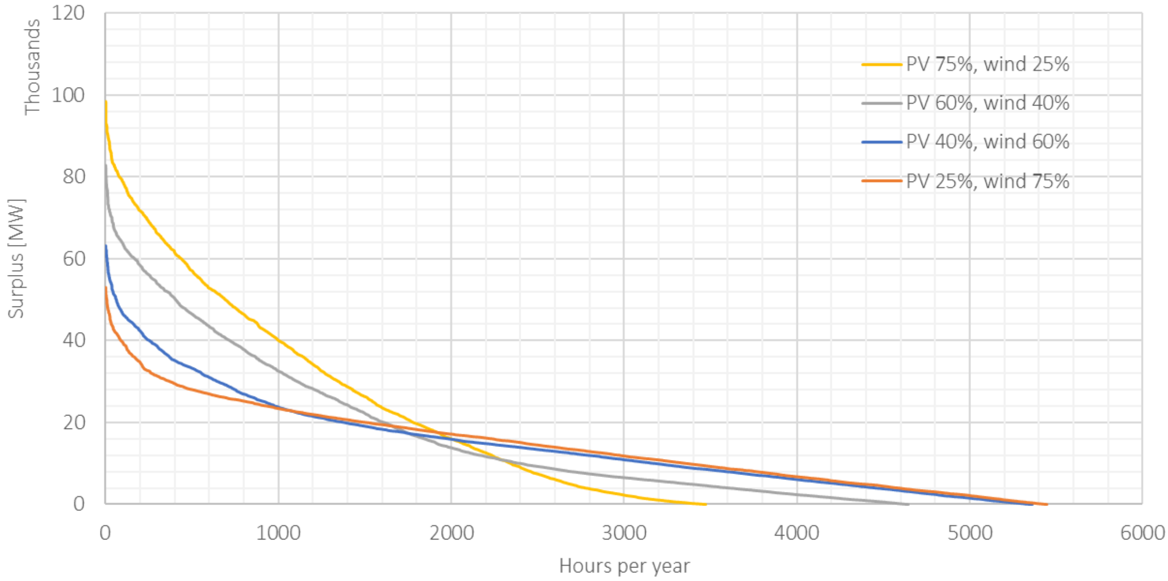

Appendix XIII: P2G storage requirements (i.e. discharge time) per P2G and G2P capacity and different generation mixes

Note that the analysis was performed using increments of 5 GW. Hence, the curves are in reality smooth lines rather than straight lines. It is furthermore assumed 5 GW CAES compression is already implemented and the generation from VRE is 415 PJ annually.

PV 25%, wind 75%

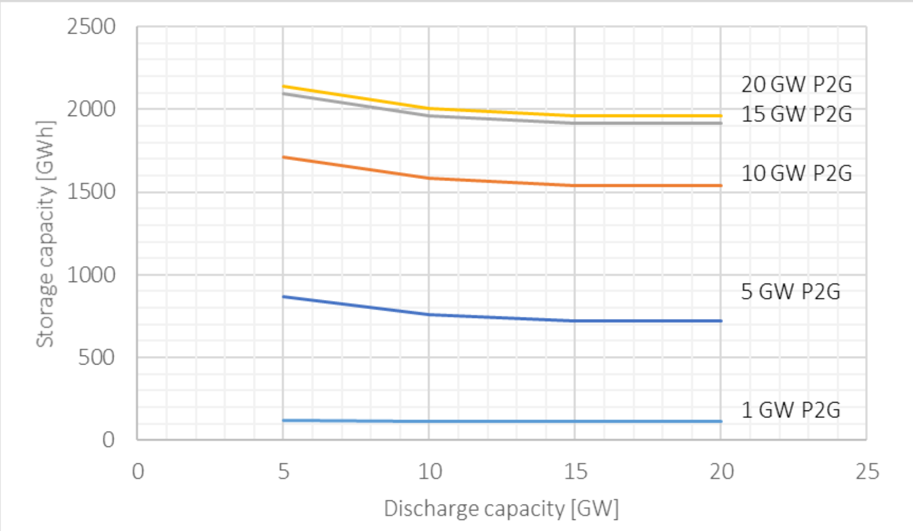

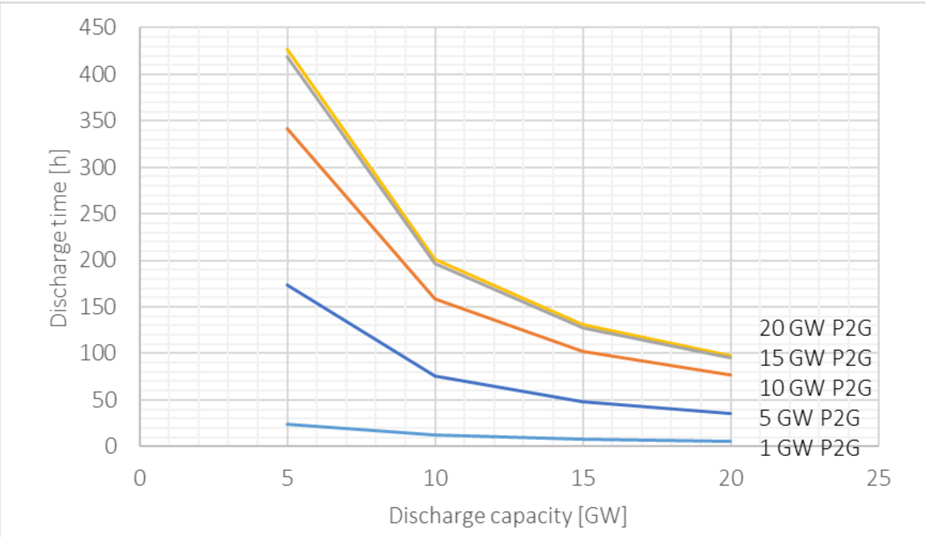

PV 40%, wind 60%

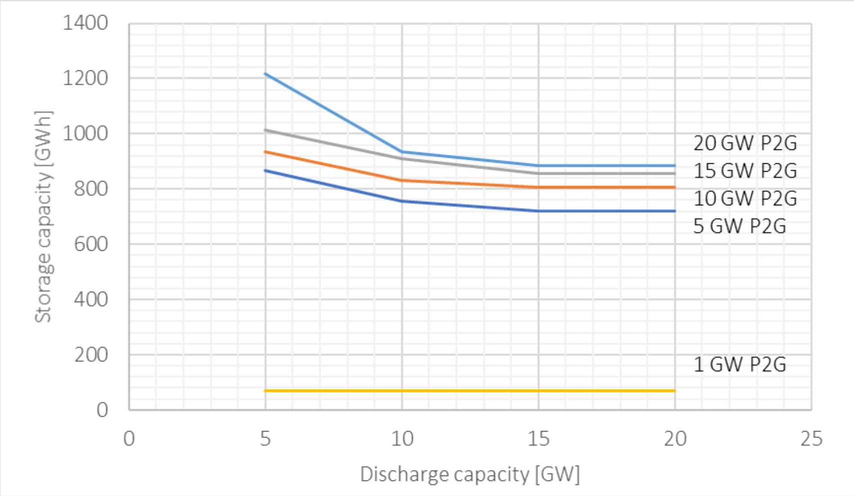
1400
1200
1000
800
600
400
200
0
Storage capacity [GWh]
0
5
10
15
20
25
Discharge capacity [GW]
20 GW P2G
15 GW P2G
10 GW P2G
5 GW P2G
1 GW P2G

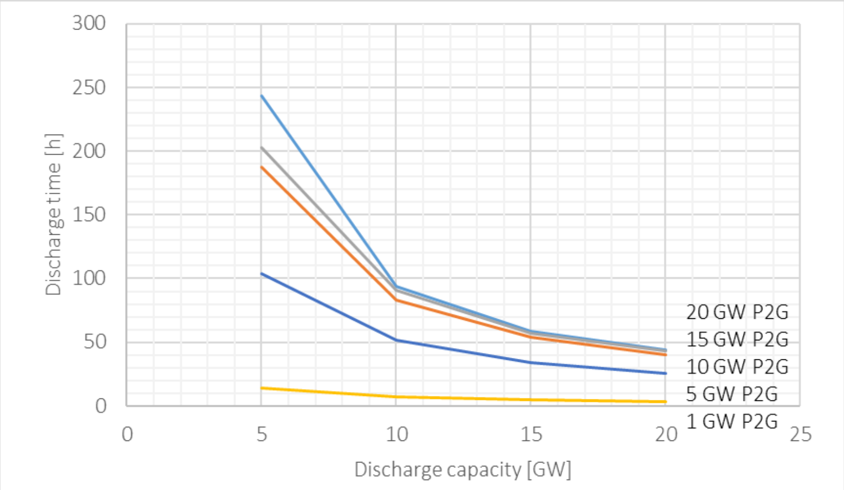
300
250
200
150
100
50
0
Discharge time [h]
0
5
10
15
20
25
Discharge capacity [GW]
20 GW P2G
15 GW P2G
10 GW P2G
5 GW P2G
1 GW P2G

Appendix XIV: Generation and surplus handling at 150% demand generation

At 5 GW CAES, 10 GW P2G with G2P, 6 GW interconnection and at a ratio of 25% PV and 75% wind.

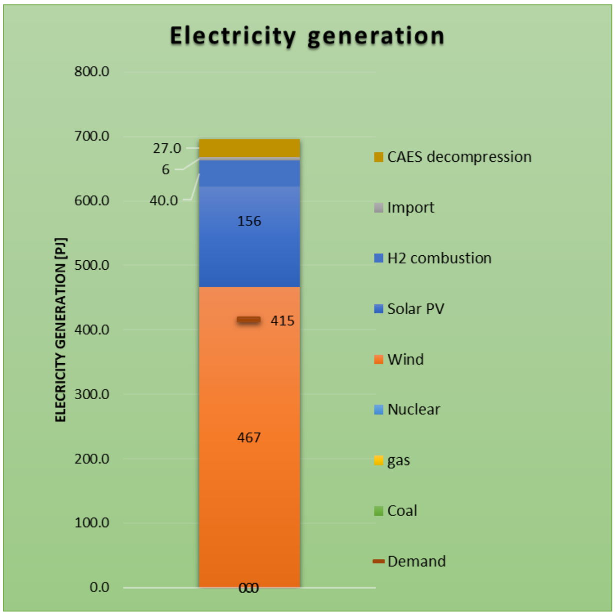

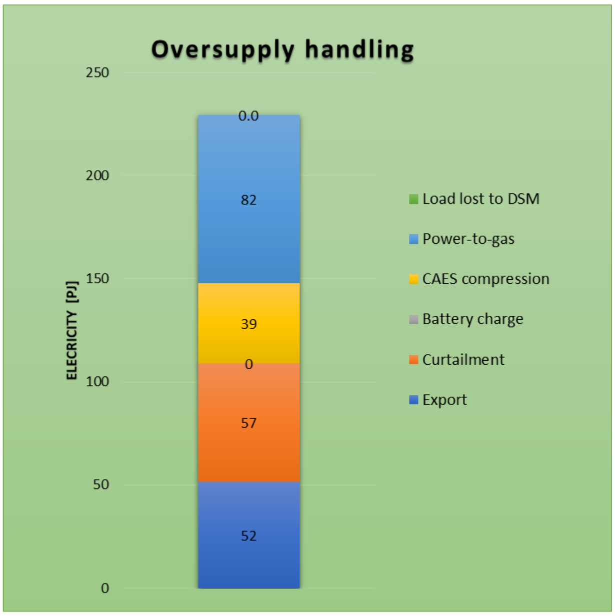

Appendix XV: LCOS per discharge time and level of operation

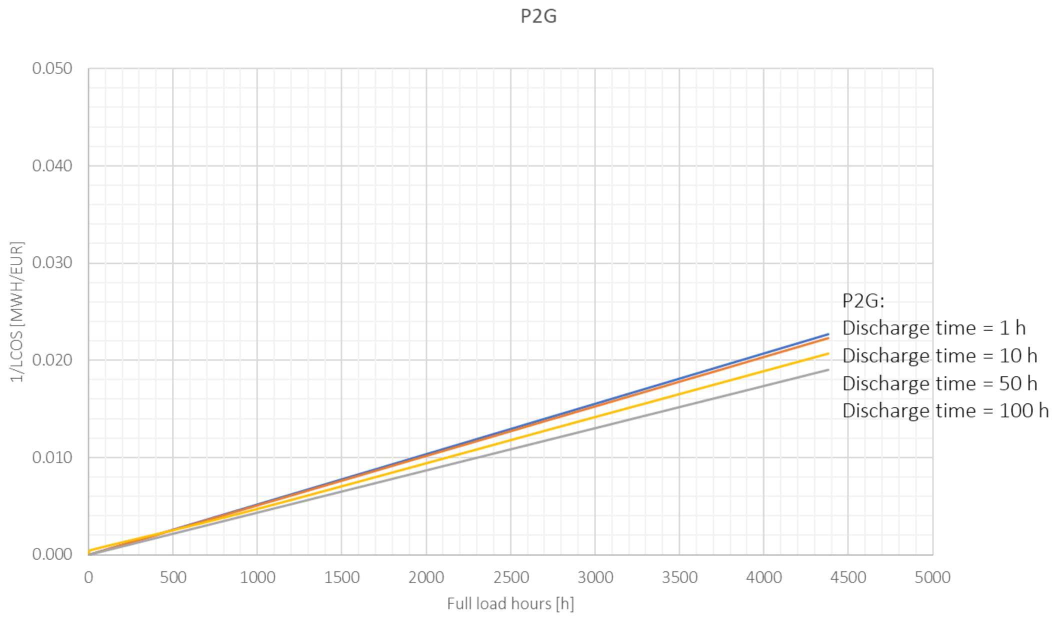

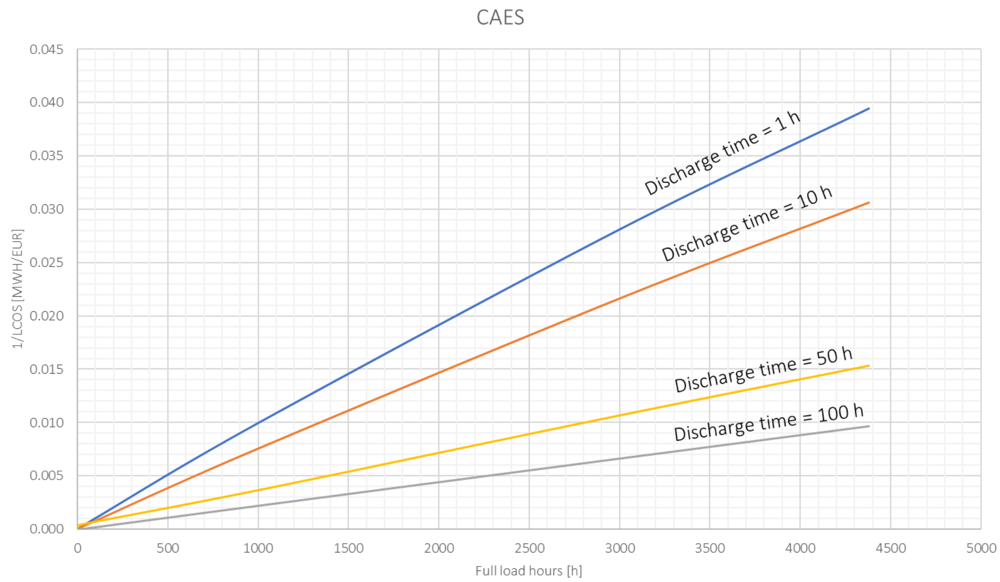

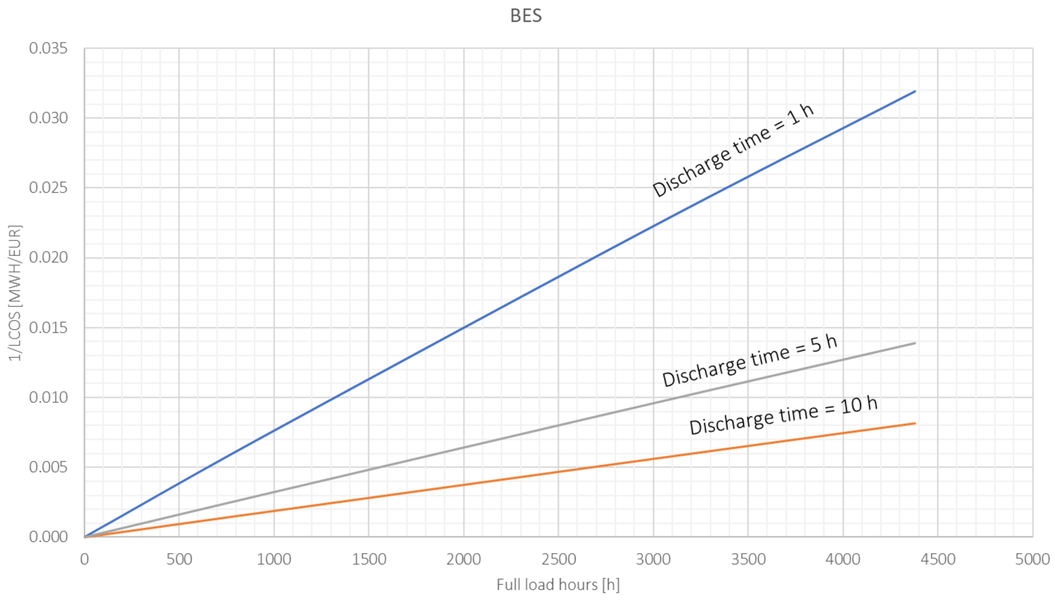
BES
0.035
0.030
0.025
0.020
0.015
0.010
0.005
0.000
1/LCOS [MWH/EUR]
Discharge time = 1 h
Discharge time = 5 h
Discharge time = 10 h
0
500
1000
1500
2000
2500
3000
3500
4000
4500
5000
Full load hours [h]

Appendix XVI: Definition and quantification of other flexibility measures

Besides EES, other drivers of grid flexibility are demand-side management (DSM), dispatchable generation and grid adaptation. Since DSM becomes increasingly important with changing demand patterns, a section is furthermore included on the effects of demand-side electrification. These sections elaborate on the summaries as presented in the theory section for additional reference.

1. Demand-side management (DSM)

1.1 Definition of DSM

DSM is a broad concept encompassing a variety of tools which aim to manage the energy demand of consumers (Kakran & Chanana, 2018), which include both residential and industrial users. IEA (2016) defines DSM as the planning, implementation and monitoring of actions that aim to alter consumers' demand pattern. It thus entails actions to actively reduce and shape the demand profile by consumers, especially in order to avoid high peak demands (Kakran & Chanana, 2018; Kool, 2011). DSM actions are generally executed by transmission or distribution system operators (TSO/DSO), parties responsible for grid balance or prosumers (Esterl et al., 2016). The aim of DSM is to increase demand-side flexibility as well as grid stability. Hence, a closely related concept is demand response (DR), which differs from DSM in the sense that it is a reactive process and the response to energy supply requirements (Kirby, 2006). In other words, one aim of DSM is to promote DR. Although the two concepts are distinctly different, DR is therefore often regarded a subdivision of DSM (e.g. Esterl, 2016; ESMAP, 2015). Other literature proposes categorisation of both DSM and DR under the encompassing category of demand-side integration (DSI) (IEA 2014; Stötzer et al., 2015).

In practice, DSM may be achieved through actively shaping the load profile of consumers through direct load control (DLC) (Kakran & Chanana, 2018). In such a case, utilities provide payments to customers for installing controllable back-up generators, interruptible generators or appliances with a remotely adjustable load (e.g. air-conditioning installations) (IEA, 2014). On the other hand, utilities can incentivise consumers to alter their consumption pattern, e.g. by increasing the electricity price at peak demands through (critical) peak pricing. Similarly, real-time pricing induces a variable electricity price, depending on the load on the system. In a similar fashion, imposing inclining block rates (IBR) cause consumers to pay a higher electricity price if they cross a consumption threshold (Bergaentzlé et al., 2014). Finally, DSM is stated to include investing in energy efficiency, which reduces total electricity demand as well as the peak loads on the system (ESMAP, 2015; Gelazanskas & Gamage, 2014).

ESMAP (2015) in turn subdivides DR into price response (PR) and automated demand response (ADR). Price response entails the reaction of consumers to shift consumption to moments of cheaper electricity, such as from day to night (Kirby, 2006). Although the electricity price is the strongest driver, consumers may further be incentivised through environmental or social signals (IEA, 2014). Gelazanskas & Gamage (2014) states that consumers can react to signals by reducing, storing or curtailing electricity at peak demands or by deploying local generation. Furthermore, electromobility poses significant integration potential for DR, as electricity surplus can be stored locally in the batteries of electric vehicles (EVs) (Pietzcker et al., 2017). Another DSM tool that stimulates PR is the implementation of demand-side bidding, where consumers can opt to participate in electricity trading by proposing changes to their demand pattern (IEA, 2014; IEA DSM, no date). For some DR concepts, the installation of hardware may be needed to allow consumers to react quickly to signals. Alternatively, ADR can be deployed causing an automated response from consumers in order to regulate and control peak loads, unforeseen system events and system frequency (ESMAP, 2015). In ADR, systems are equipped with smart hardware to act as quick ancillary services or variable loads, without human interaction.

In conclusion, the encompassing concept of DSI can be split up into DSM and DR and spans a variety of tools [Figure 4B]. In general terms, DSM indicates measures that utilities use to actively regulate and influence the consumers' demand pattern. DR is the reactive behaviour that consumers display, possibly influenced by DSM measures. Note that for consistency and readability purposes, the term DSM shall from here on be used to indicate both DSM and DR.

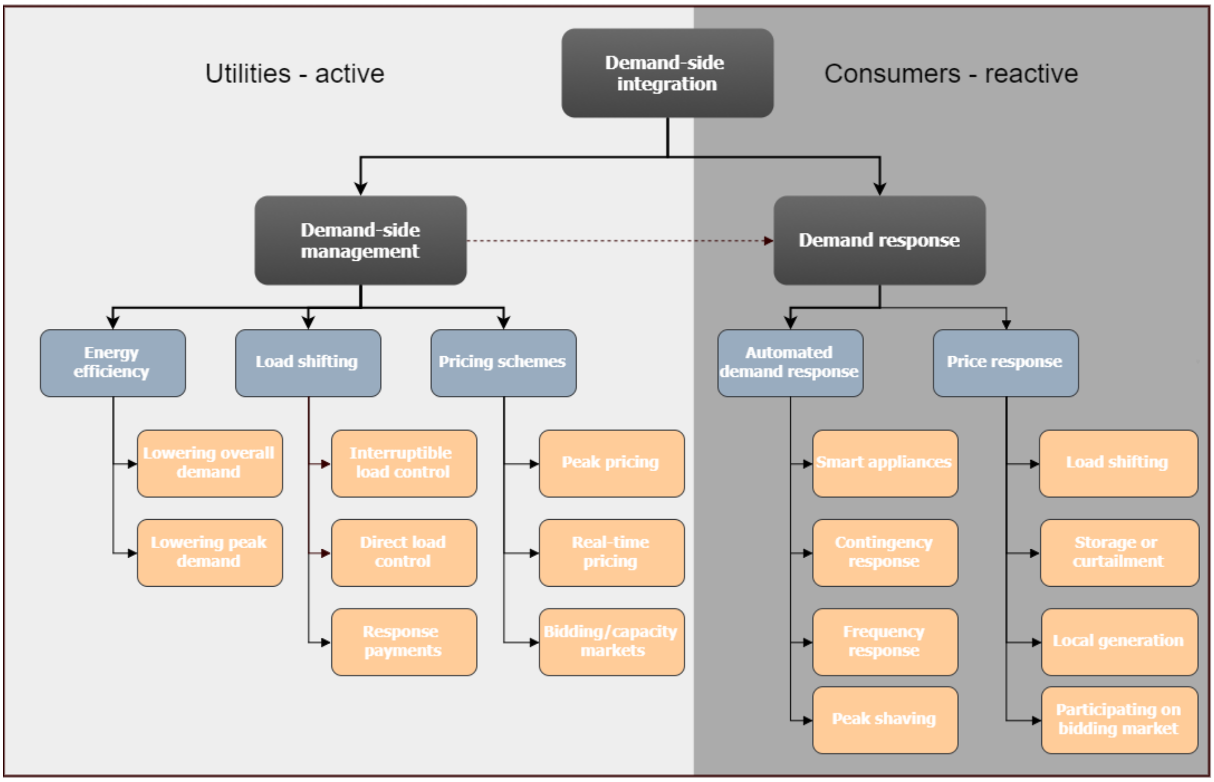

Figure 4B: Overview of DSM concepts

1.2 Quantification of DSM measures

The following section provides a literature review on reported impacts of DSM on the demand profile of consumers, as summarised in Table 9. In the table, 'diffuse' indicates that a measure reduces load spread out over periods of time, whereas 'peak' implies merely peak loads are reduced.

First of all, Bergaentzlé et al. (2014) summarises the load reductions of different price-based DSM tools. Peak pricing is shown to reduce peak loads between 4-6% for price variation between larger time segments and up to 30% for finer segments. Combining the latter with DLC is stated to allow reductions of up to 51% of the load at peak times. Furthermore, IBR tools show a varying load reduction of 5.6 to 11% over time.

In terms of response payments, IEA (2014) states that the most cost-effective payment program concerned paid shutoff of a 1300 MW load. Load shifting is furthermore stated to be most promising in EVs in the transport sector and in wet appliances (Wimmler et al., 2017). For the Netherlands specifically, wet appliances are reported to have a potential peak load reduction varying around 10% (Staats et al., 2017). It is however shown that this value varies in a large uncertain range, making wet appliances unreliable in reducing peak load.

For industrial DR, Movares (2014) reports companies that aggregate to a flexible capacity of 240-600 MW for Belgium and 1-9 GW for Germany, depending on the announcement time of required load shifting. For the Netherlands, some companies are identified eligible for DR but is acknowledged that little potential exists for an industrial DR market.

Kirby (2006) reports that a load control program of 25,000 residences led to 36 MW of interruptible load. It further provides evidence that responsive (air-conditioning) programs can follow the load pattern during the day. Verzijlbergh et al. (2015) proposes indicative values for specific flexible residential and industrial loads, which vary between 0 and 0.5 GW. It is furthermore stated that eHPs and EVs pose a controllable energy capacity of 5 and 10 GWh respectively.

Spees & Lave (2007) shows that different sources report energy efficiency potentials between 10-33% of load reduction for the USA. Furthermore, it shows that the average size of consumer contingency response loads is 158 MW. Spees & Lave (2008) provides price and demand elasticities for multiple price-based DSM tools, reporting that RTP can lead to reductions of 10-18% of peak loads.

Finally, Stötzer et al. (2015) differentiates DSI potentials for Germany into different days and seasons. It reports peak load reductions in summer of ~10% on working days up to 21% on Sundays. In winter, peak demand experiences an increase of 1.4% on working days and reductions of 22% on Saturdays. These reductions in turn lead to an increase of minimum load of 10 to 270%, depending on the day and season.

Table 9: Quantification of DSM tools

Type	Tool	Load reduction	Timeframe	Source(s)
Active	Peak pricing	4-6%[a], 30%[b]	Peak	Bergaentzlé et al., 2014
	Peak pricing + DLC	51%[b]	Peak	Bergaentzlé et al., 2014
	IBR	5.6-11%	Diffuse	Bergaentzlé et al., 2014
	Response payments	1300 MW	Peak/diffuse	IEA, 2014
	DLC (wet appliances)	0.05 GW, 10%,	Peak	Verzijlbergh et al., 2015; Staats et al., 2017
	Interuptible load	36 MW[c]; up to 0.5 GW	Peak	Kirby, 2006; Verzijlbergh et al., 2015
	Real-time pricing	10-18%	Peak	Spees & Lave, 2008
	Energy efficiency	10-33%	Diffuse	Spees & Lave, 2007
Reactive	Load shifting (industry)	Several GWs; 16%	Diffuse	Movares, 2014; Verzijlbergh et al., 2015; Stötzer et al., 2015
	Load shifting (residential/transport)	Several MWs	Diffuse	Wimmler et al., 2017
	Contingency response	158 MW[d]	Peak	Spees & Lave, 2007

[a] For broad time segments
[b] For finer time segments
[c] Considering 25,000 households
[d] Average of several DR programs

2. Electrification

Electrification implies to which extent different sectors use electrified processes rather than other resources. The shift towards increasingly electrified processes causes a change in the consumers' demand profiles. Although the concept can be argued to have implications in many sectors, its influence can broadly be divided into the residential, transport and industrial sector.

2.1 Residential electrification

Residential electrification concerns switching from fossil resources to electricity for space heating/cooling, water heating and cooking. However, since the energy used for cooking is a minor contribution, it mostly implies a shift to electric or hybrid heat pumps (EHPs) for space and water heating. EHPs efficiently transfer heat between a source and a sink, where its energy demand is generally lower than the amount of energy it supplies (REN21, 2017). The source of heat can either be air, water or ground, where air-source heat pumps are most commonly adopted. Application of EHPs is currently limited but expected to play a significant role in reducing natural gas usage in the residential sector[38]. The fact that fossil-based space heating is replaced by EHPs causes changes in the daily gas demand as well as in the electricity demand. Yet, a well-insulated house is a prerequisite for proper functioning of an EHP (Elzenga & Ros, 2014).

UK Power Network (2014) states that the daily demand profile of a household becomes more evenly distributed with the adoption of an EHP. Love et al. (2017) and UK Power Network (2014) furthermore provide daily EHP load profiles specified per month [Figure 5B]. Notably, a peak occurs in the morning, followed by a dip in the afternoon and finally a lower peak in the evening.

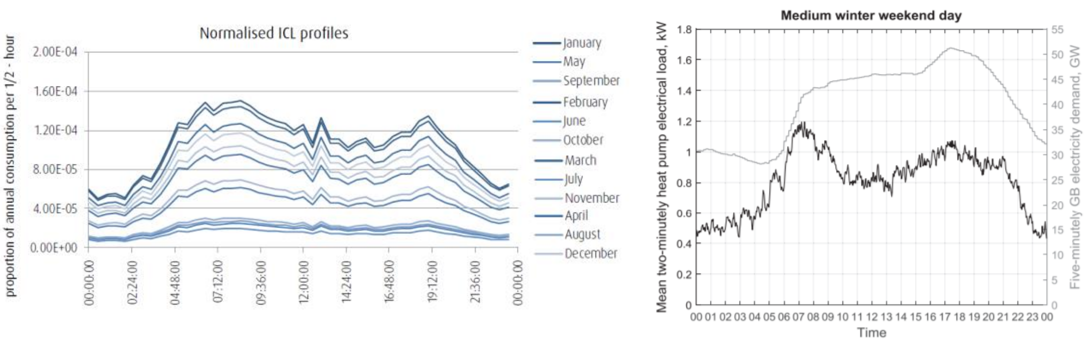

Figure 5B: Single EHP load profile per month [UK Power Network, 2014, p. 17 (L); Love et al., 2017, p. 337 (R)]

2.2 Transport electrification

The electrification of transport naturally concerns the use of (hybrid-)electric vehicles (EVs) as opposed to fossil-fuelled vehicles as a mode of transport. Although conventional vehicles remain dominant, the use of electric vehicles has experienced a rapid increase over recent years (REN21, 2017). Whereas electric passenger cars account for the majority of global EV deployment, EVs can also include electric trains, buses, trams or marine vehicles.

REN21 (2017) shows that electrifying the entire European fleet would lead to an increase of over 24% of the entire European electricity demand. Without measures to manage the charging and discharging behaviour, this thus has the potential to significantly raise loads on regional and national grids. At the same time, potential of electrified transport lies in the possibility to form a synergy with distributed energy storage. Since the batteries of electric passenger cars can be used for (dis)charging energy (i.e. vehicle-to-grid or V2G), a large increase in EVs would entail a large potential energy storage capacity (REN21, 2017). Nevertheless, Verzijlbergh et al. (2015) reports that downside to using EV

[38] ~2% of the Dutch households are equipped with an EHP, expected to reach 5% by 2020 (Schoots et al., 2016)

batteries as storage mediums include significantly reduced battery lifetimes and reduced control over the battery's state of charge.

Moreover, the way in which the daily demand profile of a household changes in response to EV adoption is dependent on the charging behaviour of the consumers. Factors that influence the demand profile include the time of day when charging occurs, the charging duration, the *smartness* of the charging and the amount of charging done at home rather than at public charging stations (Movares, 2013). UK Power Networks (2014) furthermore proposes hourly home charging loads for electric vehicles per household [Figure 6B].

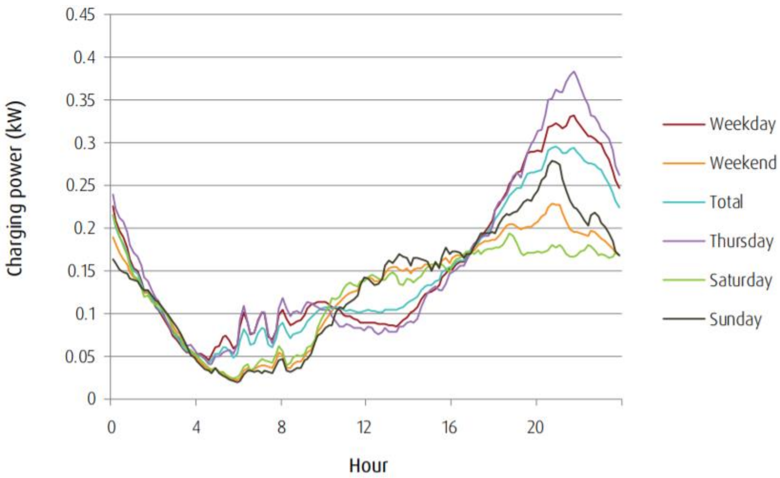

Figure 6B: Average EV charging profiles per weekday [UK Power Network, 2014, p. 27]

2.3 Industrial electrification

In terms of industrial electrification, TNO (no date) distinguishes between the conversion of power to heat, power to chemicals, power to commodities, power to specialty chemicals and power to gas. A further separation can be made between flexible and baseload electrification, where the former implies part-time use of electricity in response to the price of energy carriers such as natural gas (Berenschot, 2017). Power to heat concerns the notion of using electricity to upgrade heat and steam processes e.g. using electric boilers or heat pumps. Power to chemicals or commodities entails the synthesis of chemicals, fuels and products through the use of electricity in combination with renewable feedstock such as CO_2 or biomass. As described before, power to gas concerns the conversion of electricity into gaseous products such as hydrogen, synthetic natural gas or ammonia. Berenschot (2017) supplements these types of electrification with power to mechanical drive and power for separation. The former indicates electricity usage for replacing steam-driven mechanics and the latter involves the use of electricity for ultra- or nanofiltration and reversed osmosis. For details on the electric alternatives for a range of industrial process, Berenschot (2017) provides an overview of specific technologies for each type of industrial process.

The fact that different industrial processes shift towards electricity as their resource implies the daily electricity demand profile is prone to change. Moreover, increased electrification induces a larger DSM potential since an increasing share of processes can be controlled, shifted or interrupted. The daily electricity profile and its potential for load shifting hence both depend strongly on the type of industrial processes.

3. Dispatchable generation

Deploying dispatchable generation is the most traditional form of providing grid flexibility. Dispatchable or flexible generation implies the selective operation of power plants whenever VRE generation is insufficient to meet demand. Different aspects of power plants that influence their flexibility include short-term start-up, operation capabilities at a range of generation levels, ramping rates and response times (IEA, 2014; Verzijlbergh et al., 2015). Table 1B shows the flexibility characteristics for several conventional generation power plants: an open-cycle gas turbine (OCGT), a natural gas combined cycle plant (NGCC), a supercritical pulverized coal plant (SCPC), a nuclear power plant (NPP) and a bio energy plant (Bio). It can be concluded that OCGTs and SCPCs are generally the most flexible power plants[39] and NPPs the least flexible due to their long start-up times.

Table 1B: Power plant flexibility characteristics

Parameter	Unit	OCGT[2,5,6]	NGCC[2,4,5,6]	SCPC[1]	NPP[3, 4, 5]	Bio[4,7]
Minimum load	[%]	15-25	40-60	50	30-50	50
Cold start time	[min]	-	120-250	90	>1440	-
Warm start time	[min]	<20	90-200	45	>1440	180
Hot start time	[min]	<20	45-90	30	780-1440	-
Ramp up rate	[%/min]	20-30	4-5	2	1-5	3
Efficiency	[%]	30-42	38-60	40-45	30-33	30-35
CO_2 intensity	[g/kWh]	400	400	~800	~0	~0

[1] NETL (2012), [2] IEA (2014), [3] NEA (2011), [4] Eurelectric (2011b), [5] IEA (2012), [6] ESMAP (2015), [7] IRENA (2012)

The utilisation effect

An issue that arises when using dispatchable power to back up VRE is the utilisation effect, which entails that increased introduction of VRE generation reduces the capacity factors and thus the cost-effectiveness of back-up generators (IEA, 2014). Since VRE generation only requires additional flexible capacity during timeshares with low capacity factors, back-up capacity generators are operated during a limited period of the year. This negatively influences investment decisions for new capacity as well as the costs for operating existing power plants. Moreover, the increased VRE generation influences the operation of power plants by increasing start-ups/stops, ramping requirements and full shutdowns (IEA, 2014).

[39] Excluding pumped hydro plants

4. Grid adaptation

Adaptation of the physical grid describes all alterations to the existing power grid which aim to increase the system's responsive capabilities. In terms of grid adaptation, several factors have the potential to increase the flexibility and adaptability of the power grid. IEA (2012) proposes a distinction between three categories of grid adaptation: a) grid extension, b) grid renewal and c) renewable integration. The possible grid adaptations within each category are summarised in Table 2B and discussed below.

4.1 Grid extension

Firstly, grid extension involves connecting new firm generation capacity to existing grids (IEA, 2012). This increases the demand-matching capabilities of the system but requires investments into new power lines. Secondly, grid extension includes increasing interconnection of the grid on regional, national and international level. Since overproduction can be transferred to regions with underproduction, interconnection both promotes the smoothing of power fluctuations and reduces grid instability. Increased interconnection further lowers the need for regulation reserves and reduces congestion (IRENA, 2015b). The specific value of interconnection does however depend on whether the demand and generation profiles of connected grids coincide or complement each other (IEA, 2012). Other barriers to interconnection of high-capacity grids include their cost- and time-intensity as well as the need for a full integral grid transformation (IRENA, 2015b).

4.2 Grid renewal

Grid renewal involves upgrading the current transmission and distribution networks to accommodate changing demand and generation patterns. With an increasing need for bi-directional power flows, the grid infrastructure should be shifted away from one-way transmission, which can require upgrades to existing power lines and connection nodes (IEA, 2012; IEA, 2014). Bidirectional power flows accommodate the connection of distributed energy technologies[40] to distribution grids but increases the complexity of control and monitoring (IEA, 2012).

A trending term in the field of grid improvement is the concept of smart grids. Although the term has many implications, it broadly concerns the notion that modern infrastructures need to allow real-time and digital monitoring and managing (IEA, 2011). This implies that grids should be adapted in a way that allows flexibility measures such as DR, electricity pricing schemes and prosumer generation to occur without interruption of daily grid operation. Other factors smart grids aim to accommodate include forecasting capabilities, smart inverters and distributed storage (IRENA, 2013). Smart grids are IT-intensive since the monitoring and managing requires advanced technologies to be installed at different places in the power supply chain. Such an advanced metering infrastructure (AMI) includes communication, information and electricity infrastructure at end-user locations, transmission/distribution centres or electricity stations. Nonetheless, operating on smarter grids has the potential to pose multiple economic, technological, societal and environmental benefits (IEA, 2011). Smart grids are further acknowledged to decrease operation costs, improve grid stability, power quality and resilience to grid events (IRENA, 2013).

[40] I.e. local generation technologies and storage

4.3 Grid extension

The third form of grid adaptation involves adapting the grid specifically for increased or improved VRE integration. Expanding the geographical spread of VRE generation to different point sources in the grid can reduce the stress on the power grid due to the so-called pooling effect (Pietzcker et al., 2017). Generally, the further two VRE generators are spread out, the less their energy output correlates which reduces both the system-wide variability and curtailment of VRE (IEA, 2012; IRENA, 2015b). Although it requires ample interconnection and forecasting capabilities, efforts in strategically placing VRE generation sources can thus lower the requirements for flexibility. Furthermore, VRE integration involves connecting remote VRE generators to demand centres, e.g. through connecting offshore wind turbines to the land-based grid (IEA, 2012). This also allows connecting an overcapacity of VRE to the grid. Limitations in connecting VRE sources to existing grids include their negative effect on node voltages and thermal limits of grid components (IRENA, 2015b). Similarly, VRE connection stems additional requirements such as Fault Ride-Through[41] (FRT) capabilities, protection systems against unforeseen system events and harmonisation of communication systems.

Table 2B: Investment options for grid adaptation

Investment	Adaptation	Effects on grid
Grid extension	Connecting new capacity	+ Reduces demand-bottlenecks
	Interconnection	+ Smoothens power fluctuation + Supply-demand balance + Reduces regulation reserves, congestion and required back-up capacity - High investment costs - Requires complementary generation/demand profiles - Requires integral transformation
Grid renewal	Upgrade power lines and connection nodes (transmission & distribution)	+ Bi-directional energy flows + Enables distributed energy sources - Increased control and monitoring complexity
	Smarter grids	+ Accommodates other flexibility measures + Improves stability, resilience and power quality + Reduces system costs + Enables distributed energy sources - Hardware- and IT intensive
VRE integration	Geographical spread	+ Reduces system-level variability + Reduces curtailment - Requires ample interconnection and forecasting
	Connecting VRE sources to grids	+ Additional generation (over)capacity + Connects remote VRE sources - Negative effect on grid components - Requires FRT capabilities, protection systems and smart adaptations

[41] The ability of generators to remain operational during short-term fluctuations (IRENA, 2015b)